Experimental Investigation and Parametric Optimization of Automated Metal Inert Gas Welding Stainless Steel SS 316 with Low alloy Steel AISI 4140

Tajudin Ayub Deko

A Thesis Submitted to Department of Mechanical Engineering

School of Mechanical, Chemical and Materials Engineering

Presented in Partial Fulfillment of the Requirement for the Degree of Master's in Manufacturing Engineering

Office of Graduate Studies

Adama Science and Technology University

June-2023

Adama, Ethiopia

Experimental Investigation and Parametric Optimization of Automated Metal Inert Gas Welding Stainless Steel SS 316 with Low alloy Steel AISI 4140

Tajudin Ayub Deko

Main Advisor: Dr. Habtamu Beri (Associate Professor)

A Thesis Submitted to Department of Mechanical Engineering School of Mechanical, Chemical and Materials Engineering

Presented in Partial Fulfillment of the Requirement for the Degree of Master's in Manufacturing Engineering

Office of Graduate Studies
Adama Science and Technology University

June -2023

Adama, Ethiopia

DECLARATION

I hereby declare that this Master Thesis entitled "**Experimental Investigation and Parametric Optimization of Automated Metal Inert Gas Welding Stainless Steel SS 316 with Low alloy Steel AISI 4140**" is my original work. That is, it has not been submitted for the award of any academic degree, diploma or certificate in any other university. All sources of materials that are used for this thesis have been duly acknowledged through citation.

Tajudin Ayub Deko	______________	__________
Candidate	Signature	Date

RECOMMENDATION OF ADVISOR

We, the advisors of this thesis, hereby certify that we have read the final version of the thesis entitled “**Experimental Investigation and Parametric Optimization of Automated Metal Inert Gas Welding Stainless Steel SS 316 with Low alloy Steel AISI 4140**” Prepared under our guidance by Tajudin Ayub Deko submitted in partial fulfillment of the requirements for the degree of Mater’s of Science in Manufacturing Engineering. Therefore, we recommend the submission of the final revised version of the thesis to the department following the applicable procedures.

___________________________	________________________	________________
Advisor	**Signature**	**Date**
___________________________	________________________	________________
Co-advisor	**Signature**	**Date**

APPROVAL SHEET

We, the advisors of the thesis entitled "**Experimental Investigation and Parametric Optimization of Automated Metal Inert Gas Welding Stainless Steel SS 316 with Low alloy Steel AISI 4140**" and developed by **Tajudin Ayub Deko**, hereby certify that the recommendation and suggestions made by the board of examiners are appropriately incorporated into the final version of the thesis.

________________________ ____________________ ______________

Major Advisor/Supervisor Signature Date

We, the undersigned, members of the Board of Examiners of the thesis by **Tajudin Ayub Deko** have read and evaluated the thesis entitled "**Experimental Investigation and Parametric Optimization of Automated Metal Inert Gas Welding Stainless Steel SS 316 with Low alloy Steel AISI 4140**" and examined the candidate during open defense. This is, therefore, to certify that the thesis is accepted for partial fulfillment of the requirement of the degree of Master of Science in **Manufacturing Engineering.**

____________________ ________________ _____________

Chairperson Signature Date

____________________ ________________ _____________

Internal Examiner Signature Date

Mesfin Gizaw (PhD) [signature] 15 August/2023

Eternal Examiner Signature Date

Finally, approval and acceptance of the thesis is contingent upon the submission of its final copy to the Office of Postgraduate Studies (OPGS) through the Department Graduate Council (DGC) and School Graduate Committee (SGC).

___________________ ________________ _____________

Department Head Signature Date

____________________ ________________ _____________

School Dean Signature Date

___________________ _______________ ____________

Office of Postgraduate Studies, Dean Signature Date

ACKNOWLEDGEMENT

I express my heartfelt gratitude to the Almighty **Allah** for providing me with the mercy, blessings, protection, and patience needed to accomplish this thesis work.

I am extremely thankful to my advisor, Dr. Habtamu Beri, Associate professor in the Department of Mechanical Engineering, Adama Science and Technology University, for his supervision, guidance, and encouragement.

I would like to acknowledge the head of the Mechanical Engineering Department (Mr. Bariso Bino) for his suggestions, and cooperation in writing a request letter to get support from a different organization, and for creating a pleasant atmosphere for the success of my thesis work.

I am grateful to my esteemed teachers, Dr. Moera Gutu, Dr. Guteta Kabeta, Dr. Devendra Kumar, Dr. Sayeed G. and Dr. P.J. Ramulu in the Department of Mechanical Engineering for their valuable insights, knowledge sharing, and life experiences. Additionally, I would like to thank all the members of the department who have positively impacted my academic journey.

I am grateful for my parents whose constant love and support keep me motivated and confident. Deepest thanks to Bontu Gudata, who is my love. I am forever thankful for her unconditional love and support throughout the entire thesis process and every day.

Finally, I gratefully recognize the help of Adama Science and Technology for their education and support and for funding the thesis. I also wish to acknowledge the help provided by Manufacturing Industry Development Institute (MIDI), and Ethiopian Quality and Standard Agency for their help in providing facilities to conduct the experiments and testing during my thesis work.

TABLE OF CONTENTS

LIST OF FIGURES

LIST OF TABLES

ACRONYMS

AISI	American Iron and Steel Institute
ASME	American Society of Mechanical Engineers
ASTM	American Society for Testing and Materials
ANOVA	Analysis of Variance
AWS	American Welding Society
CFH	Cubic Feet per Hour
DMW	Dissimilar Metal Welding
DOE	Design of Experiment
GFR	Gas flow rate
GMAW	Gas Metal arc welding
GRA	Grey Relational Analysis
HAZ	Heat affected zone
LPT	Liquid Penetrant Testing
LFT	Liquid Fluorescent Testing
MIG	Metal inert gas
MSS	Mean Sum of Square
NDT	Non Destructive Testing
OA	Orthogonal Array
SEM	Scanning electron microscopy
S/N	Signal to Noise Ratio
SST	Total sum of squares
SS	Stainless steel
UTM	Universal testing machine
UTS	Ultimate tensile strength
WFR	Wire feed rate

ABSTRACT

In today's industry such as Marine, aerospace, and automotive engineering, components need to be made out of materials that have different properties in order to meet specific performance requirements. Stainless steel 316 and low alloy steel 4140 are the most commonly used materials in marine industry where corrosive resistivity and high specific strength is the design requirement. This was the main importance of welding dissimilar metal using automated MIG to improve quality and reliability. This thesis was aimed to study how different MIG process parameters (welding current, wire feed rate, gas flow rate, and welding speed) affects the mechanical properties, bead geometry, percentage of surface defects, corrosion resistivity, and microstructural properties of welding two different metals together namely stainless steel 316 and low alloy steel 4140. Taguchi L9 orthogonal array was used as Design of experiment and multi-response optimization was conducted based on Taguchi grey relational analysis. To study the significance and contribution of each parameter, Analysis of variance (ANOVA) were conducted using Minitab 21 software. Liquid penetrant was used to evaluate the welding defects according international welding defect criteria of AWS (American Welding Society). The result of microstructure analysis shows the presence of skeleton δ-ferrite and twins with fine grain structure. The result obtained from the Corrosion test was revealed that the corrosion resistivity of the weld zone was higher than the base metal of AISI 4140, heat affected zone of AISI 4140, and SS 316 by 17.30%, 41.30%, and 12.84% respectively. The tensile strength and flexural strength experimental result showed that welding current parameter has high significant effect in both cases followed by welding speed. Hardness result shows that the welding speed followed by welding current has a significant effect on hardness. The result from study of bead and surface defect shows that welding current has a significant impact on bead quality and percentage of surface defects followed by welding speed Grey relational analysis of multi-responses optimization result shows that welding current has a highly significant effect, while gas flow rate and welding speed has no significant effect. Finally the confirmation test result reveals that the experimental result at the optimum parametric setting of welding current at third level (140A), wire feed rate at first level one (7cm/s), gas flow rate at second level (9CFH), and welding speed at level one (20cm/min) (A3B1C2D1) average multi responses were enhanced by 7.78% from the initial optimal setting.

Keywords: Automated MIG welding, Grey relational analysis, Stainless steel, Low alloy steel, Weld quality, Taguchi method.

CHAPTER ONE

INTRODUCTION

1.1 Introduction to MIG welding

Welding is a technique that is used to join two similar or different metals or non-metals together using either pressure or non-pressure. It is particularly beneficial in the manufacturing industry for connecting metal components. Welding is a widely used manufacturing process for joining nearly all types of metals. One specific type of welding is metal inert gas (MIG) welding, also known as Gas Metal Arc Welding (GMAW). This process involves heating, melting, and solidifying the parent metals and a filler material in a specific area to create a joint. MIG welding uses a consumable electrode that also acts as a conductor. It is a highly efficient process with minimal material waste and can be partially or fully automated. In general, welding is a method of joining metals and plastics without the need for adhesives or fasteners (Singh and Goyal, 2017).

Metal inert gas welding is a process in which the heat source is an arc developed between a consumable metal electrode and the base metals. An externally supplied gaseous shield of inert gas, such as argon, helium, or an argon-helium mixture, protects the arc and the molten puddle from contamination by the atmosphere (i.e. oxygen and nitrogen)(Singh and Goyal, 2017). When building structures, the MIG welding process is excellent for attaching materials. The method can be applied robotically, automatically, or semi-automatically. The method has the potential to be employed in mass production units since it can create reproducible joints. (Deeksha Narwariya and Pradeep Khanna, 2020).

Two types of shielding gas process are discussed: Metal Inert Gas (MIG) and Metal Active Gas (MAG). Metal active gas welding employs a reactive gas, such as carbon dioxide (CO_2), whereas MIG welding uses an inert gas, such as argon. MIG welding is typically used for high alloy steel, stainless steel, copper, and aluminum. During MIG welding, metal can be transferred using either the spray arc or the short-circuiting arc. An arc is formed between the work item and the welding wire when using the spray arc technique. Metal pool is continuously sprayed. The arc prevents spatters while allowing for thorough base material penetration. Welding current needs to remain above a certain minimum threshold in order for a spray arc to develop. The current level is influenced by the alloy, the shielding gas, and the size of the welding wire. Overall, the current limit over 150 A is applied for wires with diameters higher than or equal to 0.8mm. There is no metal transfer across an arc during the short arc procedure. The wire is fed back into the arc as a result of the short circuits it causes between the wire and the work piece. This technique results in a minimal heat input arc (Saurabh Gandhe and Aber Wukchaure, 2019).

When welding different steels, various elements must be addressed in order to obtain a successful and high-quality weld. One such problem is the difference in physical and mechanical qualities between the two materials being welded, which can induce cracking, distortion, and poor fusion. One issue in MIG welding is determining the right welding parameters such as voltage, wire feed speed, and gas flow rate. Welding parameters must be carefully managed to achieve the optimum amount of heat input and good fusion of both materials. Another problem is maintaining appropriate weld area shielding to minimize oxidation and contamination of the weld pool. Welding different steels can bring advantages such as enhanced strength and corrosion resistance. Combining several materials can also assist produce certain mechanical or chemical qualities that a single material may not have (American Iron and Steel Institute, 1988).

1.2 Overview of Automated MIG Welding

The automated MIG welding technique uses a fully automated system to control every step of the welding procedure. This includes the welding gun's movement along the joint, which is carried on a carriage that advances at a set speed. A control panel moves the carriage while pre-programmed processes or instructions are used to adjust the welding parameters. Additionally, fixtures are used to hold the base metals in place while welding. Fixtures help to ensure uniformity in shape and size when welding and to minimize movement.

Automated MIG welding follows the same basic principle as manual or semi-automated MIG welding, which involves using a consumable wire electrode and a shielding gas to melt and join metals together at the weld joint. The heat source needed to melt the parent metal is provided by maintaining an arc between the end of the bare wire electrode and the work piece. The electrode wire's end is melted by the arc and then moved to the molten weld pool. The wire feed rate determines the arc current for a certain wire composition and diameter. An externally supplied shield gas protects the arc and the weld pool from ambient pollution. The 'flat' arc method (constant voltage) is used in metal inert gas (MIG) welding. By changing the voltage control knobs at the power supply, the desired voltage is chosen (Ketkipada and Dahisar, 2002).

MIG welding's electric arc may reach temperatures of 9,000-11,000 degrees Fahrenheit (4,982-6,093 degrees Celsius). This high temperature is required to melt the consumable electrode wire and the base metal at the weld joint, forming a molten pool of metal that cools and fuses the two parts together. The arc's heat also causes the shielding gas to ionize, resulting in a stable plasma that shields the molten weld pool from ambient contamination while also supplying extra heat for optimal bonding. It is crucial to note, however, that the actual temperature achieved by the arc will be determined by various parameters, including the welding current, voltage, and wire feed speed, as well as the kind and thickness of materials being welded (AWS, 2000). Wire diameters for general purpose welding applications generally range from 0.023 inches (0.6 mm) to 1/16 inches (1.6 mm), with 0.030 inches (0.8 mm) and 0.035 inches (0.9 mm) being the most prevalent.

1.3 Research Motivation

The most important factor in today's manufacturing industry is quality. According to some sources, quality refers to how well customers are treated when a product is provided. In many application areas, product quality is established by the requirements that are met in the product to meet your functional demands. The mechanical and microstructural properties of welded metals are significantly influenced by the quality of the welding. On the other hand, the welding process parameters have an impact on the weld's quality. MIG welding process parameters such as welding current, welding speed, wire feed rate and gas flow rate have either direct or indirect impacts on the weld's mechanical characteristics, weld bead shape, weld chemistry, and metallurgical aspects. (Greyjevo, 2014). In specifically, stainless steel SS 316 and low alloy steel AISI 4140 are the two dissimilar metals that this study is investigating the best parameters for automated MIG welding. In order to obtain the best weld quality and mechanical properties, the research aims to explore and improve the welding process parameters. The rising need for welding different metals in sectors like aerospace and automotive production is one of the driving forces for this study. Automated MIG welding is one way to solve the issue of making a reliable junction between two distinct metals with varied thermal characteristics. The goal of this study was to better understand how different process factors affect the weld quality while employing automated MIG welding to combine dissimilar metals.

1.4 Statement of the Problem

Currently, welding dissimilar metals together is widely used in many applications such as marine, automotive, aerospace, power plants, agricultural, oil and gas, petrochemical refineries, and many manufacturing industries, and many studies have been done on the welding of stainless steel with low carbon and medium carbon steel. However, only few of the studies were adequate for the aforementioned application due to a lack of fit material selection and weld quality optimization. Material properties such as flexural bending, weld beads, and percentage of surface defects have not been tested in most studies. However, little research has been conducted on the welding of stainless steel with low alloy steel, taking into account the advantages of stainless steel SS316's superior corrosion, oxidation, and high temperature creep resistance, as well as the high strength, torsional strength, fatigue strength, and toughness of low alloy steel AISI 4140 by enhancing high weld quality and better mechanical properties.

Due to variations in mechanical properties such as ultimate tensile strength and yield strength and in the chemical composition of chromium and nickel amounts, welding mutually exclusive metals such as stainless-steel SS 316 and low alloy steel AISI 4140 presents obstacles. Poor weld quality and mechanical qualities, such as weak interfaces, porosity, and cracking, can arise from insufficient selection and optimization of automated Metal Inert Gas (MIG) welding process parameters. As a result, experimental research and parametric optimization of the MIG welding process for these dissimilar metals are required to establish the ideal welding conditions, which include welding current, voltage, wire feed rate, travel speed, and shielding gas flow rate. Through experimental inquiry and statistical analysis, this study was intending to enhance the weld quality and mechanical characteristics of dissimilar metal junctions by improving the MIG welding process parameters.

1.5 Research Questions

The research questions for this study titled "Experimental Investigation and Parametric Optimization of automated Metal Inert Gas Welding Process Parameters during Welding of Stainless-Steel SS 316 with Low alloy Steel AISI 4140" are:

1. What is the optimal welding current, wire feed rate, travel speed, and shielding gas flow rate for welding stainless steel SS 316 with low alloy steel AISI 4140 using the automated MIG welding process?
2. How do the welding settings affect the joints made of different metals in terms of their mechanical properties and weld quality?
3. How do the parameters of the automated MIG welding process, such as welding current, wire feed rate, travel speed, and gas flow rate, affect the weldment of

stainless steel 316 with low alloy steel 4140, and what effect do they have on mechanical properties?

4. Does the microstructure of the welded joints change with different sets of welding parameters?
5. Does the corrosion resistivity of different zones formed during welding dissimilar metals are differ?

1.6 Objectives of the Study

The study is aimed to addresses the following general and specific objectives.

1.6.1 General Objectives

The objective of this study is to investigate the influence of welding process parameters on the mechanical properties, weld quality and corrosion resistivity of the weld joint between SS316 stainless steel and AISI 4140 low alloy steel by automated MIG welding.

1.6.2 Specific Objectives

To achieve the main objective of this thesis, the following specific objectives were designed:

1. To optimize the welding parameters (welding current, welding speed, gas flow rate, and wire feed rate) by using Taguchi Method.
2. To investigate welding quality and welding defects using liquid penetrant testing.
3. To investigate welded joint mechanical properties (tensile, hardness, flexural bending).
4. To investigate the microstructure of welded material using OM and SEM to discover grain structural changes during heating in the weld zone and heat effect zone.
5. To explore Weld bead geometry (weld width) and Percentage surface defects to examine weld quality and the range of parameters in which surface defects grow.
6. To analyze corrosion test on different zones of welded material.

1.7 Significance of the Study

This work was significant because it has the potential to improve the quality and mechanical qualities of dissimilar metal junctions by optimizing automated Metal Inert Gas (MIG) welding process parameters. Welding stainless steel SS 316 with low alloy steel AISI 4140 presents difficulties owing to variations in chemical and physical properties, which can result in poor weld quality and mechanical qualities. This work was provided a dependable solution for welding these dissimilar metals and improve the weld quality and mechanical characteristics of the joints by performing experimental investigation and statistical analysis to optimize the MIG welding settings. The study's results have potential implications in a variety of sectors, including aerospace, automotive, and marine engineering, where the welding of dissimilar metals is critical.

The following are the implications of the thesis:

- This study was focused on conducting an experimental investigation and parametric optimization of automated metal inert gas welding parameters when welding dissimilar metals (SS316 with AISI 4140 low alloy steel).
- The investigation works on bits that help to maintain the higher mechanical properties of the joints, increase the product's life time, obtain a better weld quality, and reduce welding defects on the welded joint.

Finally, the thesis was used as an input for minimum defect products to produce better weld quality in terms of strength and hardness, and this study work can benefit students studying this research area, future researchers as a literature, and manufacturing industries in need of these welded materials.

1.8 Scope and Limitation of the Study

This research was conducted an experimental examination and parametric optimization of the automated Metal Inert Gas (MIG) welding process parameters while welding stainless steel SS 316 with low alloy steel AISI 4140. Through experimental examination and statistical analysis, the study chose and optimized welding parameters such as welding current, voltage, wire feed rate, travel speed, and shielding gas flow rate. The thickness and number of layers to be welded were utilized to choose the samples for the experiment. Tensile strength, flexural strength, hardness, and microstructural analyses were used to assess the mechanical attributes and weld quality of the joints. However, there were certain limitations to this study that should be emphasized. The research only looked at the welding process parameters for dissimilar metal junctions of stainless-steel SS 316 and low alloy steel AISI 4140 utilizing automated MIG welding. It excluded TIG welding and manual MIG welding. Furthermore, the study's experimental design was confined to particular metal types, thicknesses, and layer numbers. Additionally, the welding equipment used in this study was assumed to be of good quality and consistent performance. This study focused on optimizing certain MIG process parameters and did not consider the impact of other aspects such as joint preparation or post-weld heat treatment on weld quality and mechanical properties.

1.9 Thesis Organization

This research paper consists of five chapters. The 1st chapter is about the introduction and background of the study, problem statement, objectives of the study, significance of the study, the scope of the study, and thesis organization. The 2nd chapter is about the science behind automated MIG welding process during welding dissimilar metals and optimization techniques by reviewing of different literature. Finally, the summary of the literature and the research gap is described. The 3rd chapter is about the materials utilized for the experiment, welding method, experimental principles and the equipment used, and methodology that fulfilled the aims of the study were discussed. The 4th chapter is about detailed discussion and analysis based on the experimental results. It investigates the impact of process parameters on mechanical properties and quality of the welds, the microstructure welded metals, and corrosion resistivity. Finally, the 5th chapter presents the conclusion and recommendations for future works

CHAPTER TWO

LITERATURE REVIEW

2.1 Introduction

Researchers have undertaken several studies on the welding procedure used for dissimilar metals and its influence on various aspects. These studies have mostly concentrated on the influence of the welding process on the mechanical characteristics of welded joints, as well as parameters including welding procedures, weld shape, percentage of surface defect, microstructural analysis, and corrosion test analysis. A complete literature study was undertaken under this specific sub-topic to investigate automated MIG welding of dissimilar metals.

2.2 Studies on Welding of Stainless steel SS316 to Low alloy steel AISI 4140

Reddy et al. (2014) performed research on various weldments and discovered that AISI 4140 and AISI 316 materials may be effectively welded using the GTA welding technique, both when filler wire is utilized and when it is not. In both cases, Martensite growth can be detected in the HAZ of AISI 4140. There was tensile failure at the parent metal of AISI 316 in each test for both weldments. The welds' strength is found to be higher than that of the candidate metals AISI 4140/AISI 304. Because of the appearance of coarse austenite grains in the matrix, the GTA weldments utilizing ER 309L filler exhibited a lower hardness value in the weld zone.

2.3 Optimization of Different MIG welding Process Parameters

Assefa et al. (2022) Nondestructive testing was utilized to identify welding faults, and some samples had issues with porosity, lack of fusion, and lack of penetration. The weld zone of sample number 10 displayed a very fine structural ferrite across the grain, sub-grain, and migration barriers in the plain austenitic matrix as a result of a moderate heat intake and moderate cooling rate. A higher tensile strength of 502MPa was obtained by parametrically combining 110A current, 10 L/min gas flow rate, 2.5 mm root gap, and ER-309L filler wire. ER-312 filler wire, 130A current, 10 L/min gas flow rate, and a 1.5 mm root gap were used in a parametric configuration to produce a maximum hardness of 90HRB or 183HV. Utilizing a parametric configuration of 90A current, 7 L/min gas flow rate, 1.5 mm root gap, and ER-309L filler metals, a maximum flexural strength of 692MPa was attained.

Deeksha Narwariya and Pradeep Khanna. (2020) investigated how a MIG welding power source's process parameters affected welding current, Using Taguchi's method, a mathematical model was created between the input parameters of wire feed rate (m/min), voltage (volts), and nozzle to plate distance (mm) and the response parameter of current (amp). A L8 array was used to build the model, and graphical responses were used to examine the outcomes. He ultimately got to the conclusion that Taguchi's method is suitable for looking at the current case. It has been noticed that when the wire feed is raised, it also increases the welding current. As the voltage increases, the value of the welding current decreases slightly. The welding current scarcely decreased as NPD increased.

Wang and Chetan A. Somani. (2018) conducted research on experimental Investigation of Gas Metal Arc Welding (GMAW) Process Using Developed Articulator by Shielding Gas Nozzle than an Arc under Argon-CO2 Mixtures was carried out. This discovery, however, cannot be explained by a cooling impact of the CO2 doing the work, according to the test findings. Welding voltage, welding current, and welding speed were studied in experiments and practical, and the findings for visual inspection and ultimate tensile strength are presented. Each test sample is visually examined for visual weld flaws, weld bead reinforcement over base metal, and weld metal penetration into the root of the weld groove. Visual inspection reveals that the samples are satisfactory in terms of the reinforcement and appearance of the weld bead. The lowest reinforcement seen above the weld cap is 2 mm, and the maximum is 3.5 mm due to the angle being more than 120, which satisfies ASME section IX criteria. A macro inspection at a magnification of 20 X reveals that there is enough penetration. It was determined that five out of the eight samples met the standards for ultimate tensile strength. The operating range of the welding settings is discovered. Plots showing the behavior of welding current, open circuit voltage, and welding speed as a function of control parameters show rising welding tensile strength.

Lohse et al. (2020) had carried out GMAW tests, and by changing the characteristic curve and the wire feed to the shielding gas, the process parameters had been established. These studies showed that adding more CO_2 to the combination decreased the amount of radiation-induced energy entering the shielding gas nozzle, with an 82% argon and 18% CO_2 mixture producing the local maximum. The visible arc length also reduced when CO_2 level rose, which had an effect on the radiant volume. Higher arc temperatures at 18% CO_2 than at 100% argon or 100% CO_2 are likely to counteract this drop. An arc in CO_2 emits less radiation into the shielding gas using normal settings than an arc in argon. This shows that using argon as a shielding gas is more advantageous than CO_2 in the GMAW process.

2.4 Studies on Mechanical Properties

Sapakal. (2017) conducted research concentrating on improving metal inert gas welding process factors. The purpose of this study is to look at the toughness of welding connections made of different metals. Metal inert gas welding, sometimes referred to as gas metal arc welding, and 0.8 mm diameter stainless steel filler wire were used to weld stainless steel 304 to C-25 carbon steel. Because C-25 carbon steel is inexpensive and stainless-steel resists corrosion, argon gas was employed in this procedure as a shielding gas. To satisfy the service requirements of the industry, welding of the two is necessary for all applications. It was discovered that wire feed rate was the most significant effective parameter in this experiment and that hardness is affected by a variety of parameters. Finally, it was found that the input parameters of current, voltage, and wire feed rate had a substantial impact. In this experiment, it was discovered that the wire feed rate, followed by current and voltage, is the first parameter that impacts hardness.

Wahule and Wasankar. (2018) to improve the process parameters of TIG welding for different metals (SS-304 and Fe-410), an experiment was conducted utilizing Grey Relational Analysis. Both the tensile test readings and the percent elongation are obtained. The percentage of elongation and the tensile test both approach their optimal values. The findings from the test results are as follows:

- The optimal values for tensile strength were discovered to be 120 Amps of current, 16 Lit/min of gas flow rate, and 2 mm of root spacing.
- The ANOVA findings revealed that the current made the most contribution, up to a maximum of 47.38%, followed by gas flow rate and root gap.
- For percentage elongation, it was found that 120 Amp of current, 16 Lit/min of gas flow rate, and 1 mm of root spacing were the ideal values.
- The ANOVA showed that current, which accounted for 62.88% of the total, gas flow rate, which contributed 24.08%, and root gap had the least influence.
- The optimal values for multi-objective optimization of tensile strength and % elongation was found to be 120 Amps of current, 16 Lit/min of gas flow rate, and 2 mm of root spacing.
- The ANOVA revealed that current contributed the most, at a rate of 58.73 percent, followed by gas flow rate at 27.9 percent and root gap at 0.1 percent.

Bhardwaj et al. (2017) The results of an experiment on stainless steel alloy SS-202 plate MIG welding led to the following conclusion. Welding variables including welding current, gas flow rate, welding speed, and filler material affect the welding strength or tensile strength of SS-202 weld joints. At low gas flow rates, SS-202 specimens that have been welded show good tensile strength but limited ductility. The characteristics of welded SS-202 alloy specimens can be significantly impacted by welding faults like porosity. High welding rates are more likely to result in welding flaws and inappropriate metal penetration. Due to variations in microstructure, particularly grain size, the weld zone's hardness value fluctuates with distance from the weld center. Hardness can rise for two reasons: the correct fusing of the filler metal with the base metal and the production of metal oxides at low gas flow rates. At 4 mm/min welding speed with a 200A welding current, the lowest hardness is attained, while at 4 mm/min welding speed with a 300A welding current, the greatest hardness is attained. Due to its high porosity, sample 3's tensile strength is the lowest, measuring at 5 mm/min at 100 A current and 1.5 litres/min for gas flow rate, while sample 8's tensile strength is the greatest, measuring at 3 mm/min at 300 A current and 1 litre/min for gas flow rate with 5% elongation.

Chavda et al., (2014) conducted an article titled "Parametric Optimization of MIG Welding Using Taguchi's DOE-FEA Hybrid Modeling for AISI 1045." In this work, the welding process parameters for welding stress were optimized using the Taguchi technique. We optimized four input parameters using the S/N Ratio. To increase the tension on the welding plate, the larger-is-better quality feature has been applied. To forecast the ideal collection of parameters that provides the best value of stress, a L9 orthogonal array with four parameters and three levels was employed. The Minitab software16 was used to input the FEA stress data, and the program projected that the stress would be 582.670 MPa. In other words, weld stress is influenced by weld current, weld speed, and voltage. Current is the most crucial element for weld stress. The most important factor for weld stress is current. The study shows that current 200, voltage 23.5, GFR 15, and welding speed 225 provide the best stress value. So, after experimenting with welding current, welding speed, and voltage, we can conclude that increasing the weld stress (strength) yields the best results. A design matrix is created by identifying appropriate control variables, and stress and temperature distributions are calculated using ANSYS software. By implementing FEA simulation, the FEA results obtained from the confirmation analysis using the optimum combination show excellent agreement with the predicted result. It is possible to save both material and time by simulating the analysis.

Amit Ratan Biswas et al., (2019) conducted an experiment using GMAW to weld medium carbon steel 45C8 and stainless steel AISI 304. There have been reports on yield strength, ultimate tensile strength, weld zone hardness, weld bead thickness, and welded joint reinforcement. The factors employed include welding current, voltage, speed, and gas flow rate. The Taguchi Method was employed to plan the experiment. ANOVA and S/N ratio analyses indicate that the welding current is the process parameter that has the largest impact on the results. As the welding current increases, the hardness of the welded zone decreases. Weld bead thickness has been shown to rise and reinforcing to decrease as welding current increases. The weld zone, HAZs, and base metal microstructures have all been researched. From base metal to HAZ and finally to the welded zone, the grain structure changes. The grain size shrinks in the welded area.

Kiran et al., (2022) conducted an experiment for the Optimality of GTAW Parameters on Comparable and Dissimilar Steel Substrates using mathematical and experimental studies. In this investigation, the materials EN 10025 Steel (grade S295) and D36 shipbuilding steel were joined using argon arc welding. Following that, residual stresses and micro-hardness were optimized for certain input parameters using the Taguchi orthogonal L9 array design. A genetic algorithm was used to choose the ideal settings for decreasing residual stresses and raising micro-hardness. Compressive residual stresses are produced at the base plate, whereas tensile residual stresses are produced throughout the weld length and HAZ. Due to the high heat input, it was discovered that the quantity of generated residual stresses in the component was directly related to current and gas flow rate, but inversely proportional to weld offset due to the decreased groove capacity. Because stainless steel, which is harder than EN 10025 steel, is employed as a filler rod, the weld bead zone has a high hardness. Because the temperature at the HAZ is higher than the recrystallization temperature of EN 10025 steel, brittle nature can be noticed in the HAZ (grain enlargement). As a result, the HAZ has lower hardness and tensile strength than the base plate and weld zone. Although the double V groove showed better tensile strength, both the single and double V groove welded tensile specimens failed at the HAZ. The tensile and fatigue strength of the dissimilar material is greater when compared to a sample welded from a comparable material.

(Mvola et al., 2014) did research on the use of GMAW to join different non-ferrous metals. This study explored advanced and adaptable GMAW methods as applied to dissimilar welding and spoke about fusion welding of dissimilar non-ferrous metals in an effort to enhance welding procedure parameters. Reviewing earlier research reveals the following conclusions: The quality of welding between different nonferrous metals is enhanced by the employment of an appropriate method. Mg/Al dissimilar metals were effectively bonded by CMT welding using pure copper as the filler metal. The formation of many Al-Cu intermetallic compounds resulted in a joint with a 34.7MPa bonding strength. The Mg side's fusion zone, where the micro-hardness value was highest, experienced fractures. Where embrittlement chemicals were present, fractures developed. Advanced GMAW CP was used to effectively fusion weld a 2B50 wrought aluminum alloy and an AZ31 magnesium alloy. The melting zone and HAZ of the GMAW welds have varied widths due to the use of heat-treated 6061 and 7075 alloys in diverse combinations. With time and temperature, welded metals' hardness can rise dramatically. The intermetallic formation is finished when the weld's tensile strength and hardness levels are at their highest. Zinc foil can be used as an interlayer to link aluminum and magnesium alloys, preventing weld burn-through and macroscopic cracking. Welding Al-Cu dissimilar joints using GMAW methods has not been thoroughly researched, despite the huge potential cost reductions in automobile building.

2.5 Studies on Percentage of Surface Defects

(Sheikh AA, 2008) It was discovered throughout his investigation that welding defects affect how the welded product looks. The price of the finished product will be reduced if the sheet was not properly welded. Additional expenses for repairs are required to fix these flaws. Taguchi DOE analysis was used in the tests to improve outcomes and decrease the amount of sheet welding flaws. According to the study, flaws were significantly reduced when welding current was set to 90A, arc voltage was 24V, welding speed was 40cm/min, and electrode angle was set to 60 degrees. Pinholes decreased by 30.31%, incomplete fusion by 73.72%, and porosity by 63.19%. The industry greatly benefits from this drop in the percentage of problems since it drastically lowers the expense of repairs.

2.6 Studies on Bead Geometry

(Ramos-jaime et al., 2013) carried out an investigation on the impact of process variables on robotic GMAW bead area estimate. They found that the impact of GMAW process parameters on bead geometry prediction has been documented. According to the findings of the experiments, the bead area in GMAW processes is influenced by process variables such welding travel speed, wire feed speed, and welding voltage. It is possible to accurately forecast bead dimensions with an accuracy range of 0–20% by using mathematical models created from experimental data to study correlations between process factors and bead geometry. The radial basis function neural network showed that, because the algorithm converges in all circumstances, there is little difference in estimating the distance to the centroid points using various methodologies. Contrarily, the Mahalanobis distance tends to be the Euclidean distance, which results in minimal variation in the outcomes, which are more impacted by the arbitrary distribution of the centroids. The ultimate outcomes were significantly influenced by the optimization technique used.

2.6.1 Depth of penetration of welded joints

(Ibrahim et al., 2012) performed studies on how different welding parameters are affected by GMAW (gas metal arc welding) methods. The factors in this experiment are welding current, arc voltage, and welding speed. This conclusion revealed the following: The welding current was raised by 90, 150, and 210 A, respectively, to enhance the depth of penetration. The penetration will depend on the welding current. Penetration is influenced by arc voltage and welding speed as well. The graph demonstrates that 22 V at 210 A is the optimal amount of penetration for three different welding speeds. Compared to other plots, it showed the highest penetration levels. Point 90 A has a greater hardness at the weld bead, which decreases with time to point 150 A and then slightly increases to point 210 A. The greatest hardness value measured is 26 V at 90 A and 60 cm/min welding speed. The grain boundaries of the microstructure shift from bigger to smaller when the welding settings vary. The ideal value for welding penetration at 60 cm/min is 26 V at 210 A.

2.7 Studies on Microstructure of welded joints

Chaudhari and Ingle, (2019) studied the Empirical Research on Dissimilar Metal Weld of SA335 P11 and SA312 TP304 Formed by Metal Inert Gas (MIG) Welding. The results of his investigation indicated that MIG welding is inappropriate for combining SA335 P11 alloys and SA312 TP304 steel because the junctions exhibited a lack of fusion upon macroscopic examination. In samples that underwent heat treatment and the joint broke in the weld zone, the tensile strength of the MIG welded joints reduced. This results from segregation of the carbide grain boundaries and a lack of fusion. Joint strength is unaffected by heat treatment. The greater hardness seen under heat-treated conditions supports this. Sensitization, which happens in heat-treated circumstances, is thought to be the cause of the observed abnormality. The microstructure, where carbide precipitation is seen at the grain boundary, also demonstrates this. The as-welded sample of SA312 TP304's base metal revealed carbide precipitation at the grain boundary, suggesting welding sensitization. This makes stress corrosion cracking in the joint more likely.

2.8 Studies on Corrosion Test

(Mani et al., 2018) Research was done to examine the corrosion resistance of GTAW-welded bi-metal connections between tubes made of stainless steel 316 and monel 400. This study adds to the body of knowledge on the application of austenitic stainless steels 316L and Monel 400 in industrial settings. A potentiodynamic method was used to assess how the welded joints' corrosion behavior. The base metal, heat-affected zone, and weld zone following post-weld heat treatment were all included in the analysis. The results were validated using optical microscopy. The base metal of 316L stainless steel had the maximum corrosion resistance, whereas the heat-affected zone of monel 400 alloy displayed the lowest.

2.9 Review on Optimization Techniques

Pranesh B. Bamankar, Amol Chavan, (2015) Published a review study on the use of several optimization techniques for parametric optimization of MIG welding parameters. It was come to the conclusion from his review that there has been a lot of study done on Taguchi-based parametric optimization. Numerous researchers have employed a variety of methods, including regression analysis, grey analysis, surface response approach, and others. Numerous studies examined a range of response variables, including heat affected zone microstructure (HAZ), bead width, height, and depth of penetration. Future research may make use of genetic algorithms and ant colony optimization methods.

2.10 Review on Automated MIG Welding Process

The literature has extensively investigated automated MIG welding of different metals and steels. The use of automated technologies can raise production, enhance weld quality and uniformity, and reduce human error-related mistakes. To achieve good weld formation, careful consideration of process parameters such as welding current, welding speed, and wire feed rate is necessary when using automated MIG welding to join incompatible metals and steels.

According to a literature review published in the Journal of Materials Processing Technology by (Zhang et al., 2002), various factors such as joint design, filler metal, welding parameters such as voltage, current, and wire speed, shielding gas composition, and post-weld heat treatment all affect weld quality when automated MIG welding dissimilar metals and steels. The researchers discovered that selecting an appropriate filler metal with a composition close to or compatible with the base metals was important to establishing a robust welded junction. Furthermore, adopting an adequate pre-heating and cooling technique can aid in the reduction of distortion and improvement of the mechanical qualities of the welded connection.

Automation has also resulted in advances in sensing technologies for monitoring weld quality during automated MIG welding of dissimilar metals and steels. According to a research published in Welding Journal by (Wang et al., 2020) adding sensors such as acoustic emission, ultrasonic waves, thermocouples, or X-ray analysis can offer real-time monitoring of weld quality. This technique can give useful input on weld formation, allowing modifications to be made throughout the welding process.

To summarize, automated MIG welding is an efficient method for connecting different metals and steels. According to research, choosing the right factors, such as joint design, filler metal selection, welding settings, shielding gas composition, and heat treatment, may help assure high-quality welds. Sensing technology advancements have also enhanced weld quality monitoring during the welding process.

2.11 Studies on Different Welding Methods

Kutty et al., (2018) analyzed and optimized welding settings for metals of different compositions. The dissimilar welding between mild steel and stainless-steel SS 304 was effectively BUTT-joined using MIG welding and electric arc welding. The following can be said to sum up the investigation's findings: The welding process was significantly impacted by the welding voltage since higher voltage led to defects in all test samples, such as porosity and partial fusion, as well as a worse-looking weld joint. Successful completion of a butt-joint between mild steel and stainless-steel SS 304 was achieved using a MIG welding process. Due to the low amount of free carbon in the final product (welded stainless steel with mild steel), it has increased corrosion resistance, ductility, and strength. In MIG welded connections between dissimilar metals, the proportion of dilution in stainless steel is higher, which would explain why there is reduced corrosion resistance and chromium loss because to carbon precipitation in the joints. The dissimilar metal junction of mild steel and SS 304 exhibits a low ultimate tensile stress for both welding methods when mild steel-based electrodes are utilized. Voltages between 24 and 27 volts provide the greatest penetration. Lowering the voltage prevents the base metal from penetrating and fusing, while raising the voltage over 30V increases the chance of spattering. Based on the results of this investigation, it is reasonable to draw the conclusion that stainless steel filler ER309L and a welding voltage of 24-27 V are the ideal welding parameters for combining dissimilar metals like mild steel and stainless-steel SS 304. MIG Stronger than other sorts of samples are welded samples.

Gill and Pradhan, (2022) completed a review of the welding of different metals in the manufacture of car bodies. Recent developments in lightweight materials have given the automobile sector a new lease of life. For producers, combining these disparate materials is still difficult. The most promising steel-Al alloy, steel-Mg alloy, and Al Alloy-Mg alloy dissimilar pairings, as well as associated welding metallurgical problems, have been covered in detail in this study. Improvements in resistance spot welding and electric arc welding for the integration of several materials were found to be the most practical and cost-effective options because of their established infrastructures. The improvement of the weld quality of welds between dissimilar metals was shown to be significantly influenced by the decrease of intermetallic compounds. The number of intermetallic compounds and the growth of IMC layer thickness may be successfully reduced by controlling the heat input and the alloying components used for the filler metal. As a consequence, it is possible to greatly limit the occurrence of brittle IMCs and the weld zone's susceptibility to corrosion, hence enhancing the quality of the weld. Future important research issues will include choosing alloying elements for filler metals, base metals, and base metal coatings as well as optimizing welding process parameters for the least.

(Akinlabi et al., 2019) carried out a review on TIG and MIG Hybrid Welded Steel Joint. The assessment claims that despite the Hybrid TIG/MIG process's apparent advantages. The optimization of its process parameters is not well understood. Its procedures and uses are still limited. The majority of research concentrate on experimentally examining geometric features like tensile and hardness qualities. This welding technique hasn't been applied in the structural sectors to address fatigue and associated issues. There aren't many numerical analyses carried out. The hybrid's mechanical, metallurgical, and corrosion characteristics have not been properly studied. Data on thermal behavior and temperature dispersion are likewise in short supply. In order to confirm the findings using experimental data, additional study into TIG/MIG hybrid welds is necessary, as well as numerical modeling.

2.12 Research Gap

There is an important gap in terms of the optimal parameters and process conditions for automated MIG welding of stainless steel SS316 with low-alloy steel AISI4140. Despite its potential applications in industries like as marine, power production, chemical processing, and oil and gas. Experimentation and parametric optimization studies are required to discover the most effective welding settings that create high-quality and durable connections while limiting the danger of cracking and other flaws. More research was required to determine the effect of variables such as heat input, filler metal selection, preheating method, and cooling rate on the mechanical properties and microstructure of the weld, and this knowledge gap was leads to significant improvements in the efficiency and reliability of the welding process, allowing industries to meet their demanding structural requirements.

According to a review of these studies, a number of studies on austenitic stainless steels have been conducted. The research concentrated on a specific application, different grades of material, and the optimization of a single welding parameter. While they have the same chemical composition and large applications, no such focus was given to SS316 and low-alloy steel AISI 4140 by considering the effect of wire feed rate and gas flow rate during welding and optimization of weld quality for dissimilar metals. Finally, during welding dissimilar metals of stainless steel SS316 with low alloy steel AISI 4140 by MIG welding process, parameters such as welding current, welding speed, gas flow rate, and wire feed rate were considered, and The influence of parameters on mechanical properties, microstructural change, and corrosion resistivity at welded joints were also investigated and optimized using Taguchi Orthogonal array, signal to noise (S/N) ratio, and analysis of variance (ANOVA).

CHAPTER THREE

MATERIALS AND METHODOLOGY

3.1 Introduction

Following a review of the literature, some guidance and knowledge on the proper base materials and filler material selection, controlling process parameters, research and methodology, electrode wire, and welding conditions are now accessible. Due to variations in mechanical and chemical qualities, the use of stainless-steel SS 316 and low alloy steel AISI 4140 provides obstacles to the welding process. The approach for this study comprises the use of an automated Metal Inert Gas (MIG) welding procedure to combine stainless steel SS 316 with low alloy steel AISI 4140.

Welding parameters including current, welding speed, wire feed speed, and gas flow rate are changed within a set range. Experimentation and statistical analysis are then used to evaluate the weld quality, corrosion resistivity of weld joint and mechanical properties. To manage the welding conditions and assure uniformity in the final welds, an automated control panel is employed. Welding fixtures are utilized during the experiment to keep the materials in place and guarantee exact weld joint preparation. The resultant welds are then subjected to tensile strength, impact flexural bending test, and hardness testing to determine their appropriateness for practical applications. The results of these tests are examined statistically to determine the best set of welding settings for producing high-quality welds with minimal distortion.

3.2 Experiment Procedure (Methodology)

To meet the research goal outlined in chapter 1. The schematic diagram of the frame work of the applied techniques is shown in figure 3.1.

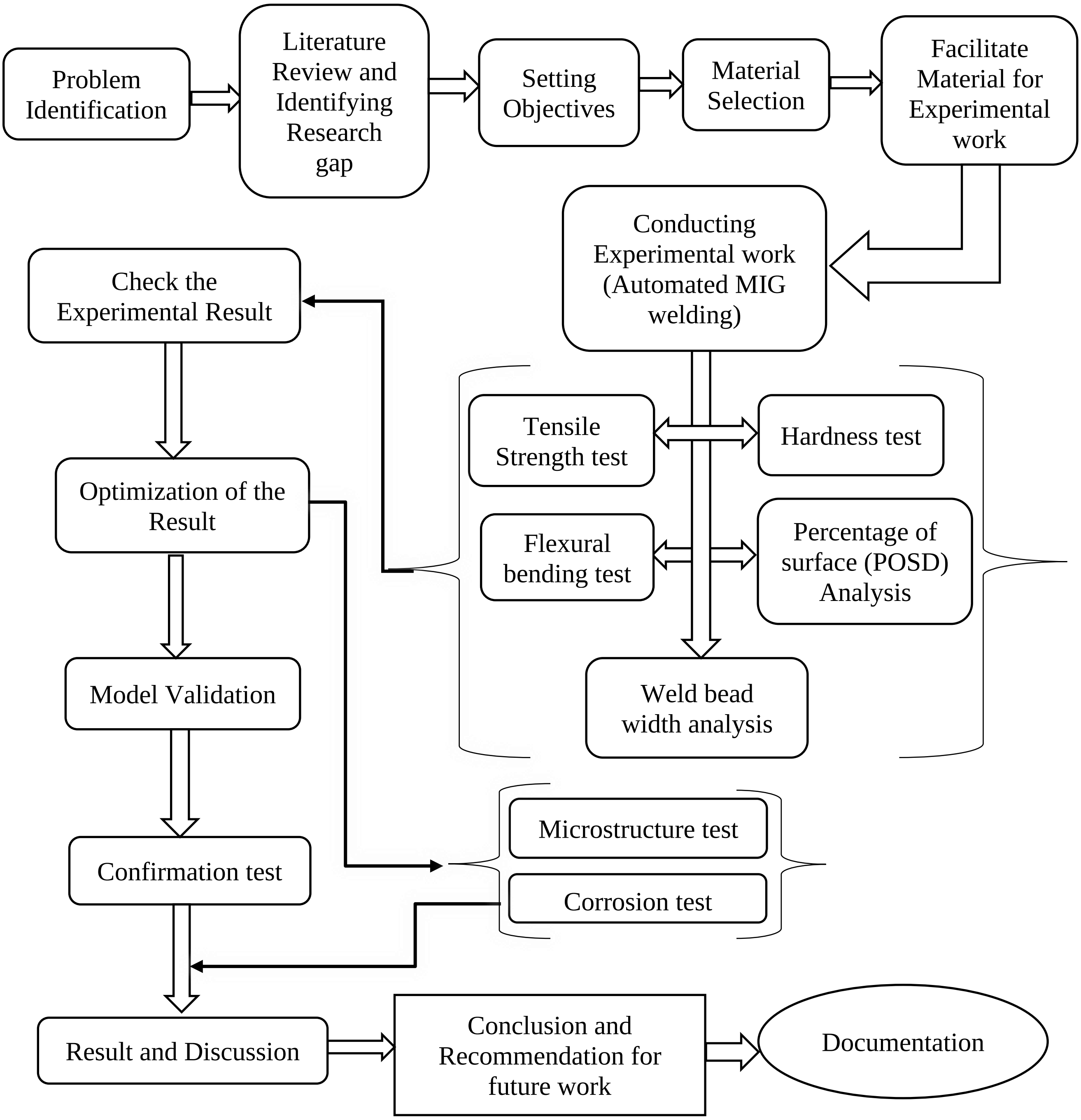

Figure 3.1: Flow chart for experimental work (research methodology)

3.3 Material Selection

The work-piece materials employed in this experiment were stainless steel (SS316) and low alloy steel (AISI4140).

3.3.1 Base Materials

3.3.1.1 SS316 Stainless Steel

Austenitic chromium-nickel stainless steel of type SS316 has a molybdenum content of 2% to 3%. Molybdenum increases both overall corrosion resistance and strength at high temperatures (Damian Kotecki, 2015). The only difference between this material and Type 304 is that it is stronger at higher temperatures. Examples of common uses include furnace parts, heat exchangers, jet engine parts, pharmaceutical and photographic equipment, valve and pump trim, chemical equipment, digesters, tanks, and evaporators, as well as pulp, paper, and textile processing equipment parts. (SS 316) (Stainles MakeItFrom, n.d.)

3.3.1.2 AISI 4140 Low alloy Steel

Low alloy AISI 4140 steel is made up of chromium, molybdenum, and manganese. Due to its durability, high fatigue strength, abrasion and impact resistance, and widespread application across many sectors, it is a great material option. The adaptability and utility of 4140 are unmatched by many grades. Chromium and molybdenum are added to increase corrosion resistance. Molybdenum can be especially helpful when attempting to stave against corrosion brought on by chlorides. Manganese is a deoxidizer and is used in AISI 4140 to promote hardenability. Manganese and sulfur can also mix in alloy steels to enhance machinability and enhance the carburizing process(Normalized 4140 Cr-Mo Steel MakeItFrom, n.d.). Low-alloy steel a versatile steel with many uses is AISI 4140. Due to its exceptional strength, hardness, and wear resistance, it is frequently utilized in the production of parts and components for the oil and gas, construction, automobile, aerospace, and automotive sectors.

3.3.2 Weldability of both materials

Due to differences in material composition, stainless steel SS316 and low alloy steel AISI 4140 have differing weldability properties. SS316 is frequently regarded as having excellent weldability, particularly when used with austenitic stainless steel filler metals. The production of chromium carbides at the grain boundaries, on the other hand, might result from excessive heating during the welding process and reduce the material's mechanical and corrosion resistant properties. To achieve an acceptable weld quality and performance, it may be necessary to adjust the heat input, inter-pass temperature, and post-weld heat treatment (PWHT). The weldability of AISI 4140 low alloy steel, in contrast, is significantly influenced by the material's specific heat treatment condition and the welding technique used. This material is susceptible to hydrogen cracking, which can occur when welding with specific filler metals and under specific welding conditions. These difficulties can be mitigated by preheating the base material, regulating the heat input, and employing low-hydrogen filler metals (Reddy et al., 2014).

When welding SS316 and AISI 4140 together, it is critical to examine each material's weldability properties and use appropriate welding procedures and filler materials. Depending on the application requirements and material thicknesses, welding methods such as Gas Tungsten Arc Welding (GTAW), Gas Metal Arc Welding (GMAW), or Submerged Arc Welding (SAW) can be used to join these materials. The selection of appropriate filler metals is critical, with corrosion resistance, mechanical qualities, and compatibility with the materials being connected all being considered. To summarize, with the proper welding techniques and processes, both SS316 and AISI 4140 can be effectively welded. To create a high-quality weld connection, considerable consideration must be paid to their particular weldability properties while welding them together (*ASM International*, n.d.).

3.3.2.1 Chemical composition the of base and filler wire metals

Composition of the steel will always be an issue of compromise. Obtaining optimum weldability and hardness can be expensive, however making a little concession in those areas might reduce the cost. The elements and their effects on weldability and other properties of the metals are listed in table 3.1, 3.2, and 3.3 below.

Carbon (C): The most significant alloying component of steel is carbon, which may be found in amounts as high as 2% (though most welded steels contain less than 0.5%). Iron may have carbon either dissolved in it or mixed with it to produce compounds like iron carbide (Fe3C). Hardness, tensile strength, and the capacity to respond to heat treatment (hardenability) all increase with increasing carbon content. On the other side, greater carbon levels decrease weldability (Gandy, 2007).

Molybdenum (Mo): The typical concentration of this element, a potent carbide forming, in alloy steels is less than 1.0%. The addition of this substance boosts temperature strength and hardenability (Gandy, 2007).

Manganese (Mn): Steels typically include at least 0.3% manganese, which has three functions: it helps the steel deoxidize, avoids the production of iron sulfide inclusions, and encourages increased strength by making the steel more hardenable. Carbon steels often contain up to 1.5% of this element (Gandy, 2007).

Nickel (Ni): Austenitic steels that are resistant to corrosion and heat are manufactured with nickel that is over 8% weight and a lot of chromium. Steel's strength and resistance to corrosion are improved. Nickel is added in modest amounts to low alloy steels to increase their strength. (Maalekian, 2007).

Chromium (Cr): In steel, chromium is a potent alloying component. It is added for two main reasons: first, it dramatically increases steel's capacity to be hardened; second, it significantly boosts iron and steel's ability to resist corrosion in oxidizing conditions. Due to its presence in some steels, the weld and the area around it may become too hard and break. More than 12% of chromium is found in stainless steel (Gandy, 2007).

Silicon (Si): When silicon is employed as a deoxidizer, it often only occurs in trace levels in rolled steel (0.2%, for instance). On the other hand, 0.35-1.0% is typical in steel castings. Iron tends to get stronger when silicon dissolves in it. As a deoxidizer, silicon is typically present in weld metal at a level of 0.5%. For improved de-oxidation and cleaning when welding on polluted surfaces, some filler metals can include up to 1.0%. The final weld metal strength will be noticeably higher when these filler metals are employed for welding clean surfaces. In rare circumstances, cracking issues might be caused by the ensuing reduction in ductility (Gandy, 2007).

Phosphorus (P): Modern steels are routinely managed to have phosphorus levels below 0.030 percent of weight. Strength and hardness are reduced while toughness and ductility are increased. Phosphorus can make some steels more machinable, but at concentrations over 0.04 percent weight, it can make welds brittle and more prone to fracture. (Sulphide and Sulphide, 2015); (Spolenak et al., 1998)

Sulfur (S): Instead, then being an alloying element, this is an unwanted contaminant in steel. When producing steel, extra care is taken to reduce or remove sulfur. It usually results in brittleness and decreases weldability at concentrations greater than 0.05%. Sulfur additions between 0.1% and 0.3% will often worsen weldability while tending to increase steel's machinability. These steel varieties can be described as free-machining (Gandy, 2007).

The chemical composition of the base and weld metals were performed at Ethiopian Quality and Standard Agency using SPECTROMAXx LMX10 ARC/SPARK spectrometer features a single air optic, with CMOS sensors. It extends the relevant and applicable elemental wavelength range from 233 to 670 nm. SPECTROMAXx has been designed to identify all the key elements in metals, including carbon and other light elements as shown in table 3.1.

Figure 3.2 below shows the tested samples under spectroscopy. Recognizing that carbon identification is of primary concern in all material verification functions, especially welding, (Oxford instruments, 2007).

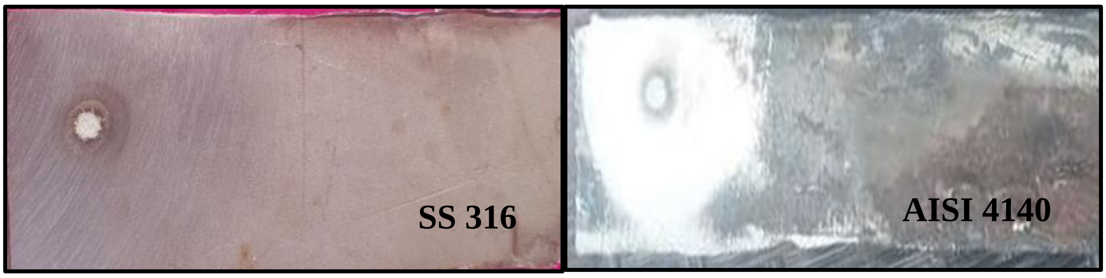

Figure 3.2: Samples for chemical composition after testing

Table 3.1: The chemical composition of base metals (Ruiz-Trabolsi et al., 2022) and (Bharath et al., 2014)

Materials		Chemical composition (wt. %)									
Elements		C	Mn	P	S	Si	Cr	Ni	Mo	N	Fe
Base metals	SS316	0.08	1.95	0.045	0.03	0.70	18	12.06	2.40	0.10	65.18
	AISI4140	0.39	0.93	0.025	0.031	0.33	1.12	0.17	0.18	-	96.82

Table 3.2: Chemical composition of electrode wire (Garcia et al., 2020)

Materials		Chemical composition (wt. %)									
Elements		C	Mn	P	S	Si	Cr	Ni	Mo	N	Fe
Wire type	ER-309L	0.03	1.75	0.04	0.03	0.40	23.50	13.20	0.75	-	60.30

Table 3.3: Mechanical properties of SS316 and AISI4140

Mechanical properties	Value	Value
	SS 316	**AISI 4140**
Ultimate tensile strength	579MPa	655MPa
Yield strength	290MPa	415MPa
Percentage elongation (in 50mm)	50%	25.70%
Rockwell hardness B	79HRB	92HRB
Mean Coefficient of thermal expansion(0-649°C)	(18.5) µm/m*K	12.2µm/m°C
Thermal conductivity (@100°C)	22.3W/mK	42.6W/mK

3.3.3 Material used for Filler

ER-309L stainless steel filler material with diameter 1.2mm was employed as filler material as shown in figure 3.3 below.

ER-309L: Austenitic stainless steel 309L is used to join stainless steel sheets from the 300 series, including 309, 309L, 304, 316, and others. Excellent for buttered passes on steel overlay work, joining stainless steel to mild or carbon steels, and welding austenitic clad stainless steel to mild or carbon steels. The weld deposit is more resistant to inter-granular corrosion caused by carbide precipitation, which may happen if using straight 309 grade, because to the lower carbon content (L). (Erl and Carolina, n.d.).

Figure 3.3: 309L stainless steel wire

Shielding gas used: Argon gas, especially pure argon, is best for keeping an arc stable. Argon facilitates a smaller penetration, which results in a cleaner weld. Process metals are heated to temperatures of more than 7000 degrees during the welding process. Most metals become liquid at these temperatures, enabling the creation of the weld. Argon is used to shield the molten metal from atmospheric components including oxygen, nitrogen, and hydrogen.

Fixed Welding Parameters

Welding voltage: Depending on the material being welded and the choice of shielding gas, several welding voltage ranges are available for MIG welding. As a general rule, the MIG welding voltage range falls between 16 and 22 volts (Nadzam et al., 2014). Due to the fact that welding voltage was not chosen as a process parameter for optimization in this experiment, a best value welding voltage of 20V was chosen by taking into account the aforementioned criteria and the trial exercise.

Arc length: A high-quality weld bead must be produced during MIG welding by maintaining an optimum arc length. The majority of industry professionals advise choosing an arc length for MIG welding that is between 9.5mm and 13mm, or about the diameter of the electrode being used (Catalogue, n.d.). The type and thickness of the material being welded, the welding location, the wire diameter, and the feed rate are all critical aspects as well. Because MIG welding is automated in this experiment, it is easy to set the arc length, and 11mm is chosen as the arc length.

Root gap: The distance between the two metal parts that need to be linked before welding is referred to as the root gap in MIG welding. Depending on the thickness of the material being welded, the welding location, and the type of joint being utilized, the appropriate root gap size for a MIG welding joint may change. After taking those factors into account and doing a trial exercise, the optimal welding penetration was found to be 1.2mm. This root gap is chosen for this experiment.

Work angle or travel angle: Depending on the thickness of the base metal and the welding position, the ideal welding gun or work angle must be chosen. Work angle is "the angle between the electrode's axis and the welder's work piece." The term "travel angle" describes the use of either a push angle (pointing in the direction of movement) or a drag angle (pointing in the opposite direction of motion). The welding operator should hold the MIG welding gun at a 90-degree work angle (relative to the work piece) when welding a butt joint, which is a 180-degree junction (Tregaskiss and Bernard, n.d.). The integrated automated MIG welding machines used in this experiment has a welding gun holder with a work angle arrangement that is simple to adjust to the necessary angle value. For this experiment, the welding gun angle is adjusted at **90 degrees** to the base metals in figure 3.4 below.

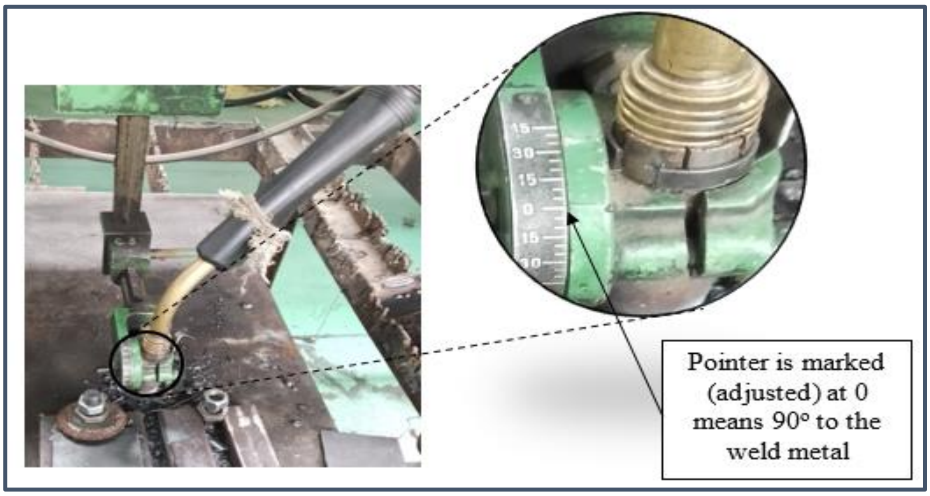

Figure 3.4: Adjustment of welding gun angle

Metal thickness: 3mm (Bharath et al., 2014) and (Assefa et al., 2022)

3.4 Sample preparation, Experimental setup, and Welding situations

Experiments have been conducted at the Manufacturing Technology and Engineering Industry Research and Development Center at the welding training center work shop on the FIMER standard TM 350 MIG welding machine integrated with welding gun fixture (carriage) machine that facilitates the automatic MIG welding process, as shown in Figure 3.7 below.

3.4.1 Basic Equipment of Automated MIG Welding

The basic MIG welding equipment consists of the following components:

- Power source
- Welding Gun
- Gas cylinders with pressure-reducing valve and flow meter
- Wire feeder unit
- Welding gun carriage with control panel
- Welding fixture

These equipment's are shown in the figure 3.5 and working principle of MIG in figure 3.6.

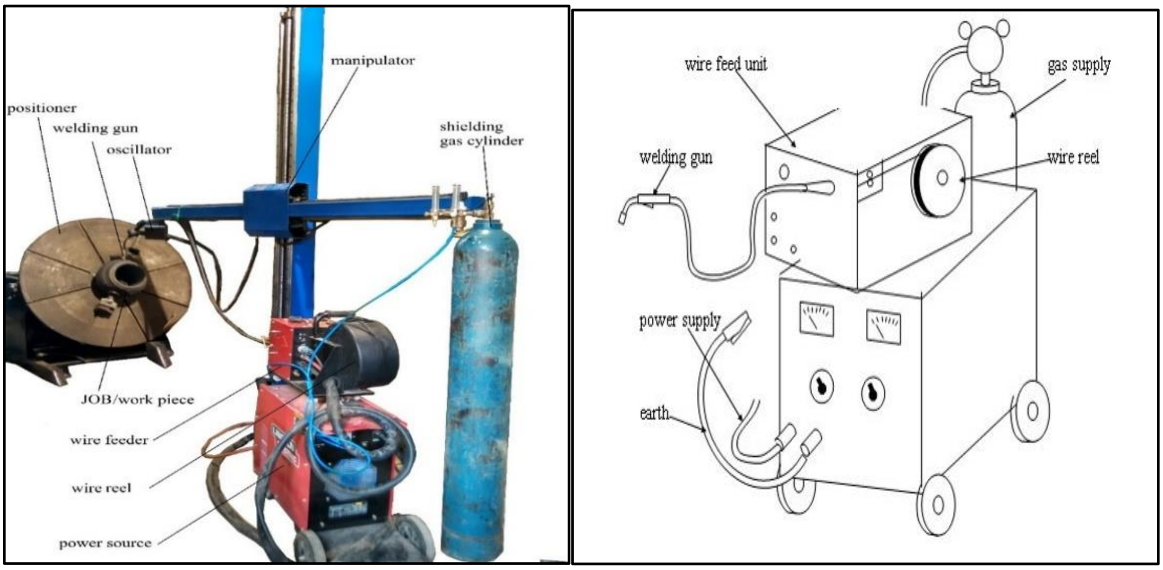

Figure 3.5: Figure of GMAW Machine (Ethan Bale, 2022)

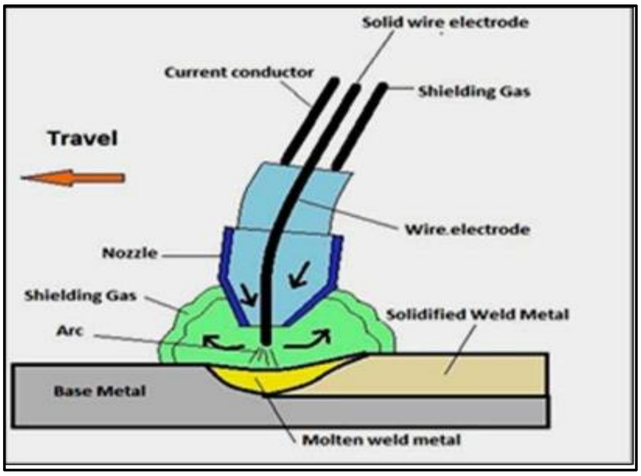

Figure 3.6: Working principles of MIG welding (Singh and Goyal, 2017)

Automatic MIG welding is a technique that may be used to regulate welding speed and produce welds that are more uniform. When MIG welding is done automatically, a machine may handle any or all of the welding tasks. Even though a human operator still prepares and positions the weld joint, the MIG gun is frequently installed on a welding gun fixture or welding carriage that is managed by a control panel or adjustment board. Automatic MIG welding has the ability to make welds more quickly and consistently than semi-automatic welding, which is one of its main advantages. The control panel knobs can be used to set the exact speed at which the electrode wire should be fed, ensuring that every weld is completed at the same rate. Automatic MIG welding can also include additional features such as adaptive control, which monitors and adjusts the weld in real-time as conditions change. This can help ensure that the weld remains consistent even if environmental factors such as humidity or temperature fluctuate during the welding process. Overall, automatic MIG welding systems are best suited for high-volume production environments where precision and speed are critical. However, they do require more specialized equipment and training than semi-automatic welding systems.

In this experiment, automatic welding mechanism is used because semi-automatic welding with a MIG welding equipment has its limitations. The gun moves at an assigned rate during automatic operation, which helps to regulate and establish the welding speed. The human respiratory system causes vibration in the hand when using a hand-moving gun, which causes the arc length to change while welding. Both the voltage and current of the operation change simultaneously when the arc length does. It is essential for the operator to pick the welding parameters, such as welding current and voltage, in accordance with the Taguchi design orthogonal array, and to control the arc length and welding speed in order to improve the quality of continuous welding. In order to take welding speed into consideration as one of the welding parameters, adopting automatic MIG welding was ultimately more beneficial than manual MIG welding.

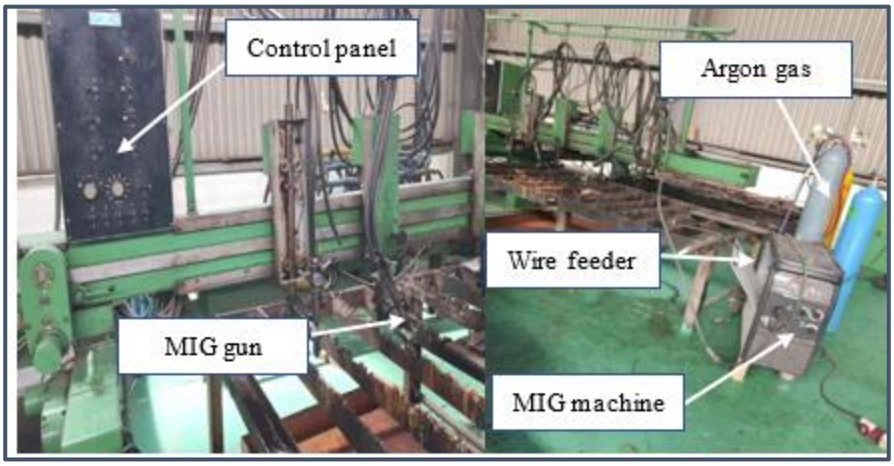

Figure 3.7: Automatic MIG welding machine (MIDI, Addis Ababa, Ethiopia)

Welding fixtures are utilized in this experiment to help manage the root gap of welding and eventually improve the weld quality. Welding fixtures can aid in preserving a constant root gap during the welding process by holding the sample firmly in place and ensuring that they are straight. This is crucial since the root gap may have an impact on the weld's penetration, strength, and general integrity. Welding fixtures are made to accommodate particular sizes and shapes of workpieces. With a predetermined root spacing, the fixture can be adjusted to keep the parts in place as shown in figure 3.8. This guarantees that before welding, each workpiece will keep a constant distance from the others. The final weld will be of higher overall quality and more constant penetration.

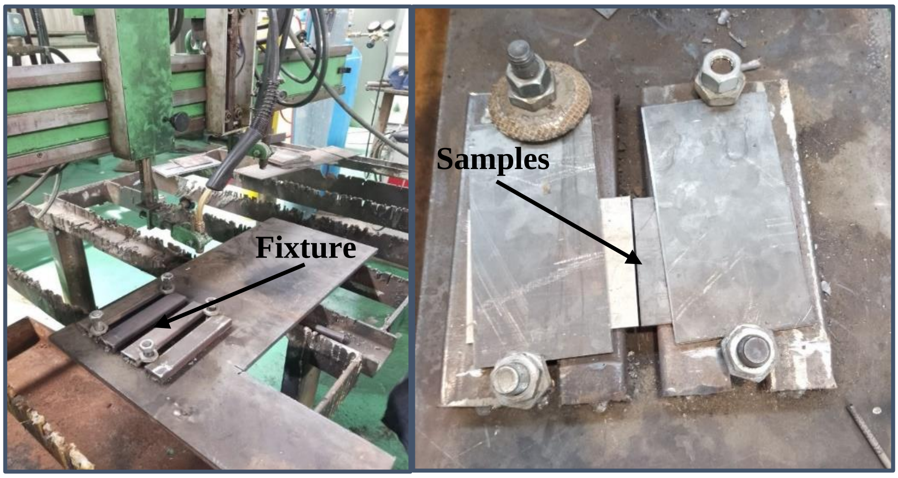

Figure 3.8: Sample holding fixture

3.4.2 Preparation of the sample and Experimental Condition

Stainless and low alloy steel sheets with dimensions of 100 mm x 75 mm x 3 mm were created using an E21S ESTUN shear cutting machine, as shown in Figure 3.7. Before welding, the edges of the work components were properly prepped. Dust was cleaned from the edges and the area around them using a wire brush. Table 3.4 displays the process variables and levels applied in this investigation. According to Taguchi's Design of Experiments, and by taking into account welding current, wire feed rate, gas flow rate, and welding speed at three levels, all of which were obtained from the L9 orthogonal array. The experiment's L9 orthogonal array is displayed in Table 3.5.

The welding process parameters and their levels are chosen according to the general approach, which entails conducting a review of the literature (Assefa et al., 2022), (Sapakal, 2017) and (Wahule and Wasankar, 2018) and trial exercises to establish the best parameters based on elements such material thickness, joint geometry, desired weld quality, and equipment accessibility. To find the settings that produce the desired outcomes in terms of weld quality and efficiency, trial exercises involve testing several parameter combinations on actual work-pieces. These levels of welding process parameters are chosen by integrating the knowledge gained from the literature review and trial activities in workshop.

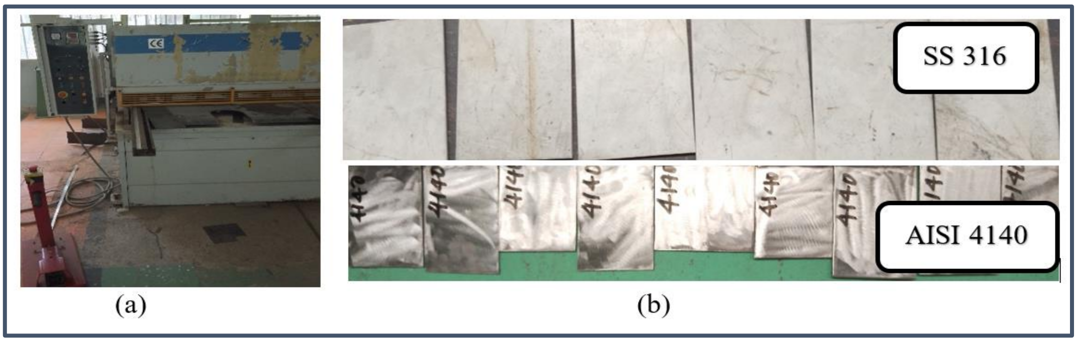

Figure 3.9: preparation of the samples: (a) shear cutting machine (at ASTU) (b) stainless steels and low alloy steels prepared

Table 3.4: Process parameters and their levels

			Levels		
S. No	**Process parameter**	**Units**	**1**	**2**	**3**
1	Welding current	Amp (A)	110	125	140
2	Wire feed rate	cm/s	7	10.5	14
3	Gas flow rate	CFH	7	9	11
4	Welding speed	cm/min	20	30	40

Table 3.5: L9 Orthogonal array developed

No of Experiments	**Control factors and levels**			
	Welding current	Wire feed rate	Gas flow rate	Welding speed
1	110	7	7	20
2	110	10.5	9	30
3	110	14	11	40
4	125	7	9	40
5	125	10.5	11	20
6	125	14	7	30
7	140	7	11	30
8	140	10.5	7	40
9	140	14	9	20

3.4.3 Experimental Welding set up

As indicated in Figure 4, the welding setup consists of the following components: MIG welding machine Current and voltage are given during welding. Gas cylinder used for gas purging: In order to establish an inert environment and maintain a steady arc, argon gas is used in this procedure and is delivered into the welding flame at a specific flow rate. Work holding table: A cast iron surface plate on which a work piece is fixed so that the welding gap between the work piece and the stainless-steel wire electrode is maintained at 1mm. welding gun carriage: utilized to adjust the arc length and welding gun angle to the ideal values for welding 3mm material thickness, which is 6mm and 90^{o} correspondingly, then move the gun of the MIG welding machine at the specified speed. However, according to nine possibilities of data from the L9 OA, the welding current, wire feed rate, gas flow rate, and welding speed varied for each test. Figure 3.10 depicts the samples after welding.

Figure 3.10: samples after welded

3.5 Weld Bead Width Geometry

The main factor affecting the quality of a MIG weld is the weld bead's geometry. Bead geometry is significantly influenced by welding process variables such welding current, shielding gas flow rate, welding speed, wire feed rate, and gap distance. The mechanical qualities of the weld are determined by factors including the heat-affected zone, bead width, bead height, penetration, and region of penetration as well as its tensile strength, hardness, and bending strength (Esme et al., 2009). With 0.01 mm least count Vernier calipers, the width of each welded sample was measured in order to calculate the bead width.

The ideal weld bead size for a given application can vary depending on a number of variables, including the base metal's thickness and composition, the joint design, and the intended use of the welded product. In general, the optimal weld bead size should be sufficient in size to guarantee strong joint penetration and low heat input while also reducing deformation and material waste. A thin weld bead may suggest that the weld has not gotten deep enough into the base metal, which would reduce the strength of the connection and raise the possibility of weld flaws. On the other hand, a large weld bead could require too much heat or cause unintended distortion in the base metal. Therefore, determining the ideal weld bead size requires balancing process variables to accomplish optimum penetration and fusion while reducing heat input and distortion. The weld bead can be made just right for the particular purpose by using the proper technique and equipment setup.

Because each welded specimen's width varied based on the factors used, the weld with the shortest bead width was deemed to be a good weld because, when there was enough welding penetration, it generated a smaller heat-affected zone. Figure 3.11 shows the weld's bead width.

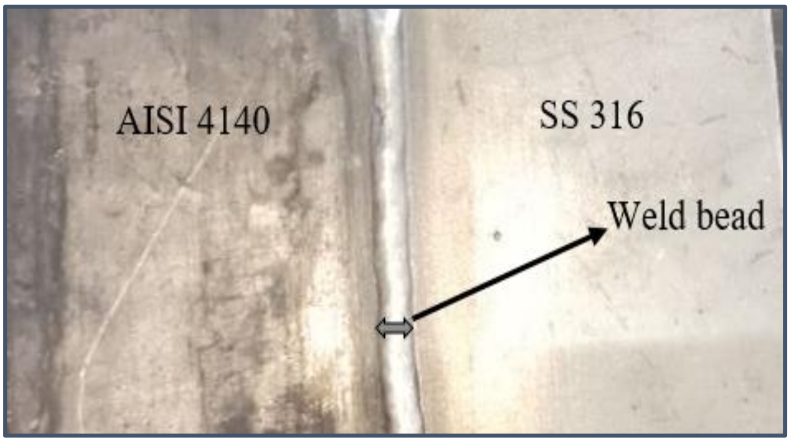

Figure 3.11: Weld bead

3.6 Welding defects Acceptance Criteria

The acceptability criteria for defects in welding such as slag, excessive reinforcing, porosity, lack of fusion, fractures, and so on are described in AWS D1.1/D1.1M:2020 and ASME Section VIII. These criteria are based on elements such as the size, position, and direction of the faults. The maximum allowed lengths for each type of fault are as follows: According to AWS D1.1/D1.1M:2020, cracks should not exceed 3mm (1/8 in), porosity should not exceed 5% of total area in a 100 mm (4 in) length of weld or 1% in a 25 mm (1 in) length of weld, lack of fusion should not exceed 3mm (1/8 in) in a single pass weld, lack of fusion should not exceed 3mm (1/8 in) in a single pass weld, slag inclusions should not exceed a depth of 3mm (1/8 in) or width of 6mm (1/4 in), and Excessive reinforcement (type of welding defect that occurs when the weld metal is deposited in excess of the required amount) and it can be determined by measuring the weld cross-section and comparing it to the required dimensions. Excessive reinforcement should not be more than three times the thickness of the base metal or 19mm (3/4 in), whichever is less. ASME Section VIII also specifies defects limitations, which may differ somewhat from those defined in AWS D1.1/D1.1M:2020 depending on the application and needs (American National Standard Structural Welding, 2020).

The acceptance criteria for surface defects in welding that allows a maximum percentage of defects of less than 5% is typically specified in welding standards and codes such as ISO 5817:2014, AWS D1.1/D1.1M:2020, and ASME Section VIII. The percentage of surface are calculated by the ratio of the sum of area of surface defects to total surface area of welded zone (weld bead).

$$\text{POSD} = \frac{\sum Ad}{Aw} \text{x100\%} \tag{3.1}$$

Where A_d = area of each surface defects and A_w = surface area of weld zone

3.7 Welding Defects Using Non-Destructive Testing (NDT)

Manufacturing, construction, and other industries that rely on welded connections frequently experience welding defects. These defects may jeopardize the joint's structural integrity and cause failures, which might be harmful in applications like pipelines, pressure vessels, ships, and bridges. Non-destructive testing (NDT) techniques offer a way to find defects in welding without causing damage to the welded connection, enabling prompt diagnosis and remedial action. In this study, this study was investigated the application of NDT techniques, particularly liquid penetrant testing (LPT) and liquid fluorescent testing (LFT), to detect and classify welding flaws. The many types of welding flaws, their causes, and the factors influencing their occurrence were also covered. After test is operated and type of defects are identified by visual inspection method and then the length of these defects are measured as shown in figure 3.12 below for further analysis.

Figure 3.12: Surface defect measurement after LPT

3.7.1 Liquid Penetrant Test (LPT)

Liquid Penetrant Testing (LPT) is a non-destructive testing method used to locate surface breaking discontinuities in a wide range of materials, including metals, polymers, and ceramics. It entails putting a liquid penetrant to the surface of the material, letting it to seep into small gaps and fractures, and then removing the surplus penetrant before applying a developer that pulls the penetrant out of the surface. LPT has several applications in areas such as aerospace, automotive, and manufacturing. It is especially effective for identifying surface cracks, porosity, laps, seams, and other defects that might compromise the integrity of a material or component. During manufacturing or maintenance, LPT is commonly used to examine welds, castings, forgings, and machined components.

The process of conducting an LPT typically involves several steps. First, the surface to be inspected is cleaned and dried thoroughly to remove dirt, grease, or other contaminants that might interfere with the test results. Then, the penetrant is applied over the entire surface using spray bottle, brush or by dipping. After a certain amount of time given in the manufacturer's instructions has elapsed (10minutes). The next step is applying a dry cloth or rag to remove any excess penetrant from the surface. This process also aids in the removal of any non-penetrated liquid on the surface, which might cause misleading signals during developer application. Then, depending on the application needs, a developer is applied to the surface such that the penetrant begins to migrate out, revealing defects wherever there are traces of penetrant. Finally, any faults discovered are reported, and the part/component can be evaluated further. Figures 3.13 below shows all processes and defects found.

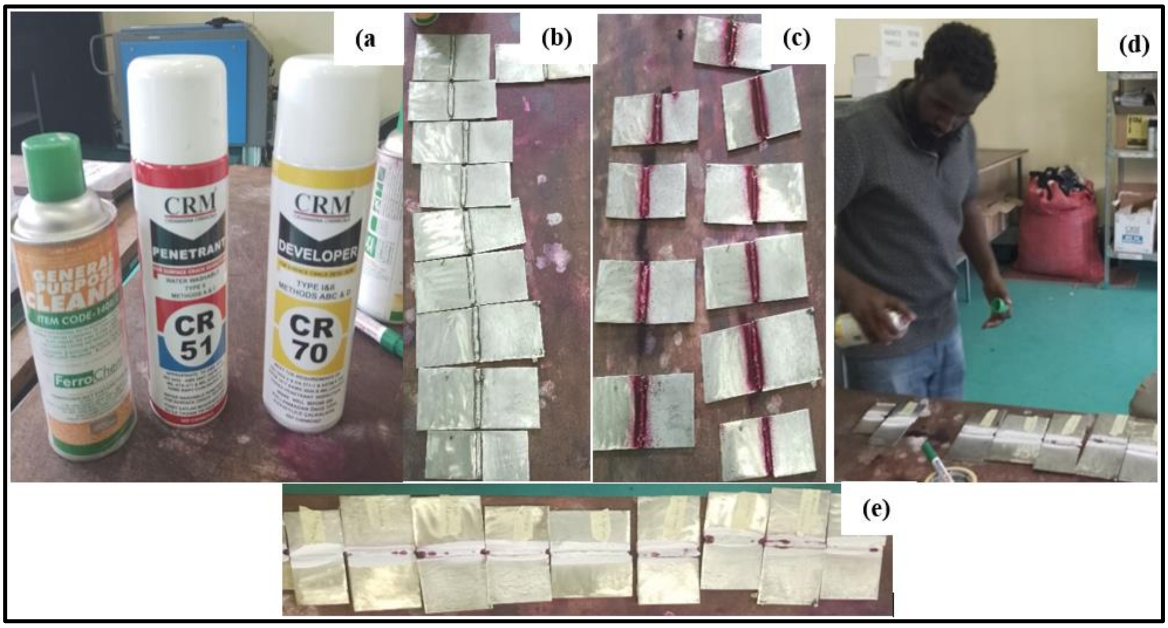

Figure 3.13: PT process: a) cleaner, penetrant and developer chemicals b) pre cleaned samples by using general purpose cleaner c) the use of penetrant fluids d) the use of developer e) examination of the test surface

3.7.2 Liquid Fluorescent Test (LFT)

The Liquid Fluorescent Test (LFT) is a sophisticated Non-Destructive Testing (NDT) method that is widely used to detect flaws in metals. It works on the same principles as LPT, with a liquid penetrant applied to the material's surface. LFT, on the other hand, employs a fluorescent penetrant that fluoresces under UV light, allowing it to identify extremely tiny defects and crack discontinuities. The procedure for doing an LFT begins with surface preparation, which includes eliminating any residues of oil or grease that may function as barriers to the penetrant. The surface is then sprayed or coated with a luminous liquid penetrant. After a certain amount of time (10 minutes), the surplus penetrant is removed with a cloth or rag. After removing any surplus penetrant from the surface, it is washed with an emulsifier to pull out any residual penetrant. The technician will utilize a black light illuminator to highlight any fluorescing indications on the surface under proper lighting circumstances. This aids in identifying possible cracks and indicators, which may then be documented and investigated further. Figures 3.14 below shows all processes and defects found.

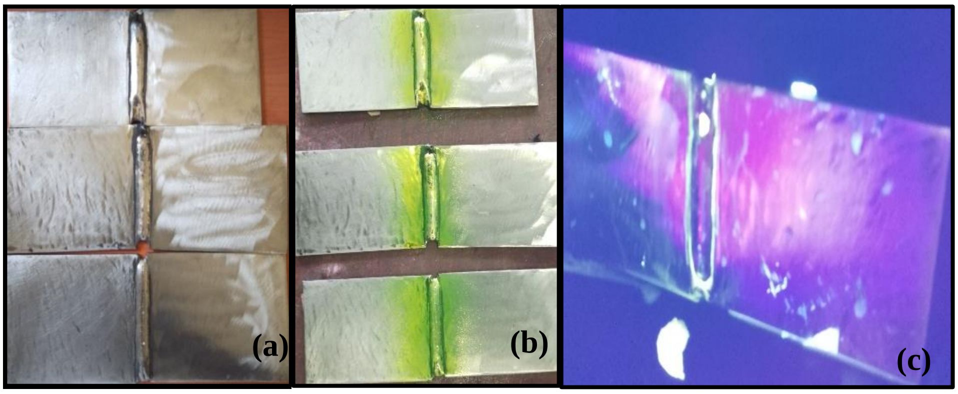

Figure 3.14: LFT processes: (a) pre-cleaning selected samples no. 3, 7, and 8 by using water and dry it; (b) sprayed samples by penetrant for segregation; (c) application of applying UV light to inspect weld surface.

3.8 Corrosion Test

Corrosion tests were performed by immersing the specimens in a 3% NaCl solution for 2 hours. The specimens for the testing were 8mm in width and 8mm in length. To eliminate any stray markings from the surface of the specimen and make it mirror polished, composite specimens were polished with emery polishing paper 800 no. and then with 12 µm diamond paste on a double disc polishing machine. An electrochemical analyzer (SP300 EC-LAB, Biologic Science Instruments, ASTU, Material science laboratory) was used to perform the electrochemical measurements in a three-electrode cell as shown in the figure 3.15 below. Tafel curves were generated by automatically adjusting the electrode potential from -250 to +250 mV versus corrosion potential (Ecorr) at a scan rate of 1mVs-1. Experiments were carried out to investigate the influence of weld zone, both heats affected zone, and both base metal of automated MIG welded optimum sample.

Mani et al., (2018) reports that the welding of dissimilar metals might occasionally result in the creation of an interphase between the different zones, which can impact corrosion. Tafel polarization curves include electrochemical characteristics such as corrosion potential (Ecorr), corrosion current density (Icorr), corrosion rate (Cr), and corrosion protection effectiveness (p). The anodic and cathodic areas of Tafel plots were used to calculate corrosion potential (Ecorr) and corrosion current density (Icorr).

$$\text{Corrosion rate in } mpy \text{ (CR)} = \frac{C.EwIcorr}{d} \quad (3.2)$$

Where C is the conversion constant (0.123), Ew is the equivalent weight of the specimen (g), d is the density of the specimen (g/cm^3).

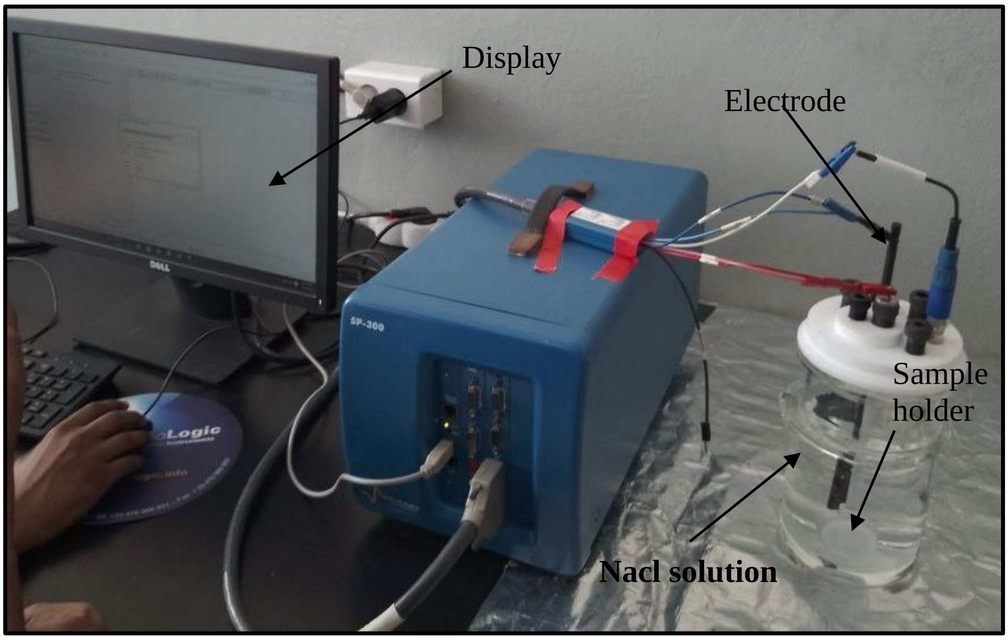

Figure 3.15: Corrosion test operation setup with potentiator

3.9 Mechanical Property Testing

MIG-welded experimental specimens made of SS316 and AISI4140 were manufactured for different mechanical tests and machined in line with ASTM standards to establish the necessary dimensions for assessing their characteristics.

3.9.1 Tensile Strength

Tensile testing is a mechanical test that determines how much stress a material can bear before it permanently breaks or deforms. The test involves applying a steadily increasing load to a sample of the material until it fails and measuring the ensuing changes in length or cross-sectional area of the sample. This test aids in determining critical mechanical properties of materials such as ultimate tensile strength, yield strength, and ductility, which are vital for designing and selecting materials for engineering applications. For conducting Tensile test Universal testing machine, a max force of 50 KN; at Adama Science and Technology University. The specimen dimensions are prepared according to ASTM E8/E8M Standard shown in table 3.16 below.

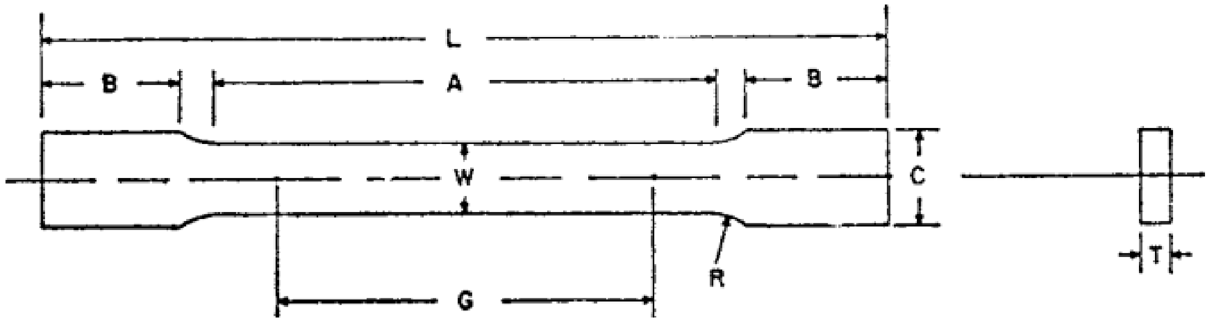

Figure 3.16: Specimen geometry for tensile test (American Association ASTM E8/E8M, 2013)

Table 3.6: ASTM Specimen standard for tensile test (American Association ASTM E8/E8M, 2013)

	Dimensions		
	Standard Specimens		Subsize Specimen
	Plate-Type, 40 mm [0.500 in.] Wide	Sheet-Type, 12.5 mm [1.500 in.] Wide	6 mm [0.250 in.] Wide
	mm [in.]	mm [in.]	mm [in.]
G— Gauge length	200.0 ± 0.2	50.0 ± 0.1	25.0 ± 0.1
	[8.00 ± 0.01]	[2.000 ± 0.005]	[1.000 ± 0.003]
W— Width	40.0 ± 2.0	12.5 ± 0.2	6.0 ± 0.1
	[1.500 ± 0.125, -0.250]	[0.500 ± 0.010]	[0.250 ± 0.005]
T— Thickness		thickness of material	
R— Radius of fillet, min	25 [1]	12.5 [0.500]	6 [0.250]
L— Overall length, min	450 [18]	200 [8]	100 [4]
A— Length of reduced section, min	225 [9]	57 [2.25]	32 [1.25]
B— Length of grip section, min	75 [3]	50 [2]	30 [1.25]
C— Width of grip section, approximate	50 [2]	20 [0.750]	10 [0.375]

The overall length should be as long as the material will allow, up to 200 mm [8.00 in.], to help with applying axial force when testing specimens that are 6-mm [0.250-in.] wide in accordance with ASTM E8/E8M standards (American Association ASTM E8/E8M, 2013). This requires a minimum overall length of 100mm, hence a 120mm overall length is used in this study as shown in figure 3.17 below.

Figure 3.17: Measurement of tensile specimen

Figure 3.18 a–d displays the tensile specimen, the welding setup, and the broke specimens following the tensile test, in that order.

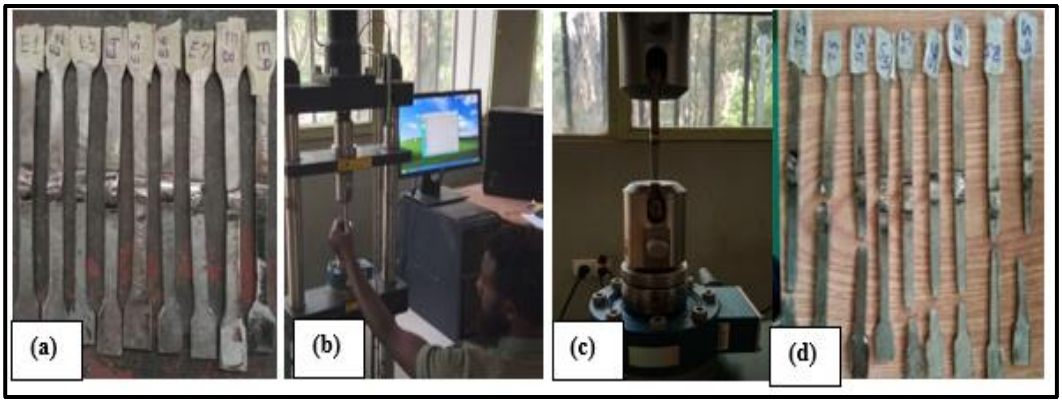

Figure 3.18: Specimen prepared for tensile strength, (a) Tensile Specimens (b) set-up, and (c) fractured specimen after force applied (d) fractured specimens (at Adama Science and Technology University)

3.9.2 Hardness Testing

In calibrated hardness testing equipment, the hardness of a weldment or welded specimen is determined by applying a specified force to a flat surface of the weldment or welded specimen, then measuring the size of the indentation that results (AWS committee, 2000). The three most common hardness tests are the Vickers, Brinell, and Rockwell tests. Hardness testing was carried out at the material engineering laboratory of Adama Science and Technology University utilizing a Vickers hardness testing equipment. Each specimen was subjected to a Vickers hardness test. The resulting impression was measured and analyzed under a microscope before being converted into a hardness number (Hultquist & Leygraf, 1980). The samples were sectioned for hardness testing using an abrasive cutter as shown in the figure 3.19.

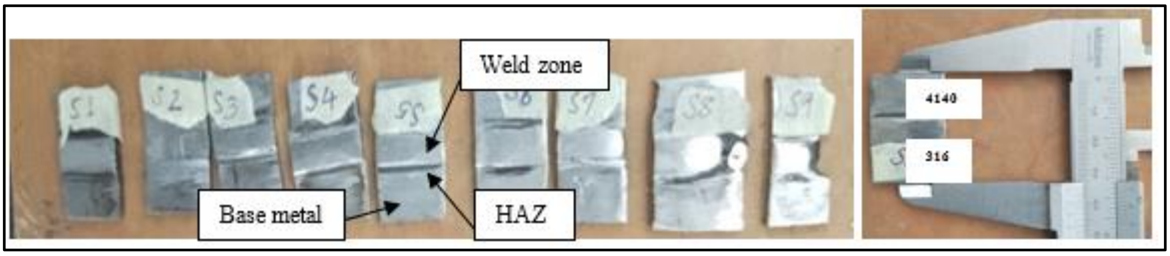

Figure 3.19: Specimens prepared for hardness test

3.9.3 Flexural Testing

The maximum stress tolerance of a material is measured by its flexural strength, which is a force (measured in newton) per unit area (Johnson, 2022). A common technique for assessing the flexural strength of a material is the four-point flexural bending test and utilized for this study.

Comparing the four-point bending test to the three-point flexural bending test, there are a number of benefits. In contrast to the three-point bending test, which concentrates the stress at two locations, it distributes the strain across a larger region, giving a more accurate picture of the material's flexural capabilities. Second, it decreases shear loads and lowers the risk of failure at the support points, improving test results. Finally, calculations are made simpler since the stress calculation formula for the four-point bending test is simpler than the one for the three-point bending test. Overall, the four-point bending test is a more reliable and accurate testing procedure for determining a material's flexural capabilities (Hein & Brancheriau, 2018).

Four-point bending or flexural tests (ASTM D 6272) standard were performed on a total of nine welded specimens using UTM with 50 KN load cell (Ribeiro, 2013). The thicknesses t = 3 mm and Overall length of 120mm as shown in figure 3.20 below and figure 3.21 illustrates the specimen before and after test.

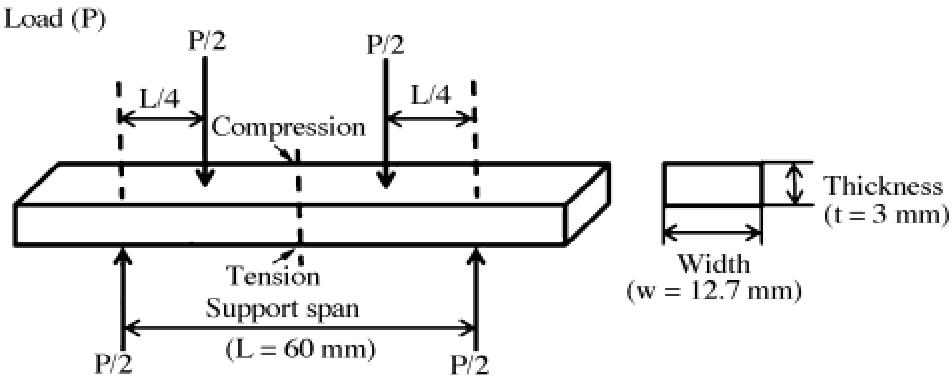

Figure 3.20: Specimen geometry of flexural test (Ribeiro, 2013)

Flexural test performed at Adama Science and Technology University. Follow these procedures to run this test: first, to get accurate findings, cut a rectangular bar-shaped sample out of the material, making sure that the length is at least four times the breadth. The samples dimensions with 3mm x 13mm x 120mm are prepared as shown in figure 3.16 below. Second, position the sample on two lower supports with the standard-recommended distance (L) between them. Utilize two top loading points that are more closely spaced apart than the bottom supports to apply the weight. Third, until the sample cracks or gets the specified deflection, apply a load at a steady pace. Keep track of the load and deflection readings during the test. Fourth, use the following formula to get the material's flexural strength: Flexural strength is calculated as

The formula for determining a rectangular specimen's flexural strength in a 4-point test (AWS, 2000) is:

$$\sigma = 3LF/(2bd^2) \tag{3.3}$$

Where L = specimen length, F = total force applied to the specimen by two loading pins, b = specimen width, and d = specimen thickness.

Fifth, use the following calculation to get the stress at maximum load: Stress is calculated as (M * c) / (I * y), where M is the maximum bending moment, c is the vertical distance in either compression or tension from the neutral axis to the extreme fiber, I is the moment of inertia of the sample's cross-section, and y is the perpendicular distance from the centroid axis to the extreme fiber. In materials science and engineering, the four-point bending test is frequently employed to evaluate the strength and stiffness of many materials, including plastics, composites, ceramics, and metals.

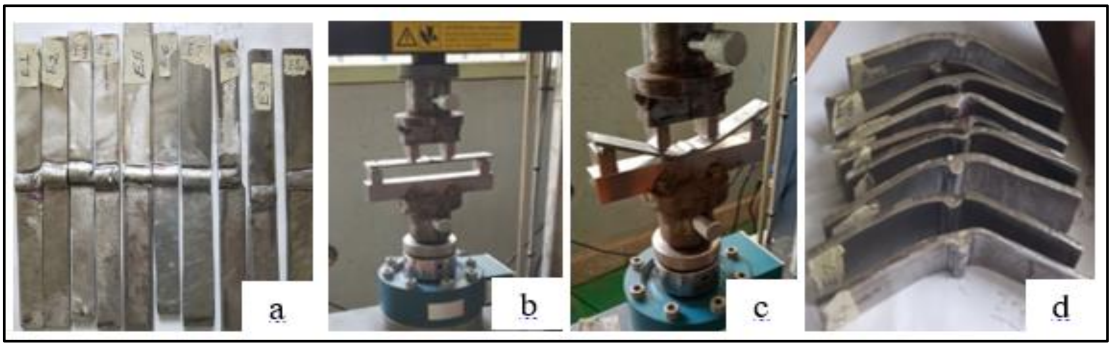

Figure 3.21: Samples: (a) before testing, (b) sample under 4-point flexural testing, and (c) samples during testing, (d) samples after testing.

3.10 Microstructure and Micro-hardness Testing

The HUVITZ HR-300 series optical microscope model was used in the material science engineering laboratory at Adama Science and Technology University (ASTU) to calculate microstructure and micro-hardness for this investigation. As seen in figure 3.23 below, micro-hardness testing was performed in the material engineering lab using a Vickers hardness testing apparatus. A Vickers hardness test was performed on each specimen. Under a microscope, the resultant imprint was measured and examined to determine its hardness. (Hultquist & Leygraf, 1980). Using an abrasive cutter and a coolant to preserve the metal's properties for testing, the samples were divided into sections for microstructural and micro-hardness testing. Then the material was put in place. The specimens were mounted, then processed using sheets of silicon carbide grit with sizes #220-600-800-1200-2000. Additionally, the samples were polished with a diamond suspension polishing agent utilizing electro-polishing equipment. Finally, a 70% nitric acid (HNO3) etching solution was used to etch the specimens for 15 seconds. This solution is depicted in figure 3.22 below. After that, a metallographic test was performed.

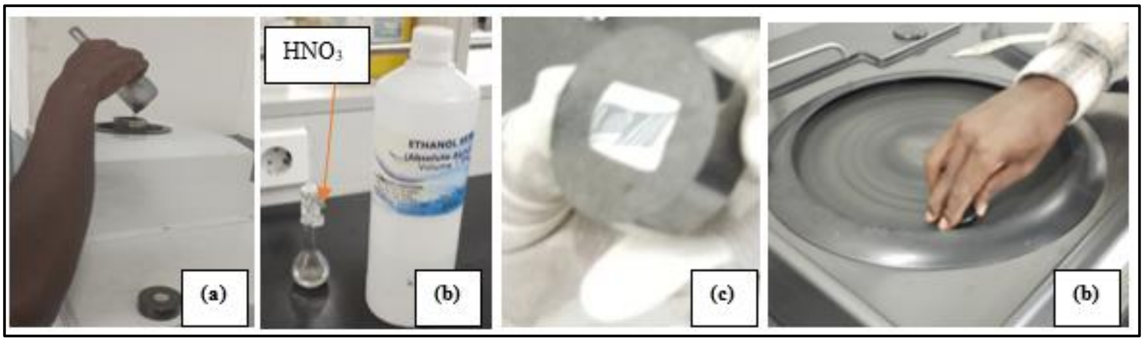

Figure 3.22: preparing a specimen for metallographic analysis, a) specimen during mounting, b) etchant solution, c) sample after etched, d) specimen polishing

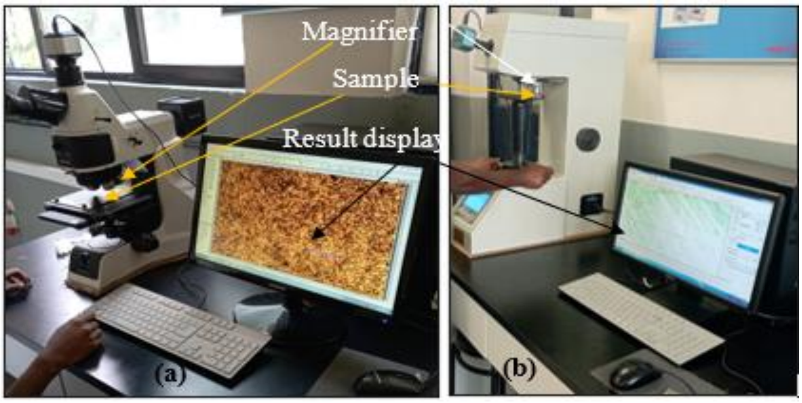

Figure 3.23: Optical microscope and Vicker's hardness testing machine (ASTU material laboratory)

3.11 Taguchi Method

Taguchi's, one of the Design of Experiment (DOE) applications, is employed to examine the effect of various factors and how they act by carrying out a limited number of experiments and assessing their influence on particular behavior. It may choose the ideal circumstances for the experiment at the same time, producing a better result. There are three main steps, according to Taguchi: planning, conducting, and analysis (Krishnaiah & Shahabudeen, 2012). In this experiment, the welding current, wire feed rate, gas flow rate, and welding speed were all investigated. The total degrees of freedom of the process parameters in the Taguchi DOE concept determines the utilization of an orthogonal array. The degree of freedom is accounted for or defined as the quantity of comparisons necessary to maximize each parameter (factor) with the chosen levels. Minitab 21 statistical software is used to create the experimental design of process parameters and numerical analysis with four elements and three levels of the experiment.

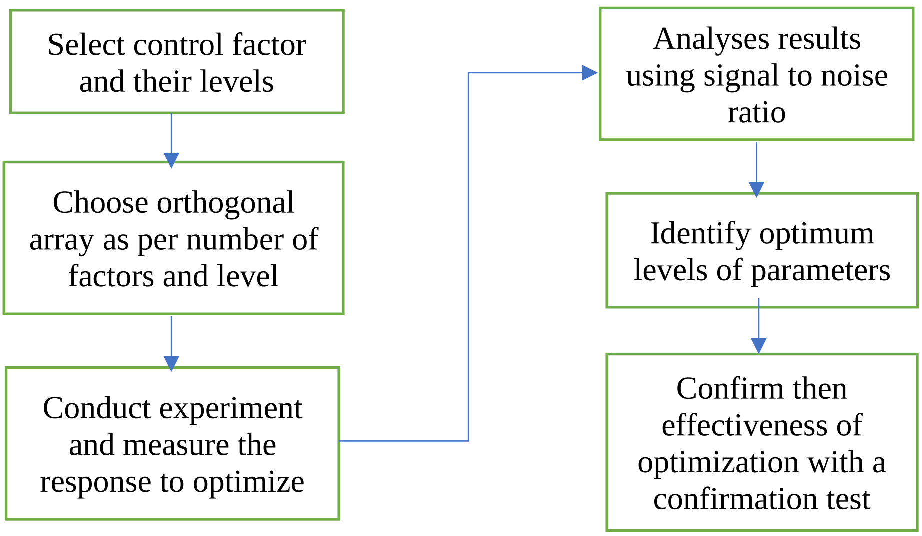

Figure 3.24: Design procedure of Taguchi methods

While MIG welding dissimilar 316 stainless steel with AISI 4140 low alloy steel, three levels of research were done to assess the impacts of welding parameters on tensile strength, hardness, flexural strength, and weld bead width. These MIG welding parameters were determined using data gathered from the literature (Sapakal, 2017) and (Wahule and Wasankar, 2018), American Welding Society (AWS) guidelines, numerous screening trials and exercises, and the guidance of knowledgeable and experienced individuals at the welding training facility, Ethiopian Manufacturing Technology & Engineering Industry Research & Development Center (MIDI) (Addis Ababa, Ethiopia).

3.11.1 Orthogonal Array

The minimum number of trials to conduct before choosing the orthogonal array should be determined based on the total degree of freedom. The number of experiments required to study the variables must not be greater than the total degrees of freedom supplied. (Krishnaiah & Shahabudeen, 2012). The choice of orthogonal array in this study was determined by the number of layers of various parameters. In the experiments, four different factors with three levels were used.

$$DOF = P*(L-1) \tag{3.3}$$

Where, DOF = Degree of freedom,

P = Number of factors and,

L = Number of levels

DOF = 4(3-1) = **8** (OA ≥ DOF, so OA has **9** experimental runs)

The number of experimental runs was determined after calculating the degree of freedom (DOF) and was selected from an orthogonal array. The L9 orthogonal array was chosen for the experiment design because the total number of orthogonal array (OA) experiments should be more than or equal to the computed value.

3.11.2 Signal to noise ratio (S/N ratio)

The Taguchi technique emphasizes the value of employing the signal-to-noise ratio when studying response variation because it reduces the effect of uncontrollable parameter fluctuation on quality attributes. The signal in the Taguchi process is the desired value (mean) for the output characteristic, whereas the noise is the unwanted value (deviation, SD). Taguchi used the S/N ratio, which is the same as the average to SD ratio, to assess the quality feature that deviates from the ideal value. Depending on the type of feature, there are a variety of S/N ratios accessible; smaller is preferable, nominal is preferable, and bigger is preferable (Karna, 2016).

A. Larger the better (Maximization)

B. Smaller the better (Minimization)

C. Nominal the best

Standard S/N ratio formula:

$$\frac{S}{N} \text{ Ratio} = -10 \left[\frac{1}{n} \sum_{j=1}^{n} \frac{1}{Y_{ij^2}}\right] \tag{3.4}$$

Where 'i' is the number of a trial; 'Yi' is the measured value of quality characteristic for the i^{th} trial and j^{th} experiment, 'n' is the number of repetitions for the experimental combination.

3.12 Multi-response optimization

A challenge to overall output response optimization is the optimization of the multi-response problem. The majority of writers employed strategies that combine all of the various response criteria into a single composite requirement when using simultaneous optimization techniques. Thus, the compromise answer is reached in a much more straightforward manner (Raissi & Farsani, 2009).

3.12.1 Grey Relational Analysis for Multi-response Optimization

A typical technique for determining the degree of connection between sequences using a grey relational grade is grey relational analysis. By utilizing the grey relational grade, researchers have used grey relational analysis to enhance control parameters with various replies. The degree of correlation between the various replies is analyzed using the grey relational grade in this method. (Obara et al., 2021) Another study used a grey relational-based strategy to tackle multi-response issues in the Taguchi methodology. For the purpose of solving optimization issues, it is common practice to integrate all the performance parameters under consideration into a single number using the Grey relational analysis.

3.12.2 Optimization Steps Used in Grey Relational Analysis

Step 1: Convert the original response data into the S/N ratio (Yij) using the appropriate formula for the kind of quality characteristic, as described in equations 2.1, 2.2, and 2.3.

Step 2: Using the following formula, standardize Yij as Zij (where 0 Zij 1). This step is required to decrease variability and eliminate the impact of different units. Normalization is the process of altering a single input to uniformly distribute and scale the data within an acceptable range. Zij is the normalized value for the jth dependent variable or response in the ith experiment or trial.

$$Zij = \frac{Yij - \min(Yij, i=1,2,3,....n)}{max(Yij, i=1,2,3,....n) - \min(Yij, i=1,2,3,....n)} \quad (3.5)$$

(To be used for S/N ratio with larger—the better case)

$$Zij = \frac{\min(Yij, i=1,2,3,....n) - Yij}{max(Yij, i=1,2,3,....n) - \min(Yij, i=1,2,3,....n)} \quad (3.6)$$

(To be used for S/N ratio with smaller—the better case)

$$Zij = \frac{Yij - T - \min(Yij - T, i=1,2,3,....n)}{max(Yij - T, i=1,2,3,....n) - \min(Yij - T, i=1,2,3,....n)} \quad (3.7)$$

(To be used for S/N ratio with nominal the best case)

Step 3: Compute the grey relational coefficient (GRC) for the normalized S/N ratio values.

$$GRCij = \frac{\Delta\min + \partial\Delta\max}{(\Delta ij + \partial\Delta\max)} \quad (3.8)$$

Where, I = 1, 2… n-experiments and j = 1, 2… m-responses

GRC_{ij} = GRC for the i^{th} experiment/trial and Δ= absolute difference between Y_{oj} and Y_{ij}

Y_{oj} = optimum performance value or the ideal normalized value of j^{th} response

Y_{ij} = the i^{th} normalized value of the j^{th} response/dependent variable Δmin = minimum value of Δ and Δmax = maximum value ofΔ

∂ is the distinguishing coefficient which is defined in the range $0 \leq \partial \leq 1$

Step 4: Compute the grey relational grade (GRG_i).

$$GRGi = \frac{1}{m}\sum GRCi \quad (3.9)$$

Where *m* is the number of responses

Step 5: Use the response graph method or ANOVA and select optimal levels for the factors based on the maximum average GRG_i value.

3.12.3 Analysis of Variance (ANOVA)

An analysis of variance (ANOVA) is used to discover which characteristics have a substantial influence on the quality feature. ANOVA is a statistical approach for determining the impact of numerous control conditions. The percentage contributions of each control factor are utilized in this research to quantify their influence on performance attributes. This analysis took a 5% significance level (or a 95% level of confidence) into account. The ANOVA findings show if there is a statistically significant variation in output characteristics. A significance level of less than 0.05 is deemed significant in ANOVA analysis, whereas a value greater than 0.05 is not. The percentage contribution calculates each term's percentage contribution to the overall sum of squares to determine the relative relevance of each model term. It is a crude but helpful guide to comprehending the significance of each model phrase. In the analysis of variance, the percentage contribution of each influential parameter was computed using the following formula (Gopalsamy et al., 2009):

$$P = \frac{SS}{SST} * 100\% \quad (3.5)$$

CHAPTER FOUR

RESULTS AND DISCUSSION

4.1 Introduction

The intention of this research was to create high-quality welded joints with appropriate mechanical qualities and corrosion resistance rates. Several tests were carried out as part of this study, and the findings were assessed to determine the efficiency of the welding procedure. The research includes a thorough examination of many aspects such as mechanical properties, percentage of surface defect, weld geometry, microstructural analysis, and corrosion test analysis. The impact of welding parameters on the mechanical characteristics, welding joint form, and microstructural characteristics of the dissimilar weld of SS316 stainless steel and AISI 4140 low alloy steels was explored. The welded samples were visually examined for defects in welding using liquid penetrant after the welding process was completed.

4.2 Liquid Penetrant and Visual Defect Testing

When the welding was being done, were visually examined. One of the welded samples exhibited an undercut at the end, too much reinforcing height, a lack of fusion, porosity, a minor fracture, and slag, among other welding defects. The samples 7 and 9 were defect-free, whereas the other samples had various types of defects. The size and type of each defect were measured in order to calculate the percentage of surface defects and to determine whether or not the welded samples with defects should be accepted in accordance with international standards like AWS D1, ASME V, and ASME VIII. Table 4.1 below shows the result of liquid penetrant test with percentage surface defects calculated and acceptability according to standard criteria.

Table 4.1: Liquid penetrant testing result for dissimilar automated MIG-welded samples

Sample No	**Non-Destructive Test Result**	Percentage of surface defects (%)
Sample 1	Porosity(d=0.8mm) and surface crack(3mm)	1.78 (Accepted)
Sample 2	Small crack(3mm) and Excessive reinforcement(5mm)	5.24 (Rejected)
Sample 3	Excessive reinforcement(6mm), small crack(2mm) and lack of fusion(6mm)	6.53 (Rejected)
Sample 4	Lack of fusion(5.8mm) and small crack(3mm)	2.53 (Accepted)

Sample 5	Lack of fusion(6.4mm)	1.82 (Accepted)
Sample 6	Small crack(2mm), slag(2mm)	1.98 (Accepted)
Sample 7	Defect-free	0.25 (Accepted)
Sample 8	Porosity(d=1mm) and small crack(3mm)	1.1 (Accepted)
Sample 9	Defect-free	0.25 (Accepted)

All samples are analyzed in terms of the type of defects and their length by calculating the surface area of each defect on the weld zone divided by total surface area of weld zone to get the percentage of defects on the surface. According to AWS D1.1/D1.1M:2020, and ASME Section VIII, the acceptance criteria for surface defects in welding that allows a maximum percentage of defects of less than 5% is typically specified in welding standards (American National Standard Structural Welding, 2020). These standards define the acceptable levels of various types of welding defects, such as porosity, undercutting, and small crack.

The acceptance criteria for welding defects such as cracks, porosity, lack of fusion, slag, and excessive reinforcement are defined in AWS D1.1/D1.1M:2020 and ASME Section VIII based on their size, location, and orientation. The maximum allowable defect lengths for each category are as follows: -

Small cracks: Samples 2, 3, 4 and 6 exhibited a small crack. This defect appeared as a result of slag inclusion due to the welding speed is too fast. AWS D1.1/D1.1M:2020 specifies that If the crack is a result of slag inclusion then the maximum length cannot exceed 1/8 in (3 mm). Therefore all samples with small crack are not exceed 3mm and accepted.

Porosity: Samples 1 and 8 exhibited a porosity. This defect was caused by trapped air in the shielding gas, which caused distributed porosity and gross surface pore breaking. According to AWS D1.1/D1.1M:2020 and ASME Section VIII, the maximum diameter of porosity in welds should not exceed 3/32 inches (2.4 mm) for most applications. Therefore sample 1 and 8 have porosity diameter of 0.8mm and 1mm respectively they are accepted

Lack of fusion: Samples 3, 4 and 5 exhibited a lack of fusion. This defect appeared as a result of low current input, arc length, electrode angle, electrode manipulation, and incorrect welding parameter settings, according to AWS D1.1/D1.1M:2020 all lack of fusion defects are accepted except lack of fusion in sample 3 which has 6.4mm in length.

Excessive reinforcement: Samples 2 and 3 exhibited an excessive reinforcement. This defect was caused at lower welding current and higher wire feed rate. According to AWS D1.1/D1.1M:2020 limits the maximum length of reinforcement to three times the thickness of the base metal or 9mm, whichever is smaller. Therefore they are accepted.

The percentage of surface defects for each sample is computed using equation (3.8), with sample 3 having the highest POSD due to the lower welding current, high wire feed rate, and high feed rate. The percentage of surface defect has been calculated for sample 3 using the taken figure 4.1 of the report of all samples obtained from the liquid penetrant testing laboratory center at the Manufacturing Technology and Engineering Industry Research and Development Center, which is provided in the appendix.

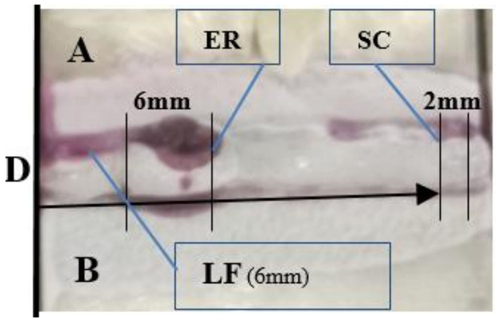

Figure 4.1: all defects and their length in sample 3

Surface area of defects:

Lack of fusion (LF) = 6mm*1mm = 6mm2, small crack (SC) = 2mm*1mm = 2mm2, excessive reinforcement (ER) = 6mm *7.03mm = 42.18mm^2, total surface area of defects (Ad) = (6+2+42.18) mm^2 =50.18 mm^2.

Weld surface area: Aw = P*L = 10.25mm^2*75 mm^2 = 768.53 mm^2, where P is the perimeter of the weld cross-section and L is length of the weld bead.

POSD = (50.18 mm2/768.53 mm^2) x 100% = 6.53%.

4.3 Microstructural Analysis of Welded Metals

An optical microscope (HUVITZ HR-300 series model) was used to study the base material and the microstructure of each MIG-welded sample. However, only two samples—samples number 7 and 3—were given basis materials. Based on the outcomes of tensile strength testing, these samples were chosen for microstructural examination. The UTS joint strength of sample number 7 was the greatest, whereas sample number 3 was the lowest. A typical optical micrograph of the base metal is shown in Figure 4.2. Figure 4.2a shows the microstructure of 316 stainless steels, which has a completely austenitic structure with minor annealing twins (Assefa et al., 2022) similar findings have been observed with stainless steel 316. Low alloy steel AISI4140 typically has a ferrite-pearlite or bainite microstructure (Figure 4.2b). Figures 4.3 and 4.4 display the optical microstructures of MIG-welded joints and the weld metal from the selected samples. The sample micrograph photos clearly show the base metal (BM), heat-affected zone (HAZ), and weld metal (WM). In samples 3 and 7, a microstructure with a delta-ferrite structure was created.

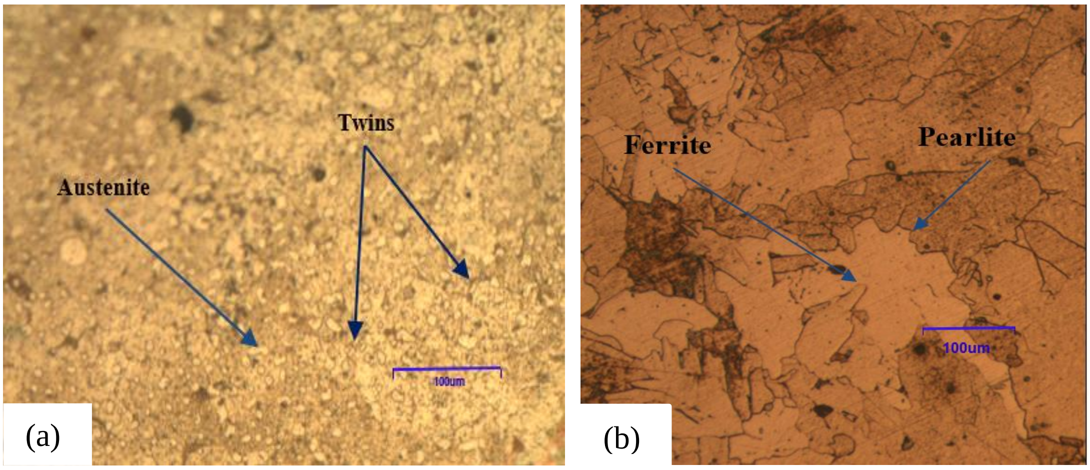

Figure 4.2: The microstructure of base metals: (a) 316 stainless steels; (b) AISI 4140

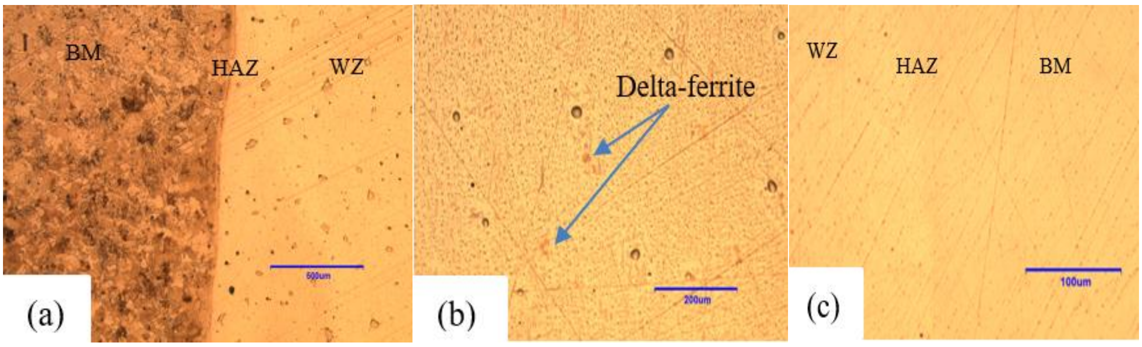

Figure 4.3: The microstructure of welded joint made of SS316 and AISI 4140 (sample 7): (a) welded joint from AISI 4140; (b) weld zone (c) welded joint from SS316

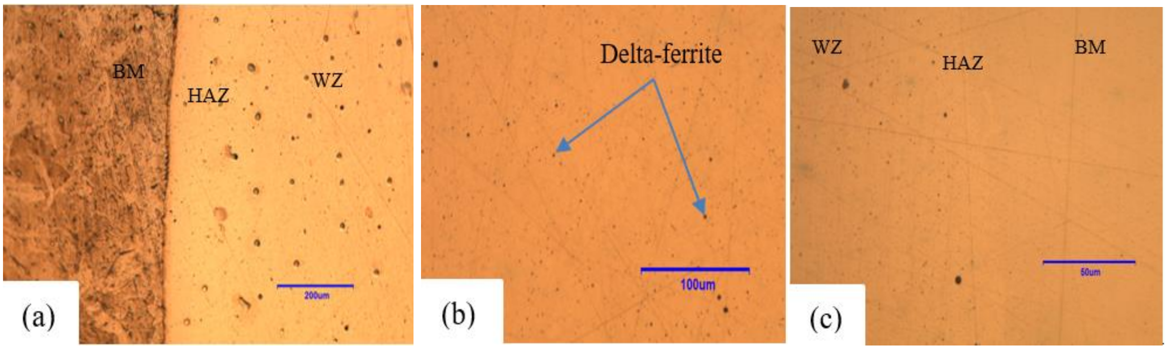

Figure 4.4: The microstructure of welded joint made of SS316 and AISI 4140 (sample 3): (a) welded joint from AISI 4140; (b) weld zone (c) welded joint from SS316.

Due to a moderate heat input and a moderate cooling rate, the weld zone of the welded specimens in sample number 7 displays a very thin delta ferrite along the sub-grain and migrating boundaries in the plain austenitic matrix, as illustrated in Figure 4.3; (Reddy et al., 2014) and (Assefa et al., 2022) reported the same result. In this weld zone, the delta ferrite (δ) is finer; the heat provided by the welding process, which was modest (140A), is related to the delta ferrite's (δ) size. When heat input is modulated, a modulated cooling rate occurs, and a finer skeletal ferrite is generated as a result. Due to very low welding heat inputs, i.e., high cooling rates (110A), the dissimilar weld metals in sample number 1 included δ-ferrite in the form of dendritic lathy-ferrite at the dendrite core surrounded by an inter-dendritic γ-phase.

4.4 SEM Microstructure

The SEM microstructure analysis conducted for the automated MIG weldments revealed no observable macro or micro-scale deficiencies, such as porosity, undercut, or lack of fusion. The microstructure studies further revealed the formation of martensite at the heat-affected zone (HAZ) of AISI 4140 as shown in the figure 4.5 below, likely attributed to the higher heat inputs involved in the welding process. In addition, the presence of carbides was observed at the HAZ of AISI 316, further indicating the reliability and effectiveness of the optimized MIG welding process parameters. Furthermore, a fine-grain structure was observed in the weld zone of optimum sample 7, demonstrating the successful execution of the welding process with optimized parameters. These findings highlight the potential benefits and applications of automated MIG welding technology for welding dissimilar metals and underscores its importance in achieving high-quality welds with minimal defects or failures (Reddy et al., 2014) shows the same result.

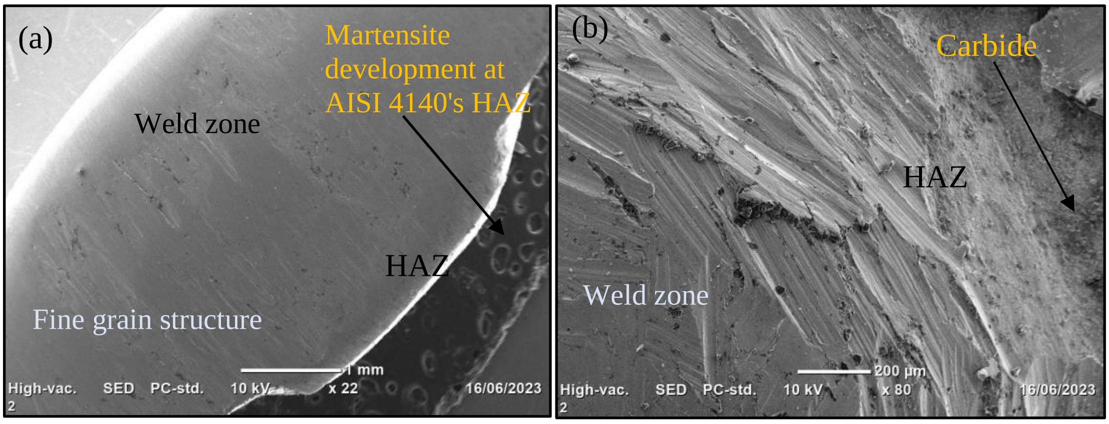

Figure 4.5: microstructure representing weld zone – HAZ of AISI 4140 and SS 316, a) cross-section of weldments, b) surface bead of weldments sample number 7

4.5 Corrosion Test Result Analysis

The research conducted an electrochemical test to determine the corrosion rate of a metal sample 7. From the graph of figure 4.6 Tafle plot obtained from the test with the equivalent weight of the sample 7 of weld zone is 3.28g, density of 7.944g/cm^3, I_{corr} = 2.838μA, so by using corrosion rate equation above calculate as CR = $\frac{0.13*3.28g*2.838uA}{7.944g/cm3} =$ 0.152mm/year, the same steps are observed for calculation of corrosion rate for base metals and HAZ of both SS316 and AISI4140 as shown in table 4.2.

Table 4.2: Corrosion rate all zones of welded joint

Material zone	E_{corr} (V)	I_{corr} (μA/cm^2)	I_{corr} (μA)	corrosion rate (mm/year)
SS 316 base	-0.232	1.545	2.056	0.11035
SS316 heat affected zone	-0.543	2.163	3.256	0.17477
Weld zone	-0.5921	1.933	2.838	0.15233
AISI 4140 heat affected zone	-0.645	2.992	4.835	0.25952
AISI 4140 base	-0.512	2.234	3.431	0.1842

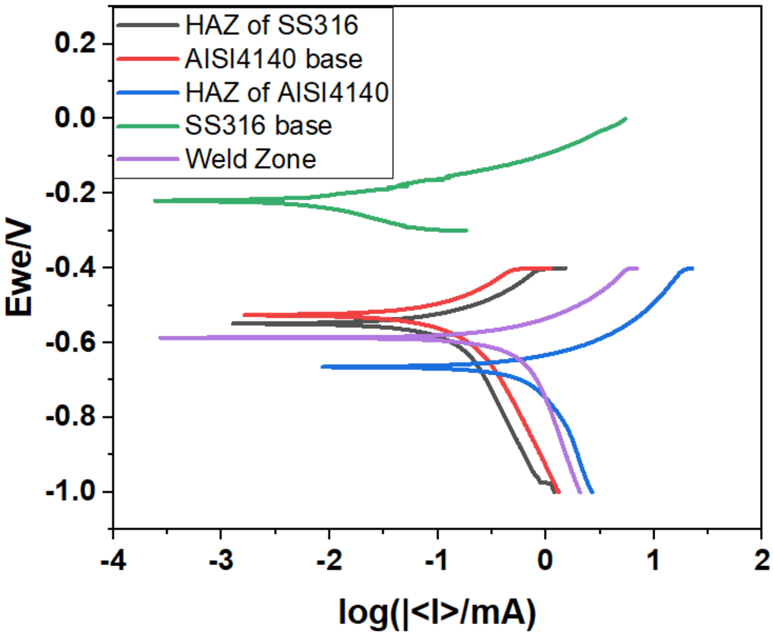

Figure 4.6: Polarization curves at all zone of selected sample

SS-316 Base - According to Table 4.2, the corrosion current density of the 316 stainless-steel base material was 1.545 µA/cm^2, the self-corrosion potential (E_{corr}) was -0.1963V, the corrosion rate of the 316L austenitic stainless-steel base was 0.11035 m/year. The SS316L base exhibits high corrosion resistance due to the formation of a protective layer that prevents corrosion. This is evident from the corrosion rate of 0.11035 m/year which is less than corrosion rate of others zone. The presence of Cr (18-20 wt. %) and Ni (10-14 wt.%) in the chemical composition also contributes to the corrosion resistance of SS316 (Mani et al., 2018) obtained the same result.

SS-316 HAZ - During welding, the heat-affected zone (HAZ) of the 316 stainless-steel base material is heated to various temperatures ranging from ambient temperature to the melting range of the alloy. In the case of the HAZ between 316 stainless steel and weld zone, the corrosion current density of the 316 stainless-steel HAZ was 2.163 µA/cm^2, the self-corrosion potential (E_{corr}) was -0.543 V, the corrosion rate was 0.17477 m/year. It is observed that the corrosion rate is 58% higher than that of the 316 stainless-steel base which indicate lower corrosion resistivity than SS316 base.

Weld Zone - The weld zone exhibits the better corrosion resistance, which can be attributed to the filler material used, ER-309L, which contains a significant amount of Cr and Ni (23.5 wt.% and 13.5 wt.% respectively). The corrosion current density of the welded zone was 1.933 µA/cm^2, the self-corrosion potential (E_{corr}) was -0.5821 V, the corrosion rate of 0.15233 m/year. It was observed that the corrosion rate is 38.04% higher than that of the 316 stainless-steel base, 12.84% lower than that of the 316 stainless-steel HAZ, 41.30% lower than that of the AISI 4140 HAZ, and 17.30% lower than that of the AISI 4140 base.

AISI 4140 HAZ - The corrosion current density of the AISI 4140 HAZ was 2.992 µA/cm^2, the self-corrosion potential (E_{corr}) was -0.645 V, the corrosion rate of the AISI 4140 HAZ was 0.25952 m/year. It is observed that the corrosion rate is 40.89% higher due to grain distortions compared to the AISI 4140 base.

AISI 4140 - The low alloy steel 4140 base had a corrosion current density of 2.234 µA/cm^2, a self-corrosion potential (E_{corr}) of -0.512 V, the corrosion rate of the AISI 4140 base was 0.1842 m/year.

4.5.1 Micro-hardness Analysis

Figure 4.7 displays the variations in Vickers micro-hardness values on either side of samples 3 and 7 as a function of the separation between the weld center and the base metals. Hardness values in each weld zone were much greater than base metal hardness values. The welded area is the most difficult component. In the fusion zone, the average hardness value of the welded metals was 502 HV. The base metals' hardness ratings were lower than those of the HAZ sides. The hardness values of the 316 stainless steel welds were 182 HV, whereas the hardness values of the AISI 4140 base metals were 300 HV.

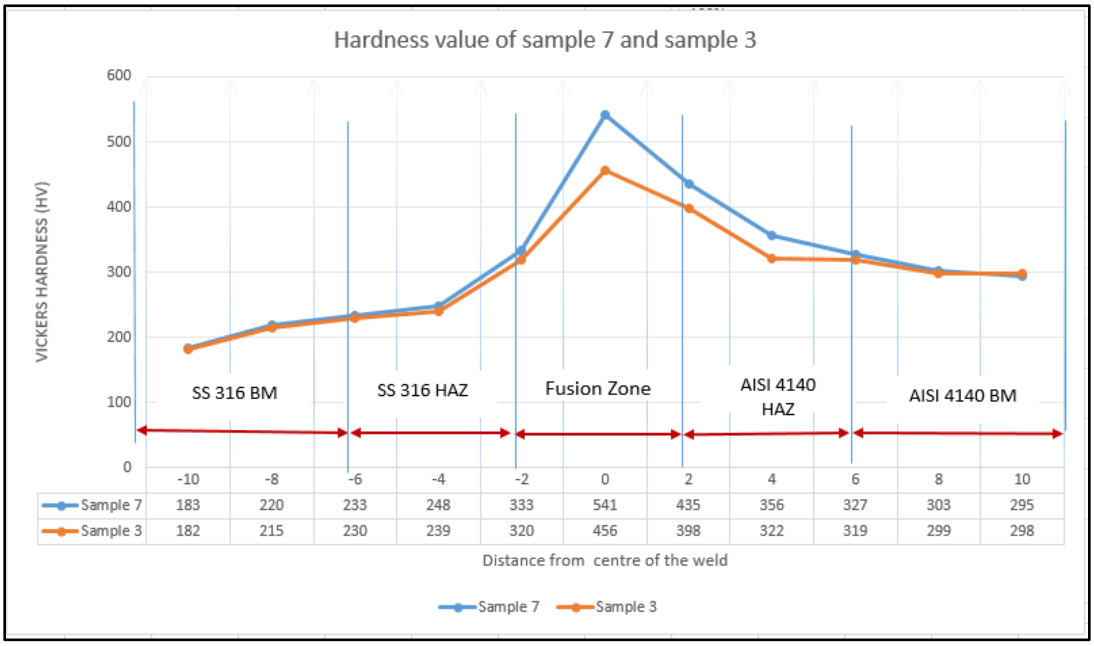

Figure 4.7: Vickers hardness of sample no. 7 and 3

4.6 Mechanical Properties

Investigating and improving automated MIG welding process parameters for welding SS 316 and AISI 4140 with dissimilar metals was the aim of this study. It is accomplished by inspecting the microstructure, mechanical attributes (hardness, tensile, flexural bending attributes), and bead width of the weldments made using these methods. Following that, the Taguchi method was used to examine the test response parameters, and analysis of variance (ANOVA) was used to calculate the percentage contribution of each parameter. Finally, the parameters were adjusted using a multi-response optimization technique using a Grey relation analysis (GRA). Table 4.3 shows the welding control parameters and levels used.

Table 4.3: Corrosion rate and Polarization resistance all zones of welded joint

S. No	**Process Parameter**	**Units**	**Levels**		
			1	**2**	**3**
1	Welding current (A)	Amp (A)	110	125	140
2	Wire feed rate (B)	cm/s	7	10.5	14
3	Gas flow rate (C)	CFH	7	9	11
4	Welding speed (D)	cm/min	20	30	40

4.6.1 Tensile Strength Result Analysis

A universal testing equipment was used to acquire tensile strength data. Each test included two specimens, with the average value being taken. Table 4.4 shows the measured experimental results of the mean tensile strength values for each trial experiment. The failure of the testing sample following the test on the stainless steel and in sample 2 and sample 3 failure occur at weld zone which shows the tensile strength of low alloy steel is better than stainless steel. Figure 4.8 and 4.9 below shows the stress strain graph for maximum and minimum tensile strength appeared in sample 7 and sample 3 respectively.

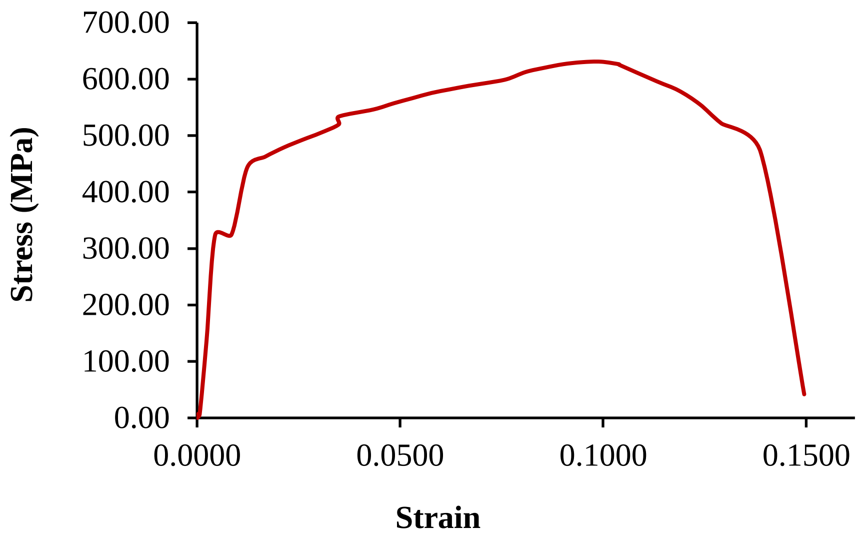

Figure 4.8: Stress strain graph of sample 7

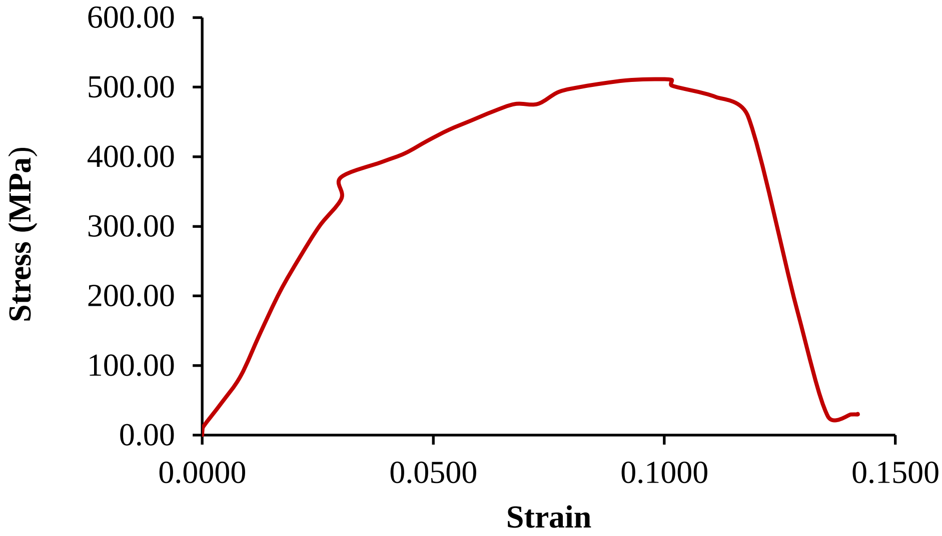

Figure 4.9: Stress strain graph of sample 3

The above graphs show that sample 3 has a higher elongation than sample 7 under tension force. This is because the defects in sample 3 provide a greater area for plastic deformation to occur. However, sample 7 has a higher ultimate tensile strength than sample 3. This is because the defects in sample 3 reduce the cross-sectional area of the weld, which reduces the load-bearing capacity of the weld. The results of this study show that the presence of defects can have a significant impact on the mechanical properties of a weld. It is important to consider the effects of defects when designing and welding joints.

Table 4.4: Mean tensile strength result

Sample No	Welding Current (A)	Wire feed rate (B)	Gas flow rate (C)	Welding speed (D)	Tensile Strength (MPa)	Signal to noise ratio
1	110	7	7	20	613	55.74921
2	110	10.5	9	30	575	55.19336
3	110	14	11	40	516	54.25299
4	125	7	9	40	602	55.59193
5	125	10.5	11	20	609	55.69235
6	125	14	7	30	599	55.54854
7	140	7	11	30	636	56.06914
8	140	10.5	7	40	612	55.73503
9	140	14	9	20	632	56.01434

4.6.1 Mean response analysis of Tensile strength

As indicated in Table 4.5, the most affected parameters were welding current (A) at level three, followed by welding speed (D) at level one, wire feed rate (B) at level one, and gas flow rate (C) at level one. Taguchi used these welding parameters (A3B1C1D1) as the initial parametric setup for the MIG-welding of stainless steel 316 to low alloy steel 4140 with a thickness of 3 mm. This implies that it is possible to employ that as a parameter combination in order to generate larger and better outcomes.

Table 4.5: Response table for Means of Tensile Strength

Level	Welding Current(A)	Wire feed rate (B)	Gas flow rate (C)	Welding speed (D)
1	568	**617**	**608**	**618**
2	603.3	598.7	603	603.3
3	**626.7**	582.3	587	576.7
Delta	58.7	34.7	21	41.3

Rank	1	3	4	2

Figure 4.10: Main effect plot for means

The numerical value at the maximum point in each graph of the main effect plot shown above figure 4.10 denotes the parameter's optimal value at that level. They also show the ideal options within the constraints of the experiment. The welding current and welding speed weight % had the biggest effects on enhancing tensile strength when compared to other welding variables. The optimal parameters (A3B1C1D1) were welding current at level three (140A), wire feed rate at level one (7cm/s), gas flow rate at level one (7 CFH), and welding speed at level one (20cm/min).

4.6.1.2 Signal to noise ratio analysis of tensile strength

According to the signal-to-noise ratio value in Table 4.6, the welding current weight percentage has the greatest influence, (Delta = 0.87; Rank = 1st) followed by welding speed (Delta = 0.63; Rank = 2nd) and wire feed rate (Delta = 0.53; Rank = 3rd). The (S/N) ratio is least affected by gas flow rate (Delta = 0.34; Rank = 4th) according to the experimental result. The initial best parameter combination for increasing weld metal strength with the greater-the-better responsiveness of automated MIG-welded of 316 stainless steel sheets with 4140 low alloy steel is **A3B1C1D1**.

Table 4.6: Response table for signal-to-noise ratios for Tensile Strength (Larger is better)

Level	Welding Current (A)	Wire feed rate (B)	Gas flow rate (C)	Welding speed (D)
1	55.07	**55.8**	**55.68**	**55.82**
2	55.61	55.54	55.6	55.6
3	**55.94**	55.27	55.34	55.19
Delta	0.87	0.53	0.34	0.63
Rank	**1**	**3**	**4**	**2**

4.6.1.3. Effect of process parameters on tensile strength

Figure 4.11 shows how these variables affect tensile strength. According to the graph when the current rises from level one to level three, the tensile strength increases significantly. The tensile strength value decreases from level one to level three as the wire feed rate rises, as well as the tensile strength value decrease from level one to level three when gas flow rate and welding speed rises (Pratiwi et al., 2023), (Ampaiboon et al., 2015) and (Miao et al., 2019) observed the same outcome.

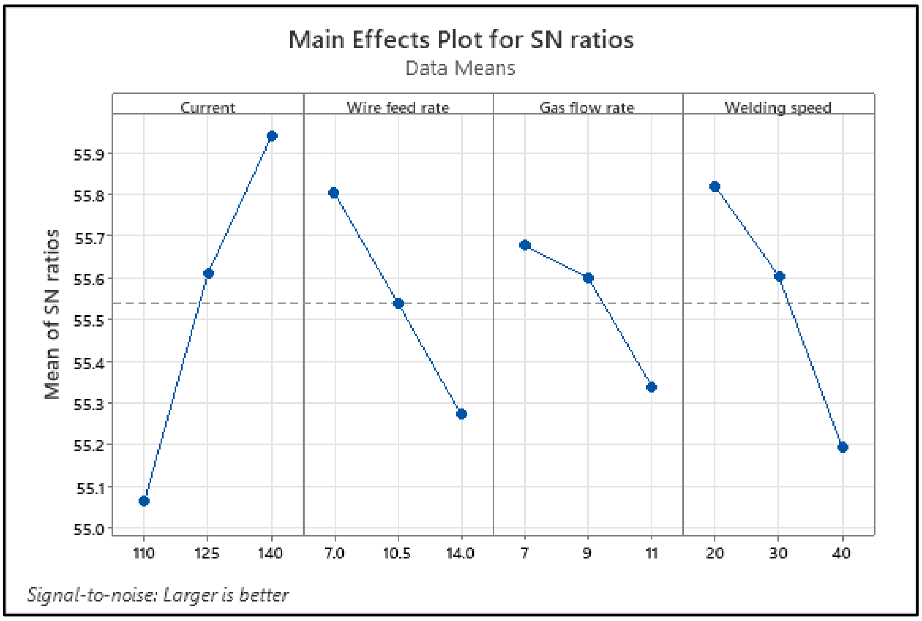

Figure 4.11: Main effect plot for signal to noise ratios for Tensile Strength

4.6.1.4. Analysis of Variance (ANOVA) for tensile strength

ANOVA was used to assess the appropriateness of the created models. The model is stated to be adequate within the confidence limit if the estimated value of the F-ratio of the produced model is less than the standard F-ratio (F0.05, 1, 8 = 5.32 from table) value at the required level of confidence of 95%. Table 4.7 shows how analysis of variance (ANOVA) is used to identify the most important characteristics that affect the tensile strength of MIG-welded steels.

Table 4.7: Analysis of variance (ANOVA) for Tensile Strength

Source	DF	Seq SS	Contribution	Adj SS	Adj MS	F-Value	P-Value
Welding Current	1	5162.7	49.66%	5162.7	5162.67	100	0.001
Wire feed rate	1	1802.7	17.34%	1802.7	1802.67	34.92	0.004
Gas flow rate	1	661.5	6.36%	661.5	661.5	12.81	0.023
Welding speed	1	2562.7	24.65%	2562.7	2562.67	49.64	0.002
Error	4	206.5	1.99%	206.5	51.63		
Total	8	10396	100.00%				

R-Sq = 98.01%, R-Sq (adj) = 96.03%, F0.05, 1, 8 = 5.32

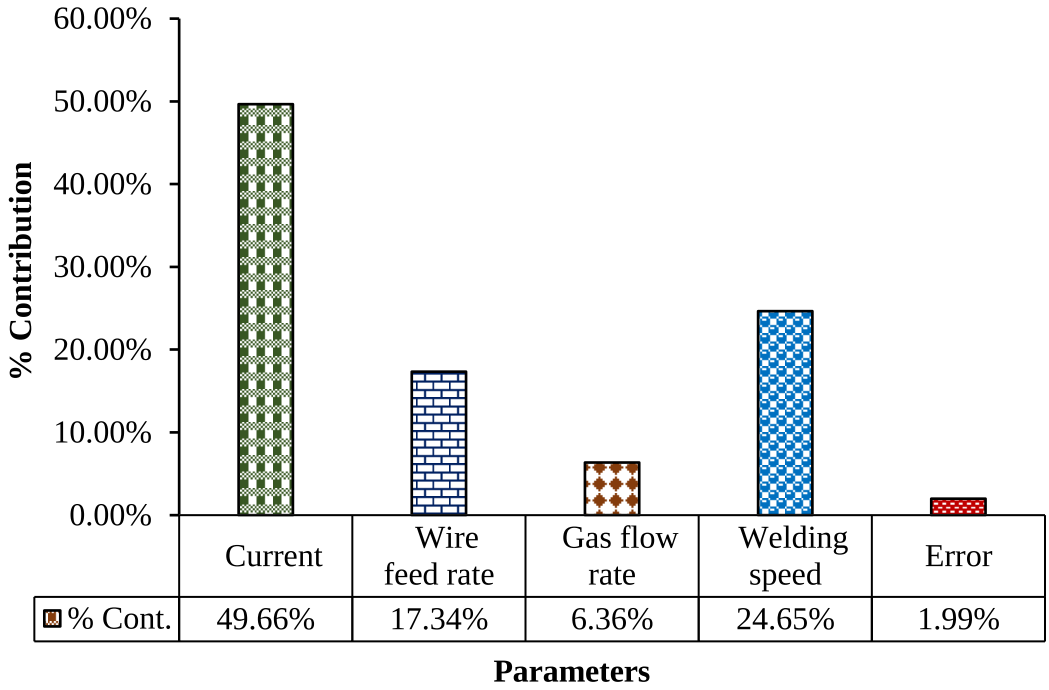

Figure 4.12: Percentage contribution of parameters for tensile strength

Since the F-value obtained from the table is 4.7, but the F-ratio obtained from the ANOVA table is substantially more than the critical F-ratio, all parameters have a significant effect on tensile strength. As shown in the figure 4.12, the welding current weight percentage (49.66%), Welding speed (24.65%), Wire feed rate (17.34%), and Gas flow rate (6.36%) all have a significant impact on the tensile strength of MIG-welded 316 stainless steel with 4140 low alloy steel sheets with a thickness of 3 mm, as indicated in the table above. The ANOVA analysis, including p-values, indicates that the percentage of contribution from all parameters significantly impacts the tensile strength ($P < 0.05$). The R-squared value, which measures the model's fit to the data, is 98.01% according to table 4.18, indicating a strong fit.

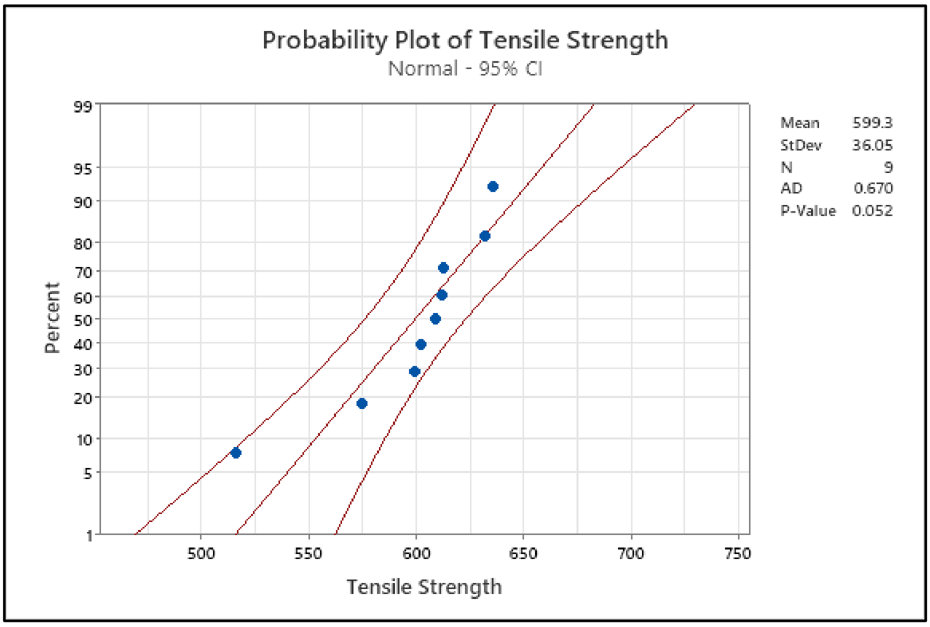

Figure 4.13: The normal probability plot for tensile strength

The errors in statistical models are believed to be regularly distributed in the design of experiments. A normal probability plot of the residuals is used to evaluate the importance of effects. If the residuals fall along a straight line on the plot, they have a normal distribution. The data points in Figure 4.13 are pretty near to the fitted normal distribution line. The residuals' normal probability plots reveal that they are pretty near to the normal probability lines. Furthermore, the p-value (0.052) in Figure 4.8 is larger than 0.05, indicating that the residuals are normally distributed and that the variables in the regression models are both significant and appropriate (Ghangas et al., 2022).

4.6.2 Hardness Test Results Analysis

Hardness measurements were taken with a Vickers hardness test machine, with each test performed on the base metal, HAZ and the weld zone. Three readings were taken in each zone, and the average value was computed. The figure 4.14 below show when Vickers hardness test machine display first trial of sample 7 which is 541HV. Table 4.8 displays the measured experimental results of the mean hardness values for each trial experiment. For superior performance qualities, the larger hardness was predicted to be the preferred alternatives.

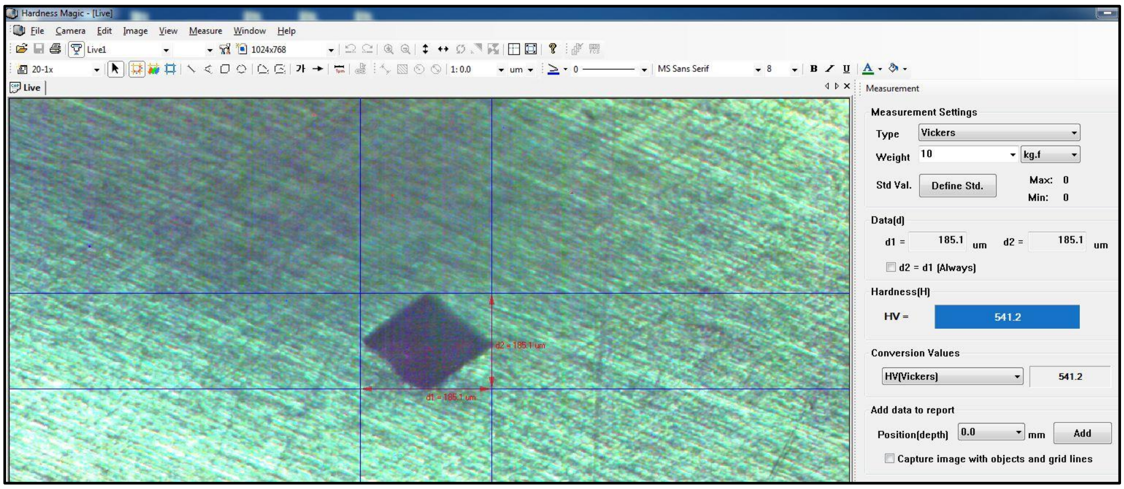

Figure 4.14: Hardness value of sample 7 trial 1

Table 4.8: Mean hardness testing result

Sample No	Welding Current (A)	Wire feed rate (B)	Gas flow rate (C)	Welding speed (D)	Hardness (HV)	Signal to noise ratio
1	110	7	7	20	482	53.6609
2	110	10.5	9	30	435	52.7698
3	110	14	11	40	456	53.1793
4	125	7	9	40	599	55.5485
5	125	10.5	11	20	435	52.7698
6	125	14	7	30	482	53.6609
7	140	7	11	30	541	54.6639
8	140	10.5	7	40	625	55.9176
9	140	14	9	20	476	53.5521

4.5.2.1. Mean response analysis of hardness

Table 4.9 shows that welding current (A) at level 3, wire feed rate (B) at level 1, gas flow rate (C) at level 1, and welding speed (D) at level 3 have the greatest value of hardness. According to the experimental response data, these welding settings (A3B1C1D3) were chosen as the first parametric configuration for hardness when MIG-welding stainless steel 316 to AISI 4140 low alloy steel with a thickness of 3 mm.

Table 4.9: Response table for means of Hardness

Level	Welding Current (A)	Wire feed rate (B)	Gas flow rate (C)	Welding speed (D)
1	457.7	**540.7**	**529.7**	464.3
2	505.3	498.3	503.3	486
3	**547.3**	471.3	477.3	**560**
Delta	89.7	69.3	52.3	95.7
Rank	**2**	**3**	**4**	**1**

Because the response is larger the better, the major influence plot for control parameters for mean hardness value is essentially the same as the main effects plot for SN ratios, therefore the impacts of the factors on hardness are evaluated from the main effect plot for SN ratios.

4.5.2.2. Signal to noise ratio analysis for hardness

The welding speed weight percentage had the biggest impact (Delta = 1.55; Rank = 1st), followed by welding current (Delta = 1.51; Rank = 2nd), and wire feed rate (Delta = 1.16; Rank = 3rd), as shown by the signal-to-noise ratio value in Table 4.10. The gas flow rate had the least impact on the S/N ratio (Delta = 0.88; Rank = 4th). Based on the larger-the-better characteristic, the Taguchi initial optimum parameter combination for increasing the hardness of dissimilar MIG-welded 316 stainless steel and AISI 4140 low alloy steel is **A3B1C1D3**.

Table 4.10: Response table for signal-to-noise ratios for Hardness (larger is better)

Level	Welding Current (A)	Wire feed rate (B)	Gas flow rate (C)	Welding speed (D)
1	53.2	**54.62**	**54.41**	53.33
2	53.99	53.82	53.96	53.7
3	**54.71**	53.46	53.54	**54.88**
Delta	1.51	1.16	0.88	1.55
Rank	**2**	**3**	**4**	**1**

4.5.2.3. Effects of process parameters on the hardness

Figure 4.15 depicts the effect of welding settings on hardness as well as the optimal values based on their rank. According to the analysis and principal effect plot graph for the S/N ratios, the ideal values for maximizing hardness include current at level 3 (140A), wire feed rate at level 1 (7 cm/s), gas flow rate at level 1 (7 CFH), and welding speed at level 3 (40 cm/min). As the current increases from level one to level three, the hardness value is increases, as shown in the graph below. (Pratiwi et al., 2023) observed the same result. The hardness of the material decreases as the wire feed rate increases from level one to level three. As the gas flow rate increased from level one to three, the hardness value is decreased. The welding speed was the most important welding factor, when welding speed rises from level one to level three the hardness value is increased. (Honarbakhsh-Raouf & Ghazvinloo, 2010) discovered the same result for weld in AISI 4140 Steel.

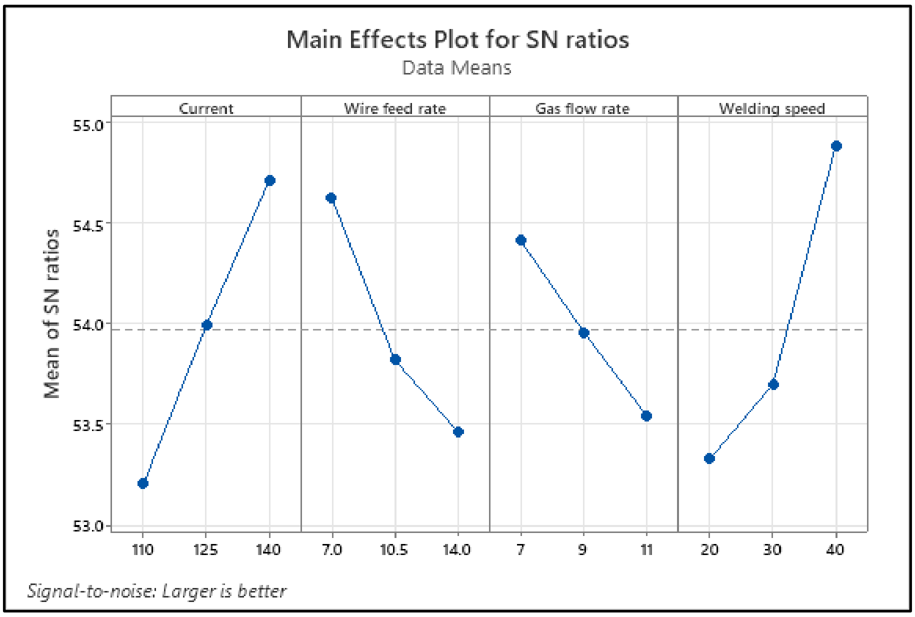

Figure 4.15: Main effect plot for signal-to-noise ratios for Hardness

4.5.2.4. Analysis of Variance (ANOVA) for hardness

The ANOVA was developed for hardness to investigate the developed experiment was adequate or not. The most critical characteristics (most significant parameters) that determine the hardness of automated MIG-welded steels are discovered and displayed in Table 4.11 using analysis of variance (ANOVA). A study was undertaken utilizing their S/N ratios to establish the percentage contribution of each component.

Table 4.11: Analysis of variance (ANOVA) for Hardness

Source	DF	Seq SS	Contribution	Adj SS	Adj MS	F-Value	P-Value
Welding Current	1	12060	31.24%	12060	12060.2	32.1	0.005
Wire feed rate	1	7211	18.68%	7211	7210.7	19.19	0.012
Gas flow rate	1	4108	10.64%	4108	4108.2	10.93	0.03
Welding speed	1	13728	35.56%	13728	13728.2	36.53	0.004
Error	4	1503	3.89%	1503	375.8		
Total	8	38610	100.00%				

R-Sq = 96.11%, R-Sq (adj) = 92.21%, F0.05, 1, 8 = 5.32

All of the parameters had a very significant effect on hardness because the F-value in the ANOVA table 4.11 was more than the F-critical. The hardness of MIG-welded 316 stainless steel and AISI 4140 low alloy steel sheets with a thickness of 3 mm was significantly affected by the welding speed percentage (35.56%), welding current (31.24%), wire feed rate (18.68%), and gas flow rate (10.64%) as shown in figure 4.16 below. The ANOVA analysis, including p-values, indicates that the percentage of contribution from all parameters significantly impacts the hardness (P < 0.05). The R-squared value, which measures the model's fit to the data, is 96.11% according to table 4.18, indicating a strong fit.

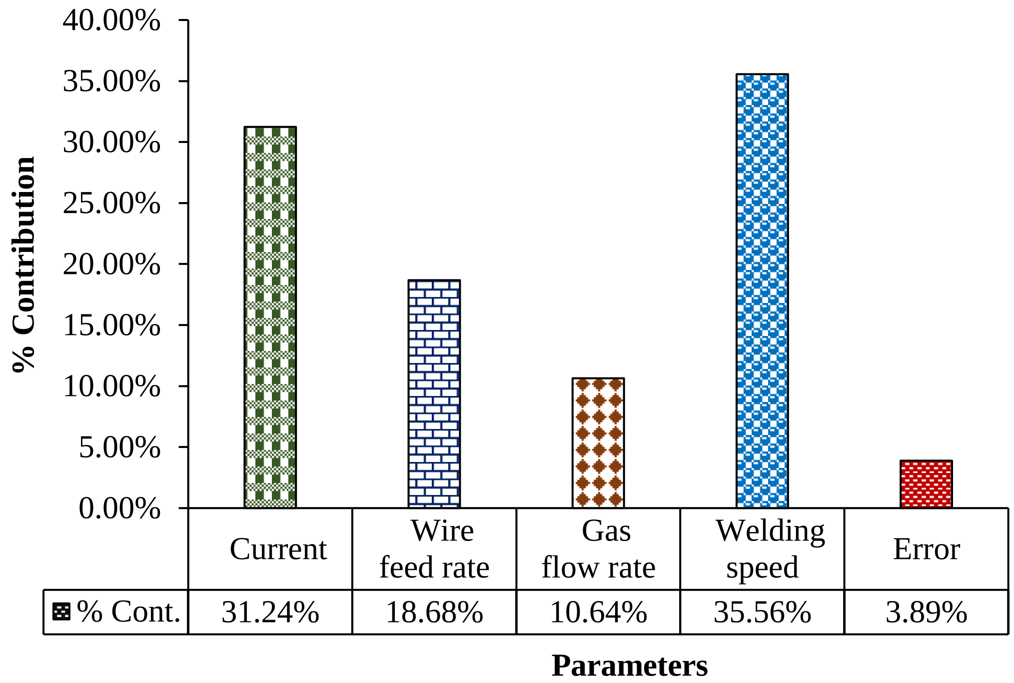

Figure 4.16: Percentage contribution of parameters for hardness

The errors in statistical models are believed to be regularly distributed in the design of experiments. A normal probability plot of the residuals is used to evaluate the importance of

effects. If the residuals fall along a straight line on the plot, they have a normal distribution. The data points in Figure 4.17 are pretty near to the fitted normal distribution line. The residuals' normal probability plots reveal that they are pretty near to the normal probability lines. Furthermore, the p-value (0.105) in Figure 4.8 is larger than 0.05, indicating that the residuals are normally distributed and that the variables in the regression models are both significant and appropriate (Ghangas et al., 2022).

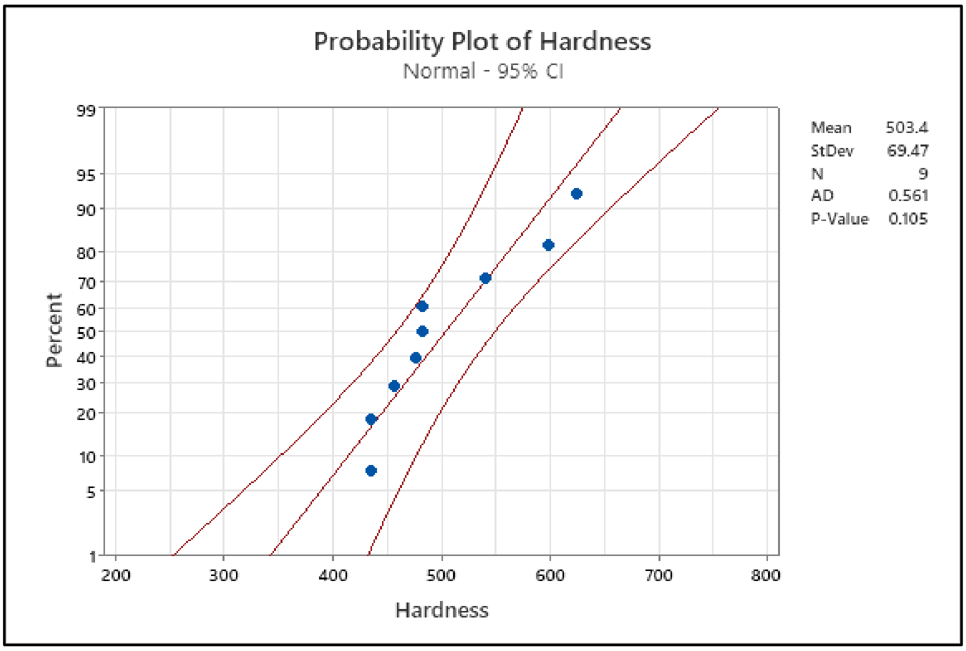

Figure 4.17: The normal probability plot for hardness

4.6.3 Flexural Strength Result Analysis

The maximum bending force was obtained via a four -point bend test performed on a universal testing machine, and flexural strength was calculated using this value and cross-section area. For each testing trial, three readings were taken, and the average result was determined. Table 4.12 displays the mean flexural strength values measured for each trial experiment.

The UTM of the curve's flexural strength test is a measure of the maximum force that may be applied to a material before it starts to deform plastically. The graph demonstrates that as the load grows, so does the material's elongation. This is due to the elastic deformation of the material. However, the material will eventually hit its elastic limit and start to distort plastically. When the force remains constant, the elongation of the material increases. The UTM of the flexural strength of the curve is the point at which the material begins to deform plastically. The maximum force of the metal's elastic limit, which is 600 N, and the maximum force at which the metal deforms plastically at constant force, which is 750 N, are both shown in figure 4.18 below on the force versus maximum change in length curve for sample 7.

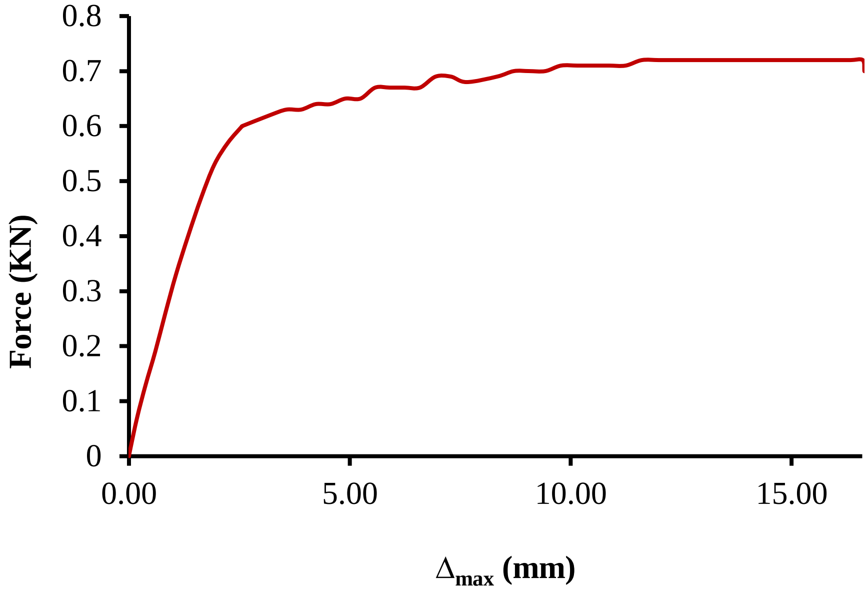

Figure 4.18: Force versus elongation of sample 7

Table 4.12: Flexural strength test result

Sample No	Welding Current (A)	Wire feed rate (B)	Gas flow rate	Welding speed (D)	Flexural strength (Mpa)	Signal to noise ratio
1	110	7	7	20	788	57.9305
2	110	10.5	9	30	556	54.9015
3	110	14	11	40	455	53.1602
4	125	7	9	40	698	56.8771
5	125	10.5	11	20	766	57.6845
6	125	14	7	30	727	57.2307
7	140	7	11	30	831	58.3920
8	140	10.5	7	40	756	57.5704
9	140	14	9	20	811	58.1804

4.5.3.1. Mean response analysis of flexural strength

Table 4.13 reveals that the highest value is for welding current (A) at level 3, followed by welding speed (C) at level 1, wire feed rate (B) at level 1, and gas flow rate (C) at level 1. These welding settings (A3B1C1D1) were chosen as the first parametric setup for MIG-welding of stainless steel 316 to AISI 4140 low alloy steel with a thickness of 3 mm. This implies that it is possible to use that as a parameter combination to produce larger, better results.

Table 4.13: Response table for means of Flexural Strengths

Level	Welding Current (A)	Wire feed rate (B)	Gas flow rate (C)	Welding speed (D)
1	599.7	**772.3**	**757**	**788.3**
2	730.3	692.7	688.3	704.7
3	**799.3**	664.3	684	636.3
Delta	199.7	108	73	152
Rank	**1**	**3**	**4**	**2**

Because the response is larger the better, the major influence plot for control parameters for mean hardness value is essentially the same as the main effects plot for SN ratios, therefore the impacts of the factors on hardness are evaluated from the main effect plot for SN ratios.

4.5.3.2. Signal to noise ratio analysis for flexural strength

As demonstrated in Table 4.14, the most important element is welding current weight% (Delta = 2.72; Rank 1st), followed by welding speed (Delta = 2.06; Rank = 2nd) and wire feed rate (Delta = 1.54; Rank = 3rd). The (S/N) ratio is least affected by gas flow rate (Delta = 1.16; Rank = 4th) according to the experimental result. The initial ideal parameter combination for increasing the flexural strength of MIG-welded 316 stainless steel with AISI 4140 low alloy steel sheets was A3B1C1D1 based on the larger-the-better flexural strength characteristic.

Table 4.14: Response table for signal-to-noise ratios of Flexural Strengths (larger is better)

Level	Welding Current (A)	Wire feed rate (B)	Gas flow rate (C)	Welding speed (D)
1	55.33	**57.73**	**57.58**	**57.93**
2	57.26	56.72	56.65	56.84
3	**58.05**	56.19	56.41	55.87
Delta	2.72	1.54	1.16	2.06
Rank	**1**	**3**	**4**	**2**

4.5.3.3. Effect of process parameters on flexural strength

The effects of welding factors on flexural strength are shown in Figure 4.18, as well as the ideal values for each rank. The optimal values for maximizing flexural strength, according to the analysis and the primary effect plot graph for the S/N ratios, are current at level three

(140A), wire feed rate at level one (7cm/s), gas flow rate at level one (7 CFH), and welding speed at level one (20cm/min), with an initial parametric setting of A3B1C1D1. The welding current weight % had the biggest impact on improving flexural strength when compared to other welding variables, while the gas flow rate had the least. As the current climbs from level one to level three, as shown in the graph below, the flexural strength increases correspondingly. The material's flexural strength decreases as the wire feed rate increases from level one to level three. The other element was the gas flow rate; as the gas flow rate increased from one to three, the flexural strength reduced dramatically. The second most critical welding attribute was the welding speed; as welding speed rises from level one to level three the flexural strength decreases (Pratiwi et al., 2023) observed the same investigation as welding speed rises from level one to level two flexural strength increase.

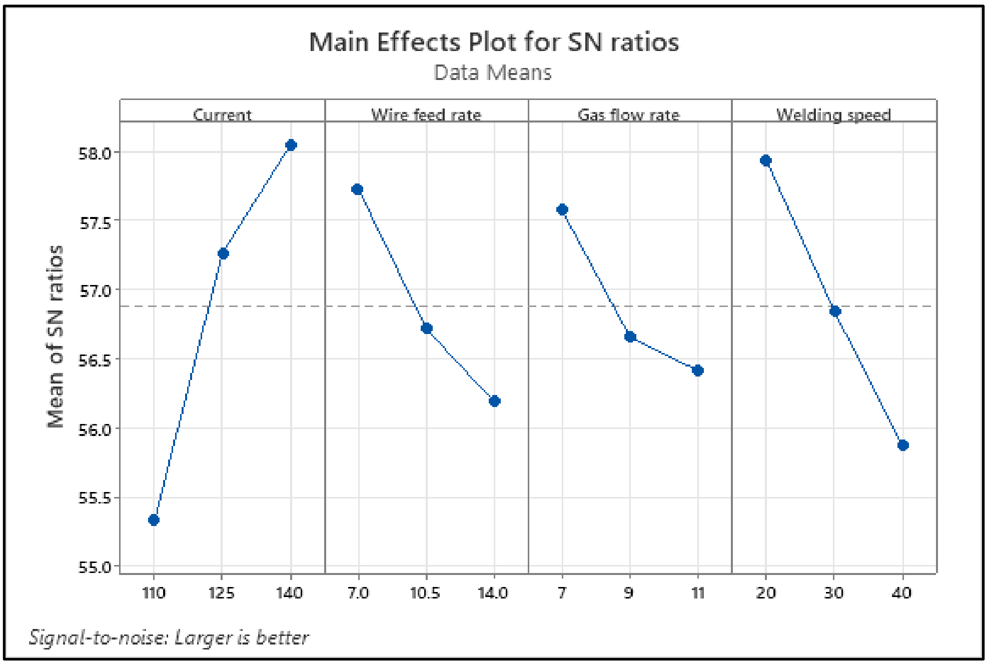

Figure 4.19: Main effect plot for the signal-to-noise ratios for Flexural Strength

4.5.3.4. Analysis of Variance (ANOVA) for flexural strength

Table 4.15 shows how ANOVA was used to evaluate the appropriateness of the developed models. The model is inadequate within the confidence limit according to this technique since the calculated value of the F-ratio of the developed model was less than the standard F-ratio (F-table value 5.32) value at the intended level of confidence of 95%.

Table 4.15: Analysis of variance (ANOVA) for Flexural Strength

Source	DF	Seq SS	Contribution	Adj SS	Adj MS	F-Value	P-Value
Current	1	59800	47.71%	59800	59800	44.25	0.003
Wire feed rate	1	17496	13.96%	17496	17496	12.95	0.023
Gas flow rate	1	7994	6.38%	7994	7994	5.91	0.072
Welding speed	1	34656	27.65%	34656	34656	25.64	0.007
Error	4	5406	4.31%	5406	1351		
Total	8	125352	100.00%				

R-Sq = 95.69%, R-Sq (adj) = 91.37%, F0.05, 1, 8 = 5.32

According to the experimental results, all parameters had a substantial effect on flexural strength since F-critical = 5.32 is less than the F-ratio. The welding current (47.71%), welding speed (27.65%), and wire feed rate (13.96%) have a highly significant impact, while the gas flow rate (6.38%) has a significant impact on the flexural strength of MIG-welded 316 stainless steel and AISI 4140 low alloy steel sheets as shown in figure 4.19 below.

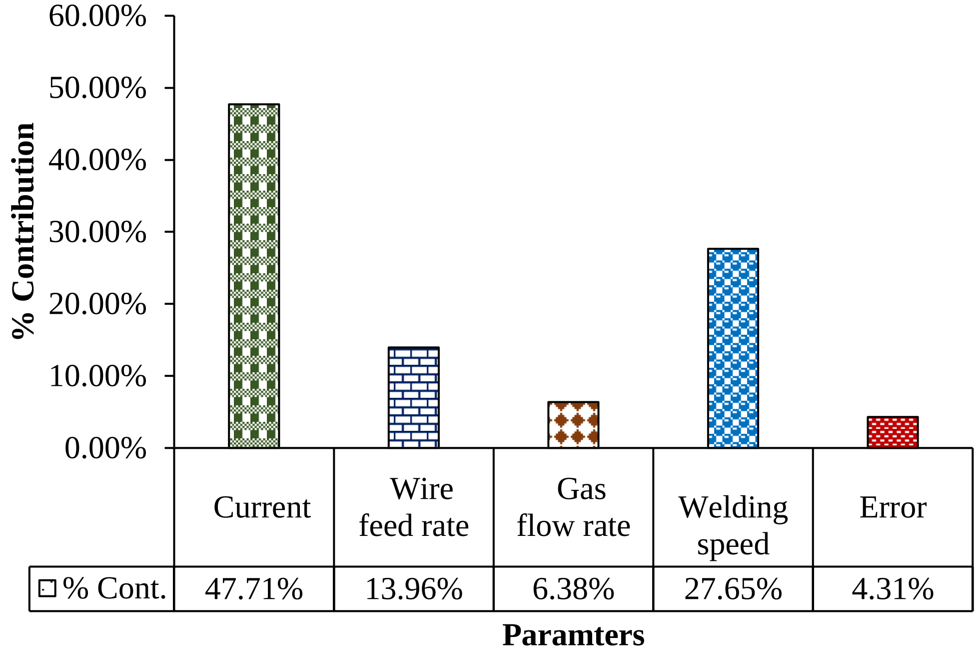

Figure 4.20: Percentage contribution of parameters for flexural strength

The errors in statistical models are believed to be regularly distributed in the design of experiments. A normal probability plot of the residuals is used to evaluate the importance of effects. If the residuals fall along a straight line on the plot, they have a normal distribution.

The data points in Figure 4.20 are pretty near to the fitted normal distribution line. The residuals' normal probability plots reveal that they are pretty near to the normal probability lines. Furthermore, the p-value (0.065) in Figure 4.8 is larger than 0.05, indicating that the residuals are normally distributed and that the variables in the regression models are both significant and appropriate (Ghangas et al., 2022).

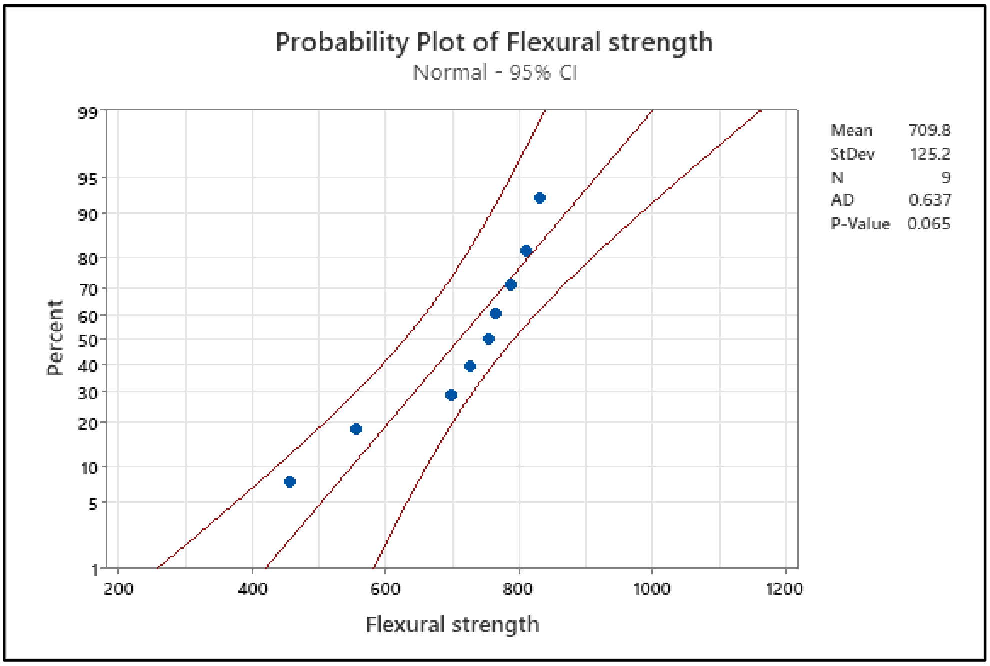

Figure 4.21: The normal probability plot for flexural strength

4.6.4 Percentage of surface defect analysis (POSD)

While welding, the occurrence of defects is a common issue that can have a negative impact on the quality of the weld. Therefore, it is important to minimize defects as much as possible. In this study, surface defects are evaluated using liquid penetrant testing, and the samples are subjected to various tests in order to measure the size of the defects. The percentage of defects at a particular parameter level is then calculated by comparing the surface area of the defects to the surface area of the weld zone. Percentage of defects for each samples are calculated and listed in the table 4.16 below.

Table 4.16: Percentage of surface defects test result

Sample No	Welding Current (A)	Wire feed rate (B)	Gas flow rate (C)	Welding speed (D)	POSD	Signal noise ratio
1	110	7	7	20	1.78	-5.0084
2	110	10.5	9	30	5.246	-14.3966
3	110	14	11	40	6.53	-16.2983
4	125	7	9	40	2.53	-8.06241
5	125	10.5	11	20	1.82	-5.20143
6	125	14	7	30	1.98	-5.9333
7	140	7	11	30	0.25	12.0412
8	140	10.5	7	40	1.1	-0.82785
9	140	14	9	20	0.253	12.0412

4.5.4.1. Mean response analysis of percentage of surface defects

The greatest value in Table 4.17 is welding current (A) at level 3, followed by welding speed (D) at level 1, wire feed rate (B) at level 1, and gas flow rate (C) at level 1. These welding settings (A2B1C1D1) were chosen as the initial parametric setup from the result for dissimilar automated MIG welding stainless steel SS316 to low alloy steel AISI4140 with thickness of 3mm. this implies that using this as parameter combination to create smaller percentage of defects on the surface of the weld but better result is viable. The main influence plot for control parameters for mean percentage of surface defects variations is shown in figure 4.21. In the main effect plot graph of the parameters below, the numerical value at the minimum point in each graph represents the parameter's best value at that level.

Table 4.17: Response table for means of percentage of surface defects

Level	Welding Current (A)	Wire feed rate (B)	Gas flow rate (C)	Welding speed (D)
1	4.5187	**1.52**	**1.62**	**1.2833**
2	2.11	2.722	2.6753	2.492
3	**0.5333**	2.92	2.8667	3.3867
Delta	3.9853	1.4	1.2467	2.1033
Rank	**1**	**3**	**4**	**2**

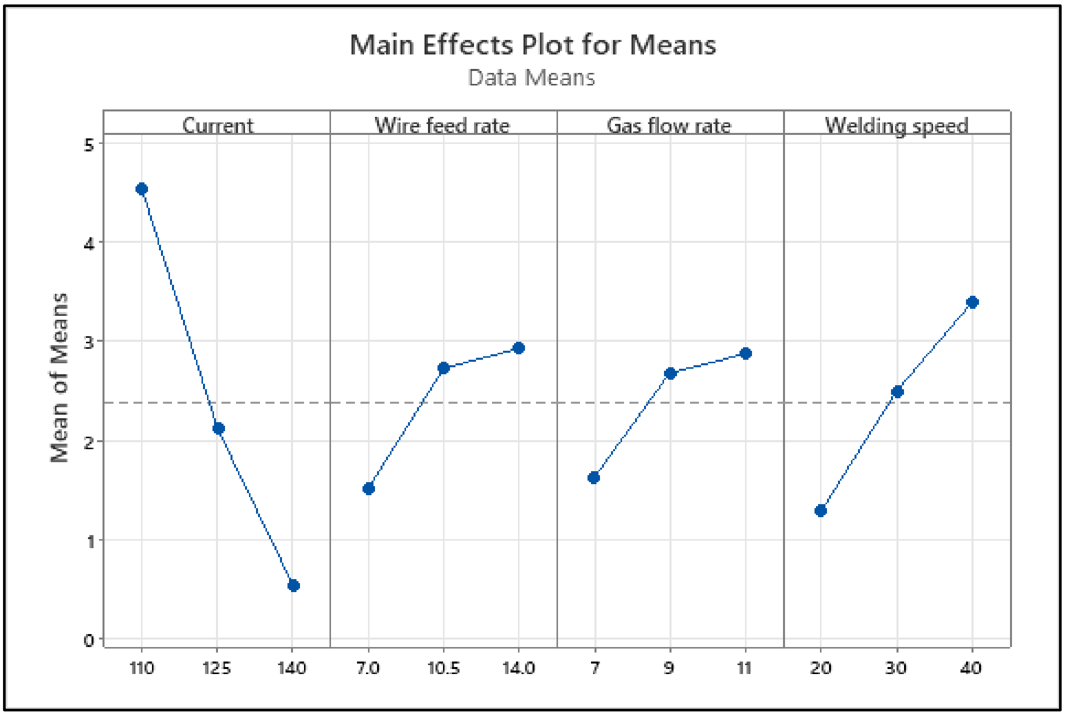

Figure 4.22: Main effect plot for the means of POSD

4.5.4.2. Signal to noise ratio analysis for percentage of surface defects

According to the signal-to-noise ratio value reported in Table 4.18, the welding current weight percentage had the greatest impact (Delta = 19.6526; Rank = 1^{st}), followed by welding speed (Delta = 9.0066; Rank = 2^{nd}), and wire feed rate (Delta = 6.4654; Rank = 3^{rd}). Table 21 shows that the gas flow rate had the least impact on the S/N ratio (Delta = 0.7704; Rank = 4^{th}). The first parameter combination for improving the percentage of surface defects of automated MIG welded SS 316 with AISI 4140 steel sheets is A3B1C3D1.

Table 4.18: Response table for signal-to-noise ratios of POSD (smaller is better).

Level	Welding Current (A)	Wire feed rate (B)	Gas flow rate (C)	Welding speed (D)
1	-11.9011	**-0.3432**	-3.9232	**0.6105**
2	-6.399	-6.8086	-3.4726	-2.7629
3	**7.7515**	-3.3968	**-3.1528**	-8.3962
Delta	19.6526	6.4654	0.7704	9.0066
Rank	**1**	**3**	**4**	**2**

4.5.4.3. Effects of process parameters on the percentage of surface defects

Figure 4.22 shows how welding factors affect percentage of surface defects, as well as the best values for each factor based on their rank. According to the study and principal effect plot graph for signal-to-noise ratios, the ideal parameters for minimizing percentage of surface defects are current at level three (140A), wire feed rate at level one (7cm/s), gas flow rate at level three (11CFH), and welding speed at level one (20cm/min). As illustrated in the graph below, the percentage of surface defects reduces as the current increases from level one to level three. The percentage of surface defects rises as the wire feed rate increases from level one to level two, which is undesired. The percentage of surface defects decreases significantly as the wire feed rate increases from level two to level three, and as gas flow rate increase from level one to level three, the percentage of surface defects slightly decreases. The second most critical process parameter was the welding speed; as the welding speed increases from level one to three, the percentage of surface defects increased; (Sheikh AA, 2008) found a similar identification.

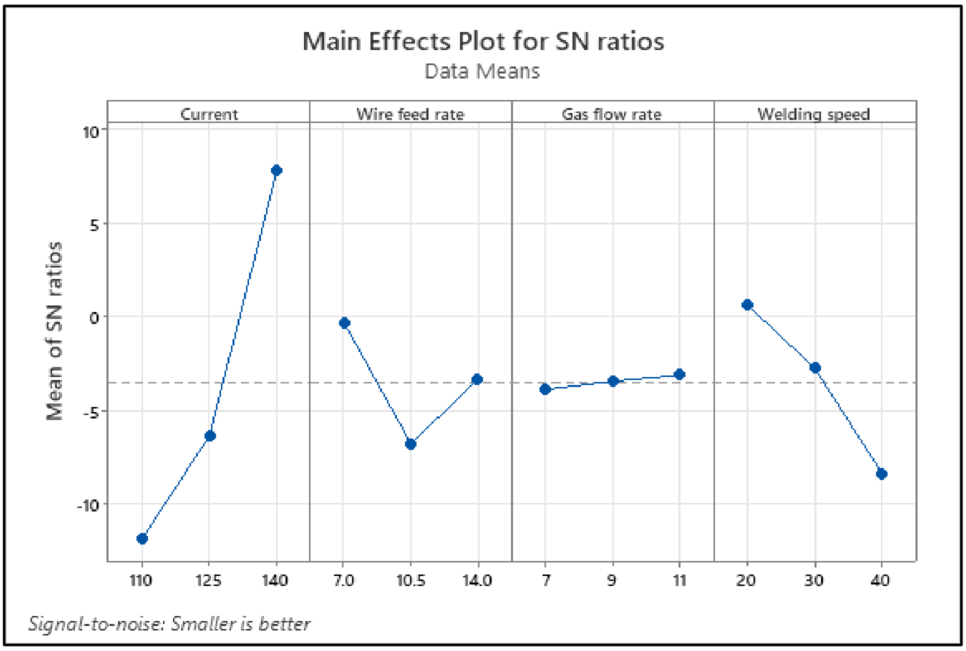

Figure 4.23: Main effect plot for the signal-to-noise ratios for percentage surface defects

4.5.4.4. Analysis of Variance (ANOVA) for percentage of surface defects

Table 4.19 shows how ANOVA was used to evaluate the appropriateness of the developed models. The model is inadequate within the confidence limit according to this technique since the calculated value of the F-ratio of the developed model was less than the standard F-ratio (F-table value 5.32) value at the intended level of confidence of 95%.

Table 4.19: Analysis of variance (ANOVA) for percentage of surface defects

Source	DF	Seq SS	Contribution	Adj SS	Adj MS	F-Value	P-Value
Current	1	23.824	64.38%	23.824	23.8243	74.88	0.001
Wire feed rate	1	2.94	7.95%	2.94	2.94	9.24	0.038
Gas flow rate	1	2.331	6.30%	2.331	2.3313	7.33	0.054
Welding speed	1	6.636	17.93%	6.636	6.636	20.86	0.01
Error	4	1.273	3.44%	1.273	0.3182		
Total	8	37.004	100.00%				

R-Sq = 96.56%, R-Sq (adj) = 92.87%, F0.05, 1, 8 = 5.32

According to the experimental results, all parameters had a substantial effect on percentage of surface defects since F-critical = 5.32 is less than the F-value. The welding current (64.38%), and welding speed (17.93%), have a highly significant impact, while wire feed rate (7.95%), and the gas flow rate (6.30%) have a significant impact on the percentage of surface defects of MIG-welded 316 stainless steel and AISI 4140 low alloy steel sheets as shown in figure 4.23 below.

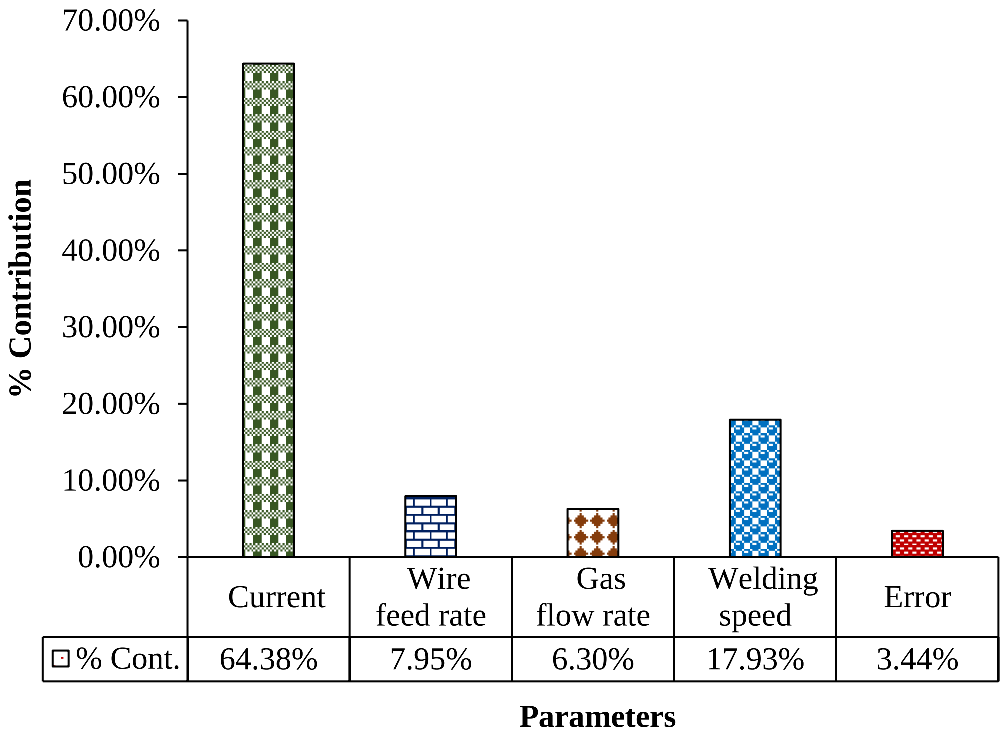

Figure 4.24: Percentage contribution of parameters for percentage of surface defects

The errors in statistical models are believed to be regularly distributed in the design of experiments. A normal probability plot of the residuals is used to evaluate the importance of

effects. If the residuals fall along a straight line on the plot, they have a normal distribution. The data points in Figure 4.8 are pretty near to the fitted normal distribution line. The residuals' normal probability plots reveal that they are pretty near to the normal probability lines. Furthermore, the p-value (0.076) in Figure 4.24 is larger than 0.05, indicating that the residuals are normally distributed and that the variables in the regression models are both significant and appropriate (Ghangas et al., 2022).

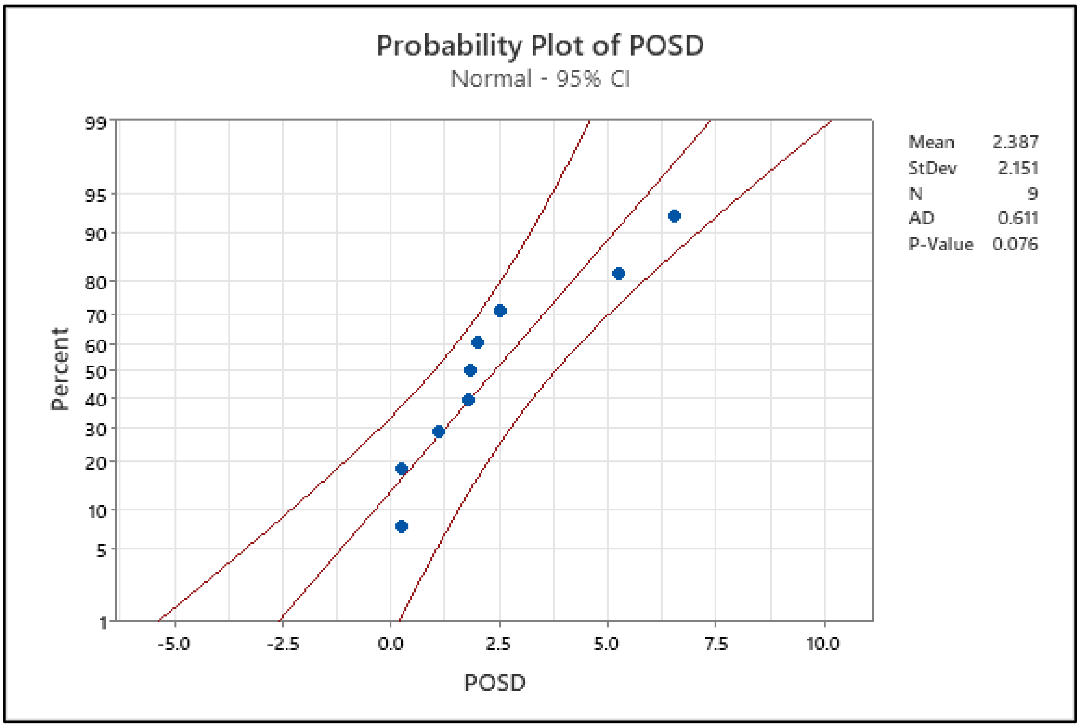

Figure 4.25: The normal probability plot for percentage of surface defects

4.6.5 Bead Width Result Analysis

In order to determine the width of the welded metal bead, a precise measurement was taken using a Vernier calliper with an accuracy of 0.01. Three measurements were taken on each welded specimen and the average value was calculated. The resulting mean bead width geometry values for each sample are presented in Table 4.20. The minimum value of the weld bead width was deemed to be the optimal weld quality, as it reduces the heat-affected zone (HAZ) area and minimizes welding defects. Therefore, a smaller width is considered to be superior.

Table 4.20: The experimental results of mean Bead width

Welding Current (A)	Wire feed rate (B)	Gas flow rate (C)	Welding speed (D)	Bead width (mm)	Signal to noise ratio
110	7	7	20	6.82	-16.6757
110	10.5	9	30	6.8	-16.6502
110	14	11	40	6.79	-16.6374
125	7	9	40	6.7	-16.5215
125	10.5	11	20	7	-16.902
125	14	7	30	7.09	-17.0129
140	7	11	30	6.98	-16.8771
140	10.5	7	40	7	-16.902
140	14	9	20	7.3	-17.2665

4.5.5.1 Mean response analysis of bead width

Table 4.21 depicts welding current (A) at level 1, wire feed rate (B) at level 1, Gas flow rate (C) at level 3, and Welding speed (D) at level 3. From the results of automated MIG-welding stainless steel 316 to AISI 4140 low alloy steel with a thickness of 3 mm, these welding settings (A1B1C3D23) were chosen as the first parametric configuration. This means that it is possible to use this as a parameter combination to produce smaller but better results.

Table 4.21: Response table for means of Bead Widths

Level	Welding Current (A)	Wire feed rate (B)	Gas flow rate (C)	Welding speed (D)
1	**6.803**	**6.833**	6.97	7.04
2	6.93	6.933	6.933	6.957
3	7.093	7.06	**6.923**	**6.83**
Delta	0.29	0.227	0.047	0.21
Rank	**1**	**2**	**4**	**3**

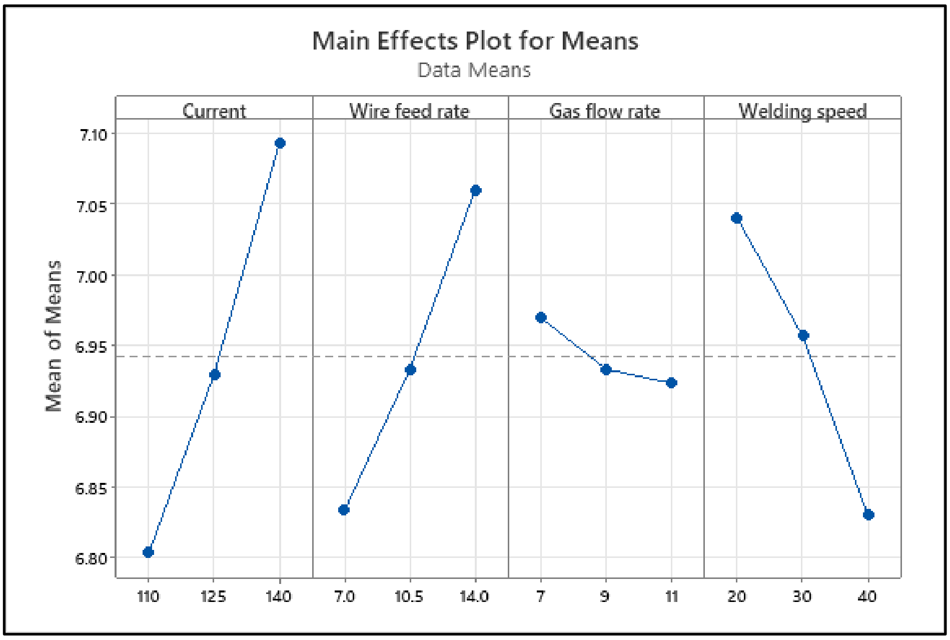

Figure 4.26: main effect plot for means of bead width

The numerical figure at the lowest point in each graph in the main effect plot graph of figure 4.25 above shows the parameter's best value at that level. They also display the best settings within the parameters of the experiment. When compared to other welding variables, the welding current weight % has the greatest impact on bead width, followed by the wire feed rate and welding speed respectively. Welding current (110A) at level one, wire feed rate (7 cm/s) at level one, gas flow rate (11CFH) at level three, and welding speed (40cm/min) at level three were the most effective settings.

4.5.5.2. Signal to noise ratio analysis for bead width

According to the signal-to-noise ratio value reported in Table 21, the welding current weight percentage had the greatest impact (Delta = 0.36; Rank = 1st), followed by wire feed rate (Delta = 0.28; Rank = 2nd), and welding speed (Delta = 0.26; Rank = 3rd). Table 4.22 shows that the gas flow rate had the least impact on the S/N ratio (Delta = 0.06; Rank = 4th).

Table 4.22: Response table for signal-to-noise ratios of Bead Widths (smaller is better)

Level	Welding Current (A)	Wire feed rate (B)	Gas flow rate (C)	Welding speed (D)
1	**-16.65**	**-16.69**	-16.86	-16.95
2	-16.81	-16.82	-16.81	-16.85
3	-17.02	-16.97	**-16.80**	**-16.69**
Delta	0.36	0.28	0.06	0.26
Rank	**1**	**2**	**4**	**3**

4.5.5.3. Effect of process parameters on bead width

Figure 4.26 shows how welding factors affect bead width, as well as the best values for each factor based on their rank. According to the study and principal effect plot graph for signal-to-noise ratios, the ideal parameters for minimizing bead width are at the initial parametric setting of **A1B1C3D3**. As illustrated in the graph below, the weld's bead width increases as the current increases from level one to level three (Assefa et al., 2022) found a similar identification. The width of the weld rises as the wire feed rate increases from level one to level three, which is undesired, and the wire feed rate at level one was the best flow for the smallest bead width. As the gas flow rate increases from level one to level two, the bead width decreases. Similarly as the gas flow rate rises from level two to level three, the bead width increase slightly. As the welding speed increases from level one to level three, the bead width decreases

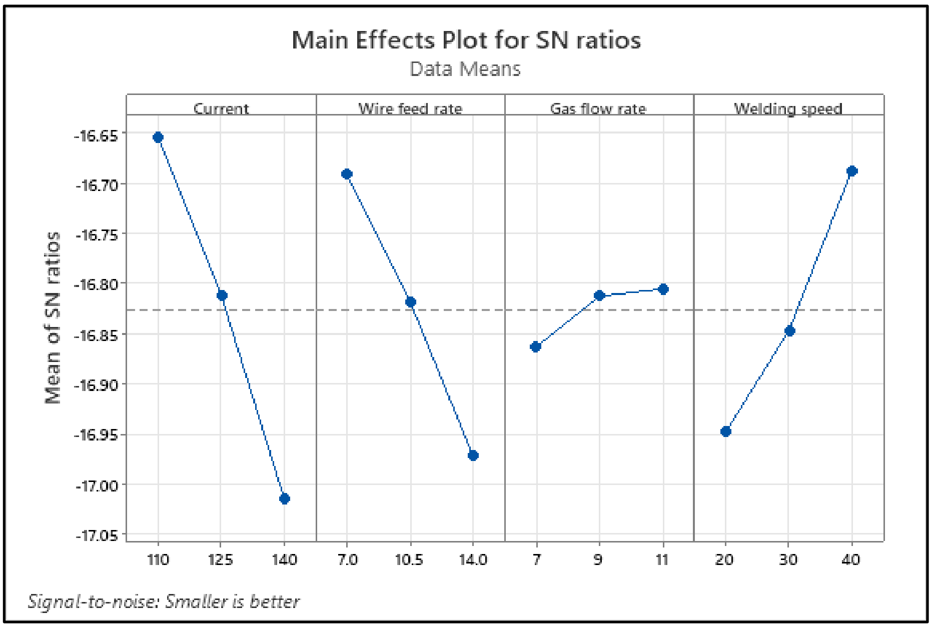

Figure 4.27: Main effect plot for the signal-to-noise ratios for bead width

4.5.5.4. Analysis of Variance (ANOVA) for bead width

Table 4.23 shows how ANOVA was used to evaluate the appropriateness of the developed models. The model is inadequate within the confidence limit according to this technique since the calculated value of the F-ratio of the developed model was less than the standard F-ratio (F-table value 5.32) value at the intended level of confidence of 95%.

Table 4.23: Analysis of variance (ANOVA) for bead width

Source	DF	Seq SS	Contribution	Adj SS	Adj MS	F-Value	P-Value
Current	1	0.12615	45.88%	0.12615	0.12615	217.29	0
Wire feed rate	1	0.077067	28.03%	0.077067	0.077067	132.75	0
Gas flow rate	1	0.003267	1.19%	0.003267	0.003267	5.63	0.077
Welding speed	1	0.06615	24.06%	0.06615	0.06615	113.94	0
Error	4	0.002322	0.84%	0.002322	0.000581		
Total	8	0.274956	100.00%				

R-Sq = 99.16%, R-Sq (adj) = 98.31%, F0.05, 1, 8 = 5.32

According to the experimental results, all parameters had a substantial effect on percentage of surface defects since F-critical = 5.32 is less than the F-value. The welding current (45.88%), wire feed rate (28.03%), and welding speed (24.06%), have a highly significant impact, while, and the gas flow rate (1.19%) has a least significant impact on the bead width of MIG-welded 316 stainless steel and AISI 4140 low alloy steel sheets as shown in figure 4.27 below.

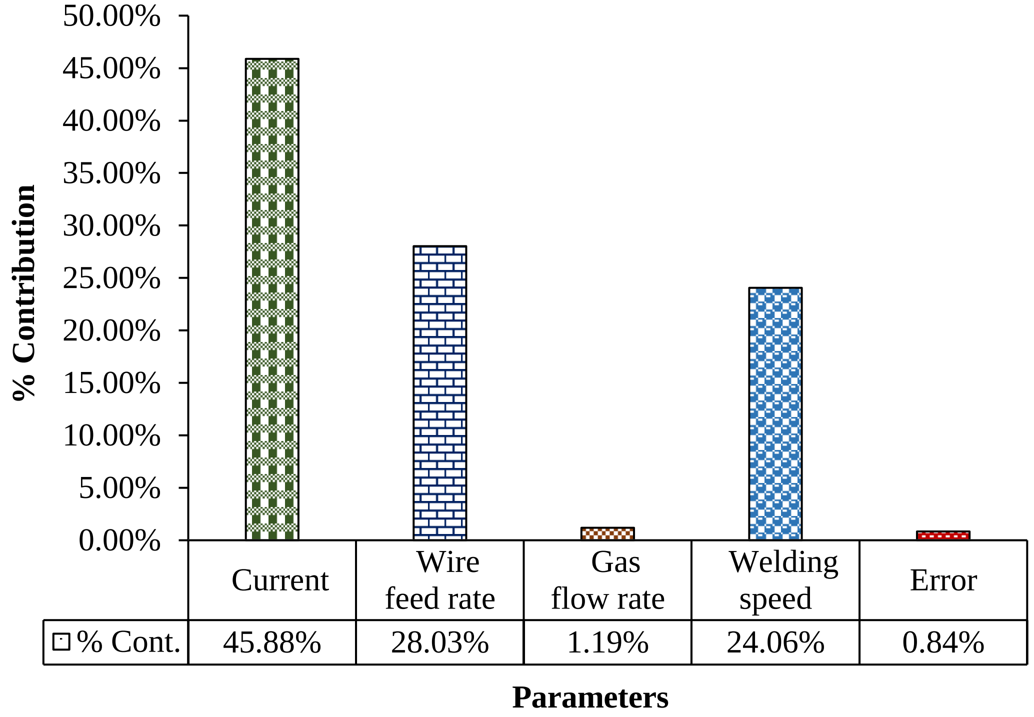

Figure 4.28: percentage contribution of parameters for bead width

The errors in statistical models are believed to be regularly distributed in the design of experiments. A normal probability plot of the residuals is used to evaluate the importance of

effects. If the residuals fall along a straight line on the plot, they have a normal distribution. The data points in Figure 4.28 are pretty near to the fitted normal distribution line. The residuals' normal probability plots reveal that they are pretty near to the normal probability lines. Furthermore, the p-value (0.440) in Figure 4.8 is larger than 0.05, indicating that the residuals are normally distributed and that the variables in the regression models are both significant and appropriate (Ghangas et al., 2022).

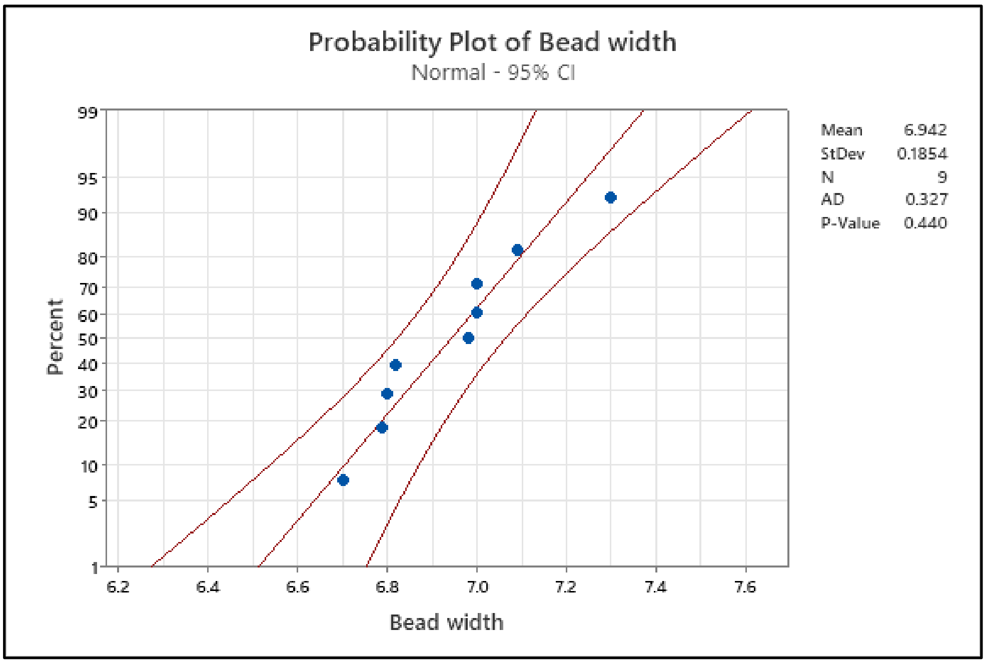

Figure 4.29: The normal probability plot for bead width

4.7 Multi-Response Optimization parametric optimization

Nowadays, multi-response optimization has become more beneficial for industries than single-response optimization. The focus of this study is to examine the impact of automated MIG welding parameters on various responses using a multi-objective technique called Grey relational analysis (GRA).

4.7.1 Grey Relational Analysis (GRA)

Step 1: Transformation of data into S/N ratios

Table 4.24: Experimental results and S/N ratio of response values

Sample No	Experimental result					S/N ratio				
	Tensile strength	Flexural strength	Hardness	Bead width	POSD	Tensile strength	Flexural strength	Hardness	Bead width	POSD
1	613	788	482	6.82	1.78	55.749	57.930	53.661	-16.676	-5.008
2	575	556	435	6.8	5.246	55.193	54.901	52.769	-16.650	-14.396
3	516	455	456	6.79	6.53	54.253	53.160	53.179	-16.637	-16.298
4	602	698	599	6.7	2.53	55.591	56.877	55.548	-16.521	-8.062
5	609	766	435	7	1.82	55.692	57.684	52.769	-16.902	-5.201
6	599	727	482	7.09	1.98	55.548	57.230	53.661	-17.012	-5.933
7	636	831	541	6.98	0.25	56.069	58.392	54.663	-16.877	12.041
8	612	756	625	7	1.1	55.735	57.570	55.917	-16.901	-0.828
9	632	811	476	7.3	0.25	56.014	58.180	53.552	-17.266	12.041

Step 2: Normalization of S/N values

Normalization of S/N values is the generation of grey relational within 0 and 1. If the response in the original sequence is larger is better, then it is normalized using Eq. (3.6), and smaller is better, then Eq. (3.7) is used for normalization.

Table 4.25: Normalized data of the experimental results

Sample No	**Normalized S/N ratio**				
	Tensile strength	Flexural strength	Hardness	Bead width	POSD
1	0.823839922	0.911790056	0.283102904	0.206979169	0.601620419
2	0.517778681	0.33282434	0	0.172736794	0.932895769
3	0	0	0.13009395	0.15557782	1
4	0.737239248	0.710441113	0.882755538	0	0.709385705
5	0.792529903	0.864779599	0	0.510717568	0.608431688
6	0.713346167	0.778024023	0.283102904	0.659670173	0.63425702

7	1	1	0.601738043	0.477356973	0
8	0.816031613	0.842963084	1	0.510717568	0.454103641
9	0.969825841	0.959554323	0.248538705	1	0

Step 3: Computation of grey relational coefficient (GRC)

Grey relational coefficient (GRC) determined using Eq. (2.8)

Table 4.26: Deviation sequence and Grey relational coefficient with $\partial = 0.5$

Sample No	Deviation sequence					GRC						
	Tensile Strength	Flexural strength	Hardness	Bead width	POSD	Tensile strength	Flexural strength	Hardness	Bead width	POSD	GRG	**Rank**
1	0.176	0.088	0.716	0.793	0.398	0.739	0.850	0.561	0.589	0.556	0.659	**7**
2	0.482	0.667	1	0.827	0.067	0.509	0.498	0.589	0.778	0.881	0.651	**8**
3	1	1	0.869	0.844	0	0.333	0.333	0.364	0.571	1	0.584	**9**
4	0.262	0.289	0.117	1	0.290	0.655	0.633	0.810	0.333	0.632	0.682	**5**
5	0.207	0.135	1	0.489	0.391	0.706	0.787	0.333	0.505	0.560	0.689	**4**
6	0.286	0.221	0.716	0.340	0.365	0.635	0.692	0.410	0.595	0.577	0.678	**6**
7	0.030	0.040	0.751	0	1	0.943	0.925	0.399	1	0.333	0.720	**1**
8	0.183	0.157	0	0.489	0.545	0.731	0.760	1	0.505	0.478	0.693	**3**
9	0	0	0.398	0.522	1	1	1	0.556	0.488	0.533	0.715	**2**

From table 4.26 above rank 1 is selected as initial parametric setting for better multi response was welding current at (140A), wire feed rate at (7cm/s), gas flow rate at (11CFH), and welding speed at (30cm/min) as shown in the table 4.27.

Table 4.27: Initial predicted parametric setting

Initial setting	**Tensile strength (MPa)**	**Hardness (HV)**	**Flexural strength (MPa)**	**Bead width (mm)**	**Percentage of surface defects (%)**	**GRG**
A3B1C3D1	636	541	831	6.98	0.25	0.720

4.7.2 Optimization of Process Parameters for Grey Relational Grade

Taguchi Signal-to-Noise (S/N) ratios, which are logarithmic functions of the desired output, serve as objective functions for optimization and aid in data interpretation and prediction of optimal outcomes. The Taguchi approach investigates GRG response variance using the Mean and signal-to-noise (S/N) ratio.

4.6.2.1. Analysis of S/N Ratio for Grey Relational Grade

To measure and characterize the hardness, the statistics formula of the larger, the better has been used. In the case of larger is the better, the ratio of signal noise can be given by equation (3.4).

Table 4.28: Signal to Noise Ratios for GRG for larger is better

Level	Welding Current (A)	Wire feed rate (B)	Gas flow rate (C)	Welding speed (D)
1	-4.007	**-3.268**	-3.394	**-3.253**
2	-3.312	-3.383	**-3.323**	-3.319
3	**-2.983**	-3.651	-3.585	-3.73
Delta	1.024	0.383	0.262	0.477
Rank	**1**	**3**	**4**	**2**

As demonstrated in Table 4.28, the most important element is welding current weight% (Delta = 1.024; Rank 1st), followed by Welding speed (Delta = 0.477; Rank = 2nd) and wire feed rate (Delta = 0.383; Rank = 3rd). The (S/N) ratio is least affected by gas flow rate (Delta = 0.262; Rank = 4th) according to the experimental result. The initial ideal parameter combination for increasing the GRG of multi response for MIG-welded 316 stainless steel with AISI 4140 low alloy steel sheets was **A3B1C2D1** based on the larger-the-better.

4.6.2.2. Effect of process parameters on GRG

The effects of welding factors on multi responses are shown in Figure 4.29, as well as the ideal values for each rank. The optimal values for maximizing GRG, according to the analysis and the primary effect plot graph for the S/N ratios, are current at level three (140A), wire feed rate at level one (7cm/s), gas flow rate at level two (9CFH), and welding speed at level one (20cm/min), with an initial parametric setting of A3B1C2D1. The welding current weight % had the biggest impact on improving GRG when compared to other welding variables. As the current climbs from level one to level three, as shown in the graph below, the GRG increases correspondingly. The GRG decreases as the wire feed rate increases from level one to level three. The other element was the gas flow rate; as the gas flow rate increased from one to two, the GRG was increased and then reduced as gas flow rate was increases from level two to three. As welding speed rises from level one to level three the GRG decreases.

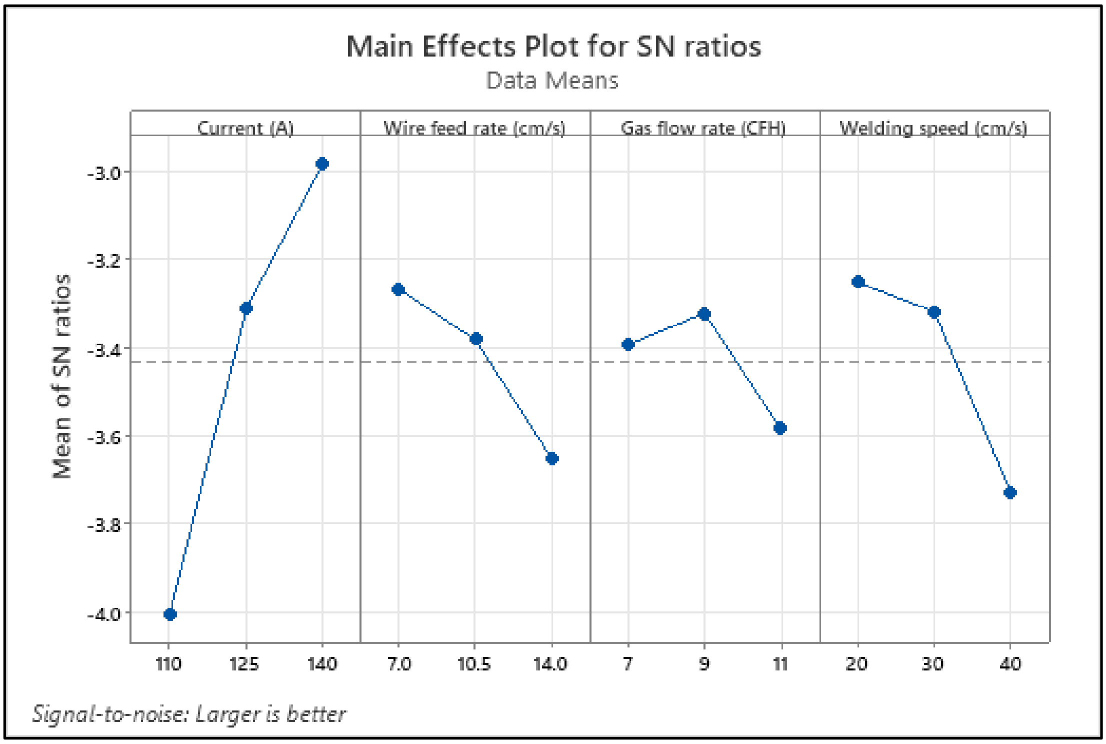

Figure 4.30: Main effect plot for the signal-to-noise ratios for GRG

4.6.2.3. Analysis of Variance (ANOVA) for GRG

Table 4.29 shows how ANOVA was used to evaluate the appropriateness of the developed models. The model is inadequate within the confidence limit according to this technique since the calculated value of the F-ratio of the developed model was less than the standard F-ratio (F-table value 5.32) value at the intended level of confidence of 95%.

Table 4.29: Analysis of variance (ANOVA) for GRG

Source	DF	Seq SS	Contribution	Adj SS	Adj MS	F-Value	P-Value
Current (A)	1	0.009146	68.50%	0.009146	0.009146	37.66	0.004
Wire feed rate (cm/s)	1	0.001149	8.61%	0.001149	0.001149	4.73	0.095
Gas flow rate (CFH)	1	0.000224	1.67%	0.000224	0.000224	0.92	0.392
Welding speed (cm/s)	1	0.001862	13.94%	0.001862	0.001862	7.67	0.05
Error	4	0.000971	7.27%	0.000971	0.000243		
Total	8	0.013351	100.00%				

R-Sq = 92.73 %, R-Sq (adj) = 85.45%, F0.05, 1, 8 = 5.32

According to the experimental results, all parameters had a substantial effect on GRG since F-critical = 5.32 is less than the F-ratio except the wire feed rate and gas flow rate has no significant effect on GRG since, with F-value of 4.73 and 0.92 < 5.32 respectively. The welding current (68.50%), welding speed (13.94%), have a highly significant impact, and wire feed rate (8.61%) has a least significant impact, while the gas flow rate (1.67%) has a no significant impact on the GRG of MIG-welded 316 stainless steel and AISI 4140 low alloy steel sheets as shown in the figure 4.30.

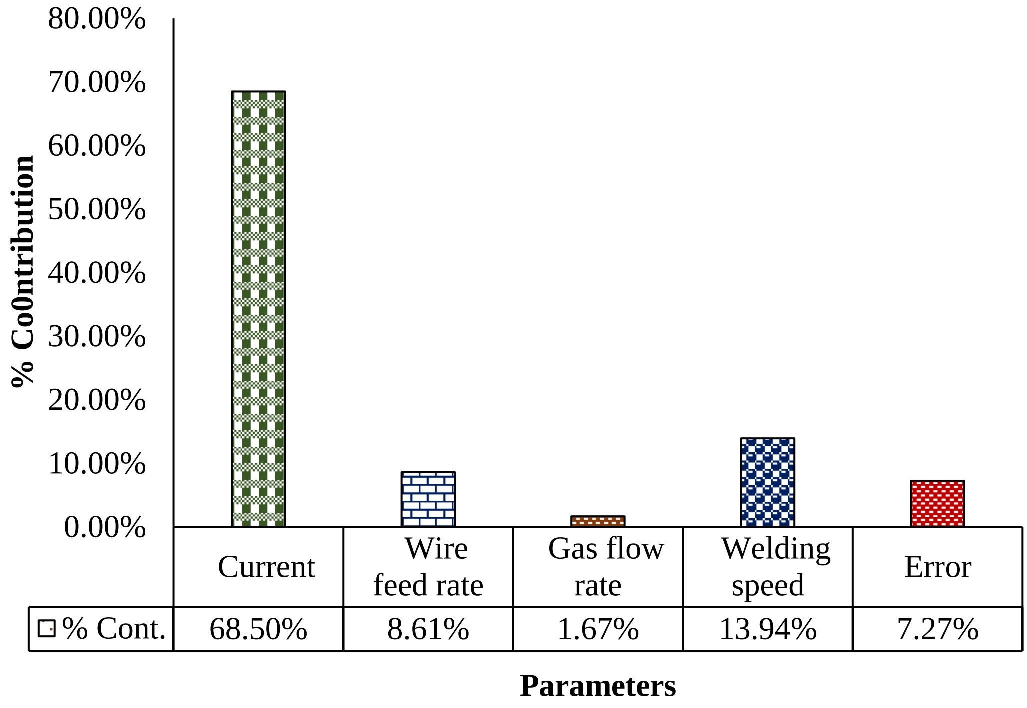

Figure 4.31: Percentage contribution of parameters for GRG

The errors in statistical models are believed to be regularly distributed in the design of experiments. A normal probability plot of the residuals is used to evaluate the importance of effects. If the residuals fall along a straight line on the plot, they have a normal distribution. The data points in Figure 4.8 are pretty near to the fitted normal distribution line. The residuals' normal probability plots reveal that they are pretty near to the normal probability lines. Furthermore, the p-value (0.221) in Figure 4.31 is larger than 0.05, indicating that the residuals are normally distributed and that the variables in the regression models are both significant and appropriate (Ghangas et al., 2022).

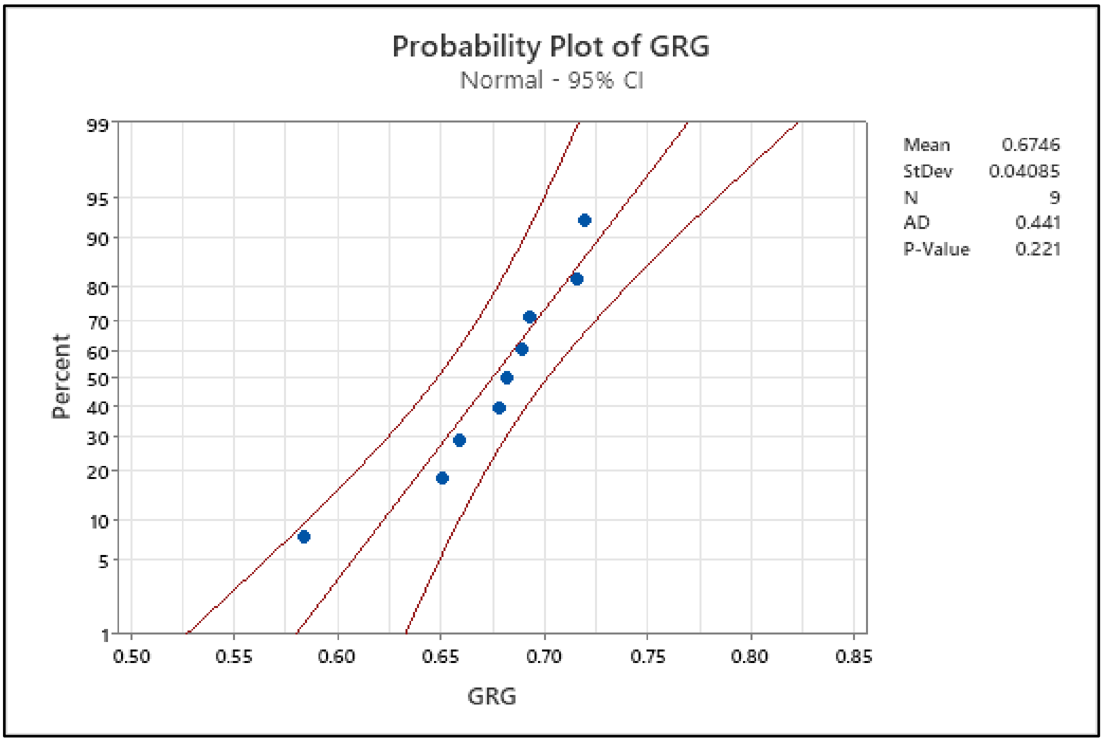

Figure 4.32: The normal probability plot for GRG

After analyzing the percentage of surface defects on several welding samples and evaluating them based on specific criteria, it was determined that sample number 2 and sample number 3 did not meet the required standards as they had surface defect percentages of 5.24% and 6.53%, respectively. Additionally, these two samples exhibited lower tensile and flexural strength when compared to the other samples. This suggested that as the percentage of surface defects increased, the welding's tensile and flexural strength decreased. On the other hand, sample number 7 had the lowest percentage of surface defects among all the samples evaluated and demonstrated high tensile and flexural strength.

4.8 Confirmation Test

After the experimental optimization, a confirmation test was necessary to validate the optimized parametric configuration. As a result, the confirmation was performed at the Ethiopian Technical Institute's Engineering Center of Excellence's welding training center. The results of the confirmation tests coincided with the projected optimum parametric setting result with a percent of improvement from initial condition around 7.78%, as shown in Table 4.30.

Table 4.30: Comparison Summary of confirmatory experiments

	Initial Condition	Confirmatory Experiment Results GRG	Improvement from Initial Condition (%) GRG
Tensile Strength (MPa)	636	675.3	6.18
Flexural strength (MPa)	831	895	7.70
Hardness (HV)	541	598.5	10.63
Bead width (mm)	6.98	6.52	6.60
POSD (%)	0.25	0.23	8.0
Optimal Condition	**A3B1C3D2**	**A3B1C2D1**	
Grey Relational Grade	0.720	0.776	7.78

CHAPTER FIVE

CONCLUSION AND RECOMENDATION

5.1 Conclusion

In this work, welding variables such welding current, gas flow rate, wire feed rate, and welding speed were examined and optimized for automated metal inert gas welding with regard to dissimilar steels (SS316 and AISI 4140). Using a Taguchi L9 orthogonal array and the signal-to-noise ratio approach to examine the experimental findings, each parameter's effect was determined using ANOVA. To examine their effects on mechanical, corrosion resistance of the weld zone, and microstructural features, as well as bead size, and percentage of surface defects, GRA was used to perform multi-response optimizations of the input parameters. As a result of the experimental results, the following conclusions were reached:

- Nondestructive testing was performed using LPT to detect welding defects, and problems such as porosity, lack of fusion, and small crack were detected in a different samples. For the acceptability of these samples they are evaluated according to International welding criteria AWS D1 and ASME VII.
- Due to a moderate heat input and moderate cooling rate, the weld zone of sample number 7's welded material showed a very thin skeletal ferrite along the grain, sub-grain, and migration boundaries in the plain austenitic matrix. Due to very low welding heat inputs, i.e., high cooling rates, sample number 3 had δ-ferrite in the form of dendritic lathy-ferrite in the dendrite core surrounded by an inter-dendritic γ–phase.
- The corrosion behavior of the welded joints was evaluated using an electrochemical test. The analysis included the base metal, heat-affected zone, and weld zone. The heat-affected zone of low alloy steel AISI 4140 showed the lowest corrosion resistance because low alloy steel 4140 contains a lower amount of chromium and nickel and is exposed to heat. It was observed that the corrosion rate of the weld zone is the corrosion rate of 0.15233 m/year which is 38.04% higher than that of the 316 stainless-steel base, 12.84% lower than that of the 316 stainless-steel HAZ, 41.30% lower than that of the AISI 4140 HAZ, and 17.30% lower than that of the AISI 4140 base, The weld zone is composed of stainless steel SS316 with 18% Cr, filler metal ER 309L with 23% Cr, and low alloy steel 4140 with 1% Cr. The presence of chromium in these materials enhances the corrosion resistance of the weld.

- A higher tensile strength of 636MPa was obtained by parametrically combining 140A welding current, 7cm/s wire feed rate, 11CFH gas flow rate, and 30cm/s welding speed. According to ANOVA, welding current and welding speed were the two factors that had the greatest impact on tensile strength.
- 140A welding current, 10.5cm/s wire feed rate, 7CFH gas flow rate, and 40cm/s welding speed were used in a parametric configuration to produce a maximum hardness of 625HV. An analysis of variance (ANOVA) revealed that welding current was the second-most important factor for hardness after welding speed.
- A parametric setup of 140A welding current, 7cm/s wire feed rate, 11CFH gas flow rate, and 30cm/min welding speed resulted in a maximum flexural strength of 692. Welding current, followed by welding speed, was found to be the most crucial component in flexural strength by analysis of variance (ANOVA).
- Minimum percentage of surface defects of 0.25% was achieved at a parametric combination of 140A welding current, 7cm/s wire feed rate, 11CFH gas flow rate, and 30cm/min welding speed. Analysis of variance (ANOVA) shows welding current was the most significant parameter for percentage of surface defects followed by welding speed.
- To achieve a minimum weld width of 6.21 mm, a parametric combination of 125A welding current, 7cm/s wire feed rate, 9CFH gas flow rate, and 40cm/min welding speed was employed. An analysis of variance (ANOVA) revealed that welding current, followed by welding speed, was the factor that had the greatest impact on weld width.
- According to the GRA optimization results, and confirmatory experiment all responses was improved from the initial value to the optimum parametric setting, which increased UTS from 636 MPa to 675.3 MPa (6.18%), hardness from 541 HV to 598.5 HV (10.63%), flexural strength from 831 MPa to 895 MPa (7.7%), bead width from 6.98 mm to 6.52 mm (6.60%), and overall Grey relational grade from 0.720 to 0.776 (7.78%). (**A3B1C2D1**), this set of parameters was compatible with the confirmation test's findings.

5.2 Recommendation and Scope for Future Work

The following recommendation and scope for future work are made based on the study's findings and conclusion.

- Investigate the effects of pre-weld heat treatment on the properties of welded joints produced by automated MIG welding, particularly in relation to the joint interface area, and Utilize post-weld heat treatment to improve the properties of welded joints produced by automated MIG welding, particularly those involving dissimilar metals such as SS 316 and AISI 4140.
- Automated MIG welding of SS 316 with AISI 4140 was employed in this study, and it can be extended to other materials, particularly those with differing thicknesses and unique material properties to investigate the effect of welding parameters on the mechanical and microstructural properties.
- Based on the research conducted on Automated Metal Inert Gas welding of Stainless Steel SS 316 with Low alloy Steel AISI 4140, it is recommended that industries such as aerospace, automotive, and marine consider the optimal welding process parameters of welding current 140A, wire feed rate 7cm/s, gas flow rate 9CFH, and welding speed 20cm/min.
- Only four welding parameters were studied in this thesis: welding current, wire feed rate, gas flow rate, and welding speed. Future research could investigate the effects and analysis of welding voltage, root gap, welding angle, shielding gases, base metal thickness, electrode size and types interaction effect of them during automated MIG welding of SS 316 with AISI 4140.
- The focuses of these experiments was on the effects of welding parameters on mechanical and microstructural properties of dissimilar metals, but this can further investigated using Robotics-assisted AMIG welding and ATIG welding.

SPECIAL ACKNOWLEDGEMENT

This research work is funded by Adama Science and Technology University under the grant number ASTU/SM-R/916/23, Adama, Ethiopia.

REFERENCES

AISI 316 (S31600) Stainless Steel MakeItFrom. (n.d.).

Akinlabi, S. A., Mashinini, M. P., Abima, C. S., Fatoba, O. S., & Akinlabi, E. T. (2019). TIG & MIG hybrid welded steel joint: A review. *Proceedings of the International Conference on Industrial Engineering and Operations Management*, *April*, 801–811.

American Iron and Steel Institute. (1988). Welding of Stainless Steels and Other Joining Methods. *NiDI and Aisi*, 1–46.

American National Standard Structural Welding. (2020). Aws D1 .1/D1 .1 M:2020. In *Structural Welding Code—Steel, ANSI/ AWS D1.1*.

Ampaiboon, A., Lasunon, O. U., & Bubphachot, B. (2015). Optimization and Prediction of Ultimate Tensile Strength in Metal Active Gas Welding. *Scientific World Journal*, *2015*. https://doi.org/10.1155/2015/831912

Assefa, A. T., Ahmed, G. M. S., Alamri, S., Edacherian, A., Jiru, M. G., Pandey, V., & Hossain, N. (2022). Experimental Investigation and Parametric Optimization of the Tungsten Inert Gas Welding Process Parameters of Dissimilar Metals. *Materials*, *15*(13). https://doi.org/10.3390/ma15134426

AWS. (2000). *Welding Inspection Handbook*. 256.

Bharath, P., Sridhar, V. G., & Senthil Kumar, M. (2014). Optimization of 316 stainless steel weld joint characteristics using taguchi technique. *Procedia Engineering*, *97*, 881–891. https://doi.org/10.1016/j.proeng.2014.12.363

Bhardwaj, B. (2017). To Study The Effects of Welding Parameters on MIG Welding of Stainless Steel Alloy-202. *International Journal of Science Technology and Engineering*, *4*(1), 131–140.

Catalogue, P. (n.d.). *WE SHAPE THE FUTURE OF WELDING AND CUTTING . 10*.

Chaudhari, R., & Ingle, A. (2019). An empirical research on dissimilar metal weld of sa335 p11and sa312 tp304 formed by metal inert gas (Mig) welding. *International Journal of Recent Technology and Engineering*, *8*(2), 5008–5012. https://doi.org/10.35940/ijrte.B1079.078219

Chavda, S. P., Desai, J. V, & Patel, T. M. (2014). *Parametric Optimization of MIG Welding using Taguchi's DOE-FEA Hybrid Modelling for AISI 1045*. *3*(4), 209–219.

Deeksha Narwariya, & Dr. Pradeep Khanna. (2020). To Investigate the Effects of Process Parameters on Welding Current of a MIG Welding Power Source. *International Journal of Engineering Research And*, *V9*(05), 185–188. https://doi.org/10.17577/ijertv9is050180

Embrittlement of Steels | Properties and Selection: Irons, Steels, and High-Performance Alloys | Handbooks | ASM International. (n.d.).

https://dl.asminternational.org/handbooks/book/16/chapter-abstract/250376/Embrittlement-of-Steels?redirectedFrom=fulltext

Engineering, M. (2014). *the Effects of Welding Parameters on Butt Joints Using*. *6*(June), 988–994.

Erl, A. W. S. A., & Carolina, N. (n.d.). *Inweld 309L*. 94621.

Esme, U., Bayramoglu, M., Kazancoglu, Y., & Ozgun, S. (2009). Optimization of weld bead geometry in TIG welding process using grey relation analysis and Taguchi method. *Materiali in Tehnologije*, *43*(3), 143–149.

Gandy, D. (2007). Carbon Steel Handbook. *Carbon*, *3*(3), 172.

Garcia, D. N., Ferraresi, V. A., & Da Mota, C. A. M. (2020). Metallurgical and mechanical behaviors of 309l-si and ernicrmo-3 dissimilar weld on ASTM A182 F22 steel. *Materials Research*, *23*(3). https://doi.org/10.1590/1980-5373-MR-2019-0680

Ghangas, G., Singhal, S., Dixit, S., Goyat, V., & Kadiyan, S. (2022). Mathematical modeling and optimization of friction stir welding process parameters for armor-grade aluminium alloy. *International Journal on Interactive Design and Manufacturing*. https://doi.org/10.1007/s12008-022-01000-1

Gill, D., & Pradhan, M. K. (2022). A Review on Advances in Friction Welding of Dissimilar Metals. *Lecture Notes in Mechanical Engineering*, *38*(1), 181–197. https://doi.org/10.1007/978-981-19-0676-3_15

Gopalsamy, B. M., Mondal, B., & Ghosh, S. (2009). Taguchi method and anova: An approach for process parameters optimization of hard machining while machining hardened steel. *Journal of Scientific and Industrial Research*, *68*(8), 686–695.

Hein, P. R. G., & Brancheriau, L. (2018). Comparison between three-point and four-point flexural tests to determine wood strength of Eucalyptus specimens. *Maderas: Ciencia y Tecnologia*, *20*(3), 333–342. https://doi.org/10.4067/S0718-221X2018005003401

Honarbakhsh-Raouf, A., & Ghazvinloo, H. R. (2010). Influence of wire feeding speed, welding speed and preheating temperature on hardness and microstructure of weld in RQT 701-British steel produced by FCAW. *Indian Journal of Science and Technology*, *3*(5), 588–591. https://doi.org/10.17485/ijst/2010/v3i5/29760

Hultquist, G., & Leygraf, C. (1980). Materials Science and Eng. *Materials Science and Engineering: A*, *42*(1), 181.

Ibrahim, I. A., Mohamat, S. A., Amir, A., & Ghalib, A. (2012). *The Effect of Gas Metal Arc Welding (GMAW) processes on different welding parameters*. *41*(Iris), 1502–1506. https://doi.org/10.1016/j.proeng.2012.07.342

Johnson, L. (2022). *How to Calculate Flexural Strength | Sciencing*. https://sciencing.com/calculate-flexural-strength-5179141.html

Karna, S. K. (2016). *An Overview on Taguchi Method An Overview on Taguchi Method*. *August*, 10–17.

Kiran, B., Nagaraju, D., Selvaraj, S. K., & Molla, B. (2022). Experimental and Mathematical Studies for Optimality of GTAW Parameters on Similar and Dissimilar Steel Substrates. *Advances in Materials Science and Engineering*, *2022*. https://doi.org/10.1155/2022/5118566

Krishnaiah, K., & Shahabudeen, P. (n.d.). *APPLIED DESIGN OF EXPERIMENTS AND*.

Kutty, H. (2018). *Analysis and Optimization of Parameters of Dissimilar Metal Welding*. *4*(9), 10–15.

Lohse, M., Trautmann, M., Füssel, U., & Rose, S. (2020). *Influence of the CO 2 Content in Shielding Gas on the Temperature of the Shielding Gas Nozzle during GMAW Welding*.

Mani, C., Karthikeyan, R., & Vincent, S. (2018). A study on corrosion resistance of dissimilar welds between Monel 400 and 316L austenitic stainless steel. *IOP Conference Series: Materials Science and Engineering*, *346*(1). https://doi.org/10.1088/1757-899X/346/1/012025

Miao, H., Li, C., He, Q., Zhang, S., Zhang, Y., & Liu, S. (2019). The Effect of Welding Speed on the Micromorphology and Mechanical Properties of Laser-Sealed Vacuum Flat Glazing Joints. *Advances in Materials Science and Engineering*, *2019*. https://doi.org/10.1155/2019/2657810

MIG Welding Basics: Techniques and Tips for Success - Tregaskiss and Bernard. (n.d.). https://www.tregaskiss.com/mig-welding-basics-techniques-and-tips-for-success/

Mvola, B., Kah, P., & Martikainen, J. (2014). Welding of dissimilar non-ferrous metals by GMAW processes. *International Journal of Mechanical and Materials Engineering*, *9*(1), 1–11. https://doi.org/10.1186/s40712-014-0021-8

Nadzam, J., Armao, F., Byall, L., Kotecki, D., & Miller, D. (2014). Gas Metal Arc Welding Product and Procedure Selection. *Tech Rep. C4.200*, 96. www.lincolnelectric.com

Normalized 4140 Cr-Mo Steel MakeItFrom. (n.d.).

Obara, C., Mwema, F. M., Keraita, J. N., Shagwira, H., & Obiko, J. O. (2021). A multi-response optimization of the multi-directional forging process for aluminium 7075 alloy using grey-based taguchi method. *SN Applied Sciences*, *3*(6). https://doi.org/10.1007/s42452-021-04527-2

Pranesh B. Bamankar, Amol Chavan, T. P. (2015). A Review on Parametric Optimization of MIG Welding Parameters by using Various Optimization Techniques. *International Journal of Engineering Technology, Management and Applied Sciences*, *3*(10), 2349–4476.

Pratiwi, D. K., Arifin, A., Gunawan, Mardhi, A., & Afriansyah. (2023). Investigation of Welding Parameters of Dissimilar Weld of SS316 and ASTM A36 Joint Using a Grey-Based Taguchi Optimization Approach. *Journal of Manufacturing and Materials Processing*, *7*(1). https://doi.org/10.3390/jmmp7010039

PRINCIPLES OF MIG WELDING TECHNOLOGY - ppt download. (n.d.). https://slideplayer.com/slide/12841566/

Raissi, S., & Farsani, R. E. (2009). Statistical process optimization Through multi-response surface methodology. *World Academy of Science, Engineering and Technology*, *39*(March), 280–284.

Ramos-jaime, D., López-juárez, I., & Perez, P. (2013). Effect of process parameters on robotic GMAW bead area estimation. *Journal of Materials Processing Tech.*, *7*, 398–405. https://doi.org/10.1016/j.protcy.2013.04.050

Reddy, M. P., William, A. A. S., Prashanth, M. M., Kumar, S. N. S., Ramkumar, K. D., & Arivazhagan, N. (2014). Assessment of mechanical properties of AISI 4140 and AISI 316 dissimilar weldments. *Procedia Engineering*, *75*, 29–33. https://doi.org/10.1016/j.proeng.2013.11.006

Ruiz-Trabolsi, P. A., Chino-Ulloa, A., Miranda-Hernández, J. G., Tadeo-Rosas, R., Carrera-Espinoza, R., Velázquez, J. C., & Hernández-Sánchez, E. (2022). A Comparative Analysis of the Tribological Behavior of Hard Layers Obtained by Three Different Hardened-Surface Processes on the Surface of AISI 4140 Steel. *Crystals*, *12*(2). https://doi.org/10.3390/cryst12020298

S. V. Sapakal, M. T. T. (2012). Parametric Optimization of Mig Welding Using Taguchi Design Method. *International Journal of Advanced Engineering Research and Studies*, *1*(IV), 2–4.

Saurabh Gandhe, E., & Aber ProfDr Wukchaure, Y. Y. (2019). Review for Effects of Different Paran1eters on the Throat Thickness of the 1110 Welded Joints. *I Ijirt I*, *6*(4), 2349–6002.

Sheikh AA, K. P. (2008). Optimization of welding process parameter to minimize defect in welding of sheet. *International Research Journal of Engineering and Technology*, *9001*, 4310. www.irjet.net

Singh, S., & Goyal, S. (2017). *A Review on Optimization of Welding Parameters in Arc Welding Process using Taguchi Parametric Optimization Technique*. *5*(09), 902–907.

Spolenak, R., Kraft, O., & Arzt, E. (1998). Effects of alloying elements on electromigration. *Microelectronics Reliability*, *38*(6–8), 1015–1020. https://doi.org/10.1016/S0026-2714(98)00110-3

Sulphide, M., & Sulphide, M. (2015). *Effects of Mn, P, S, Si & V on the Mechanical Properties of Steel* (pp. 10–11). http://www.leonghuat.com/articles/elements.htm

the R Core Team. (2015). Changes in R. *R Journal*, *7*(2), 293–297.

Wahule, A., & Wasankar, K. (2018). Multi-response Optimization of Process Parameters of TIG Welding for Dissimilar Metals (SS-304 and Fe-410) using Grey Relational Analysis. *International Research Journal of Engineering and Technology*. www.irjet.net

Wang, H., Liu, D., Lippold, J. C., & Daehn, G. S. (2020). Laser impact welding for joining similar and dissimilar metal combinations with various target configurations. *Journal of Materials Processing Technology*, *278*, 116498. https://doi.org/10.1016/J.JMATPROTEC.2019.116498

Wang, L. L., & Lu, F. G. (n.d.). *Experimental Investigation of Gas Metal Arc Welding (GMAW) Process Using Developed Articulator Experimental Investigation of Gas Metal Arc Welding (GMAW) Process Using Developed Articulator*. https://doi.org/10.1088/1757-899X/455/1/012073

Zhang, Y. M., Li, P., Chen, Y., & Male, A. T. (2002). Automated system for welding-based rapid prototyping. *Mechatronics*, *12*(1), 37–53. https://doi.org/10.1016/S0957-4158(00)00064-7

APPENDICES

Appendix 1: Liquid penetrant test report from MIDI

	MANUFACTURING INDUSTRY DEVELOPMENT INSTITUTE MANUFACTURING TECHNOLOGY AND ENGINEERING INDUSTRY RESEARCH AND DEVELOPMENT CENTER	QMS.TM.03A ; Rev. 0
	LIQUID PENETRANT TESTING REPORT	Effective Date: January 2019

Date: 15/05/2023

To: Tajudin Ayub Deko from Adama Science and Technology University
Report No: NDT/PT005/2015
Sub: Liquid Penetrant Test Report for welded LED stand steel structures
Ref No: EALBM/CEO/339/2022

Signature :-	Signature :-	Signature :-

Additional Information:

No.	Part NO	Material type	Indication type and location	Length		Photo	Result	Remarks
1	Sample 1	SS316 with AISI4140 Welded sheet	P & SC	Length -200mm Width – 75mm Thickness – 3mm	D	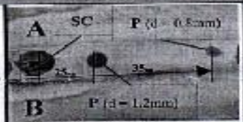	Accepted With POSD = 1.78%	
2	Sample 2	SS316 with AISI4140 Welded sheet	ER, SC & LF	Length -200mm Width – 75mm Thickness – 3mm	D	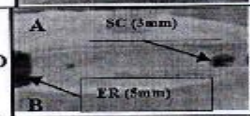	Rejected With POSD = 5.24%	POSD > 5% is rejected
3	Sample 3	SS316 with AISI4140 Welded sheet	SC & BT	Length -200mm Width – 75mm Thickness – 3mm	D	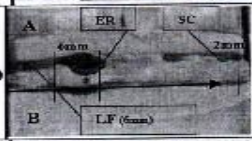	Rejected With POSD = 6.53%	POSD > 5% is rejected
4	Sample 4	SS316 with AISI4140 Welded sheet	SC & LF	Length -200mm Width – 75mm Thickness – 3mm	D	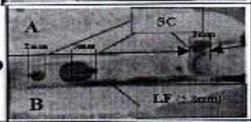	Accepted With POSD = 2.53%	s
5	Sample 5	SS316 with AISI4140 Welded sheet		Length -200mm Width – 75mm Thickness – 3mm	D		Accepted With POSD = 1.82%	
6	Sample 6	SS316 with AISI4140 Welded sheet	LF	Length -200mm Width – 75mm Thickness – 3mm	D		Accepted With POSD = 1.98%	
7	Sample 7	SS316 with AISI4140 Welded sheet		Length -200mm Width – 75mm Thickness – 3mm	D		Accepted With POSD = 0.25%	
8	Sample 8	SS316 with AISI4140 Welded sheet	SC & S	Length -200mm Width – 75mm Thickness – 3mm	D	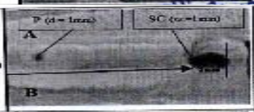	Accepted With POSD = 1.1%	
9	Sample 9	SS316 with AISI4140 Welded sheet		Length -200mm Width – 75mm Thickness – 3mm	D	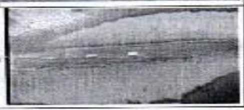	Accepted With POSD = 0.25%	

Note: P: Porosity **LF:** Lack of Fusion **UC:** Undercut **SC:** Crack **CP:** Clustered Porosity **IP:** Incomplete Penetration **S:** Slag **ER:** Excessive reinforcement **POSD:** Percentage of Surface Defects

Tested by	Checked by	Approved by
Name Misgana G/Silase	Name Nardos Mekoya	Name Tewodros Alebachew
Date :- 15/05/2023	Date :- 15/05/2023	Date :- 15/05/2023
Signature :-	Signature :-	Signature :-

Endeshaw Shanko Oumer
Design, Manufacturing, Quality, Standard and Laboratory Development Sector Lead Executive

Appendix 2: Corrosion rate calculation from tafel plot

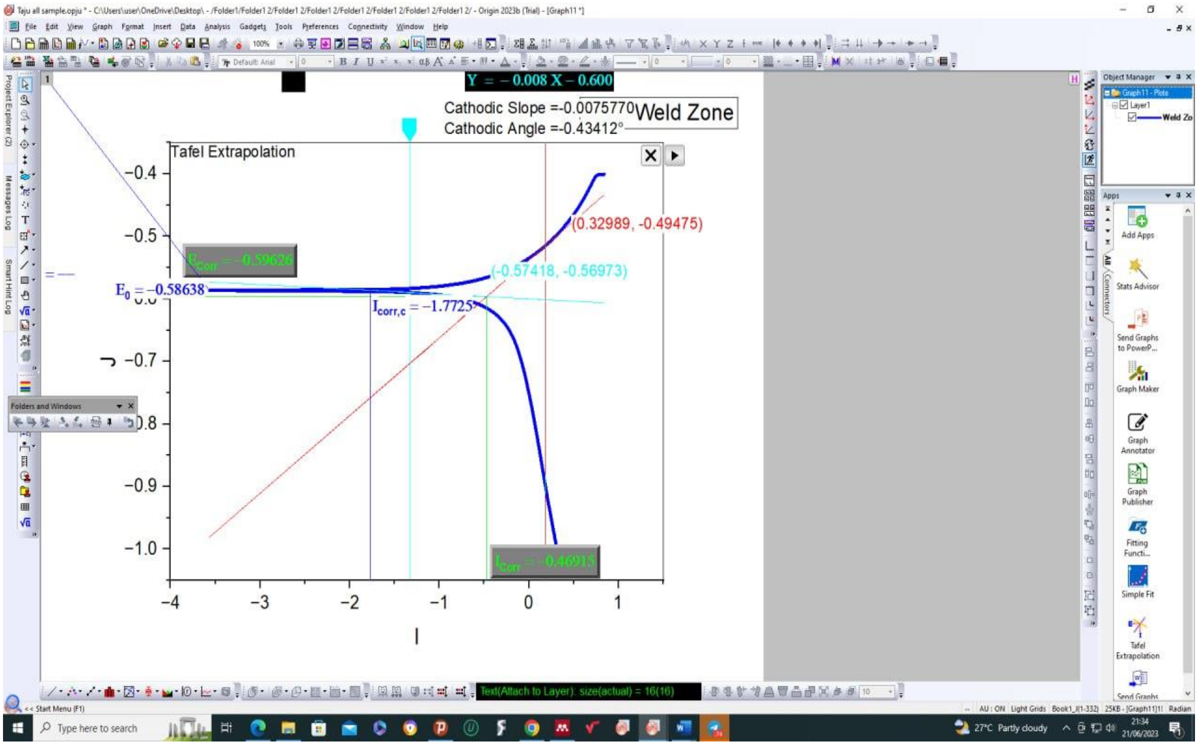

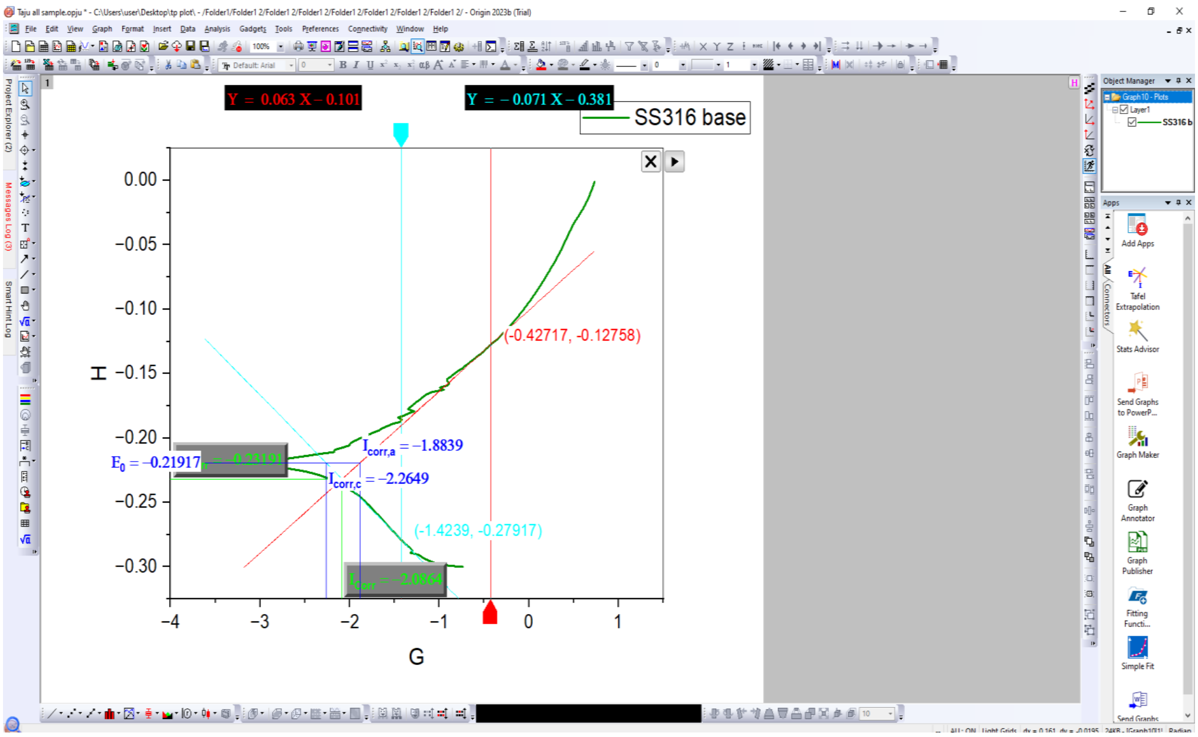

Appendix 3: Micro-Hardness Result for S-1 trial 1 and S-4 trial 2 (From Vickers Hardness)

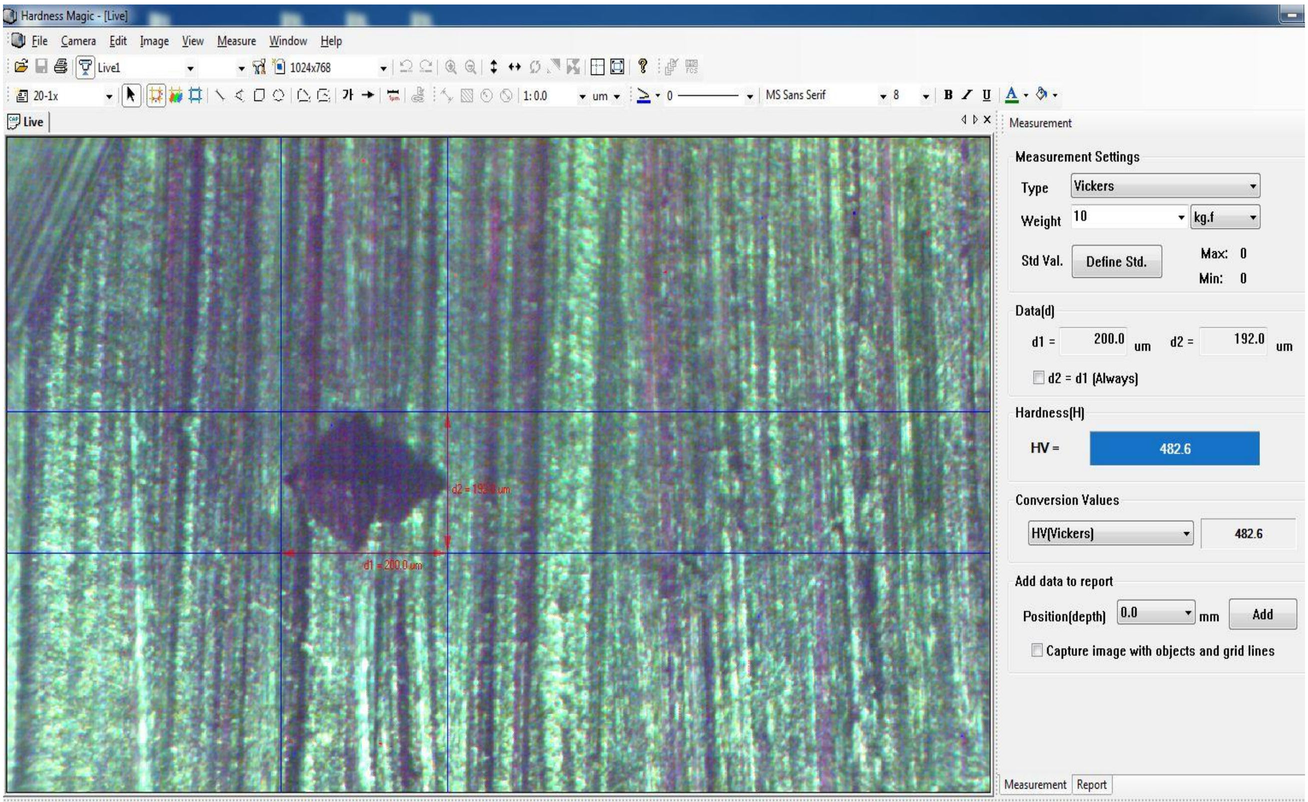

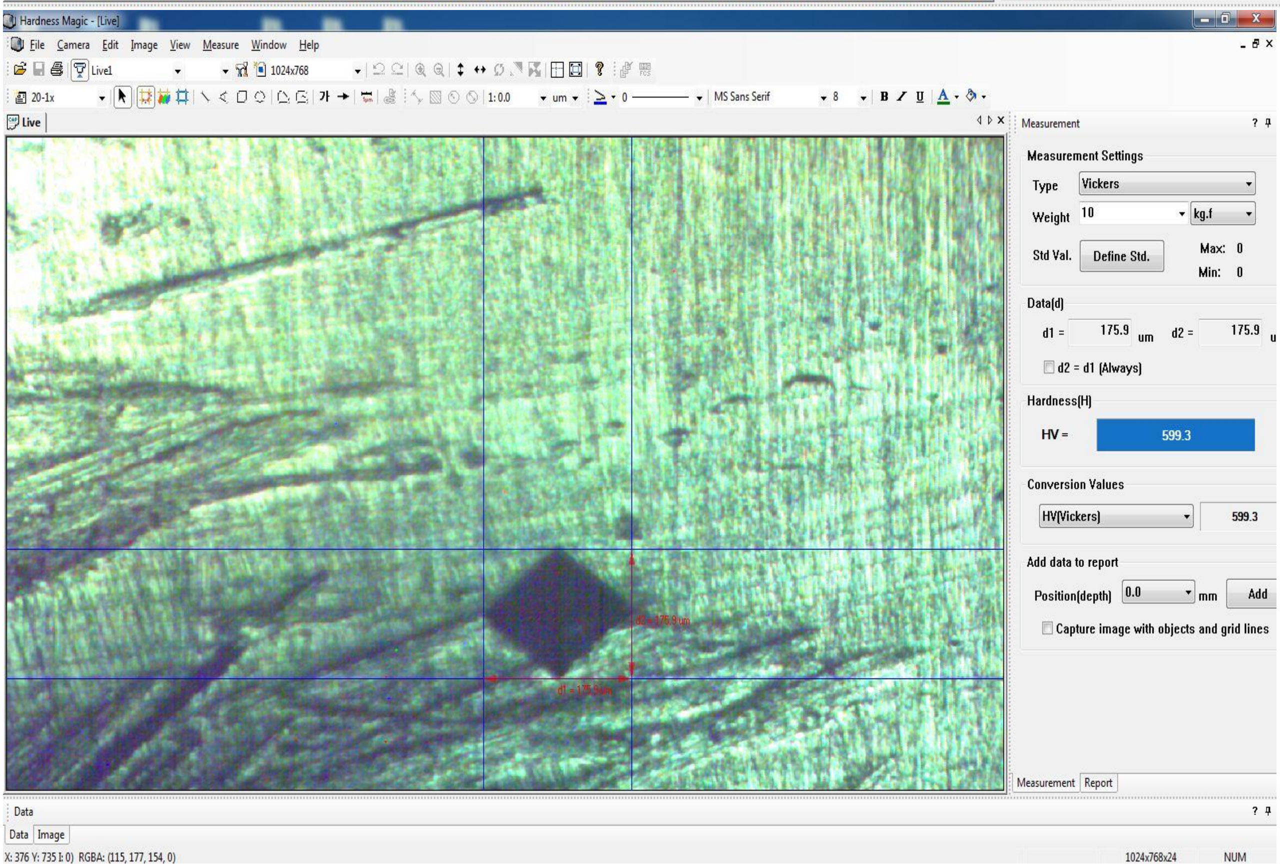

Appendix 4: Tensile Strength Stress- strain graph for Sample-7, Sample-9 and Sample-3 (From UTM)

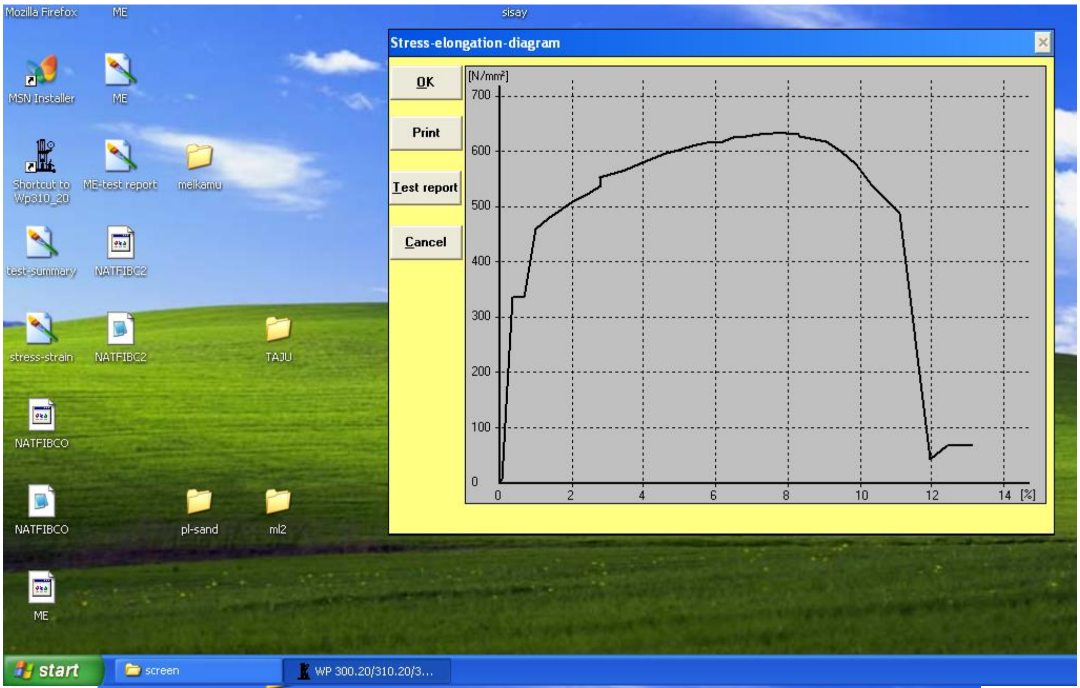

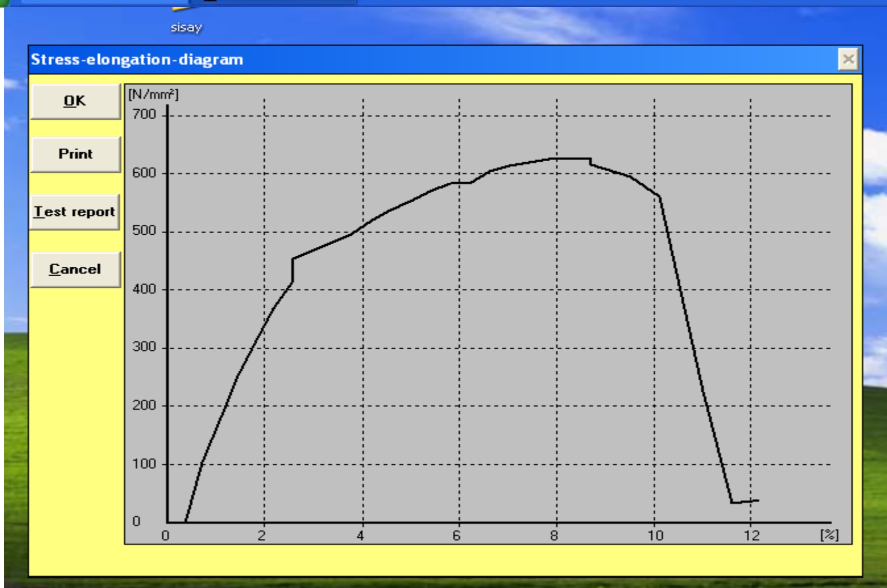

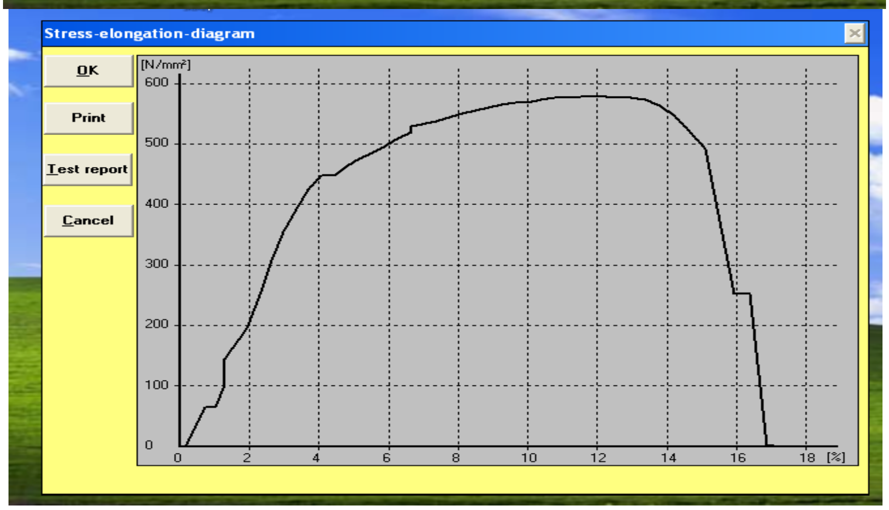

Appendix 5: Flexural Strength Stress- strain graph for Sample-3 and Sample-7 (From UTM)

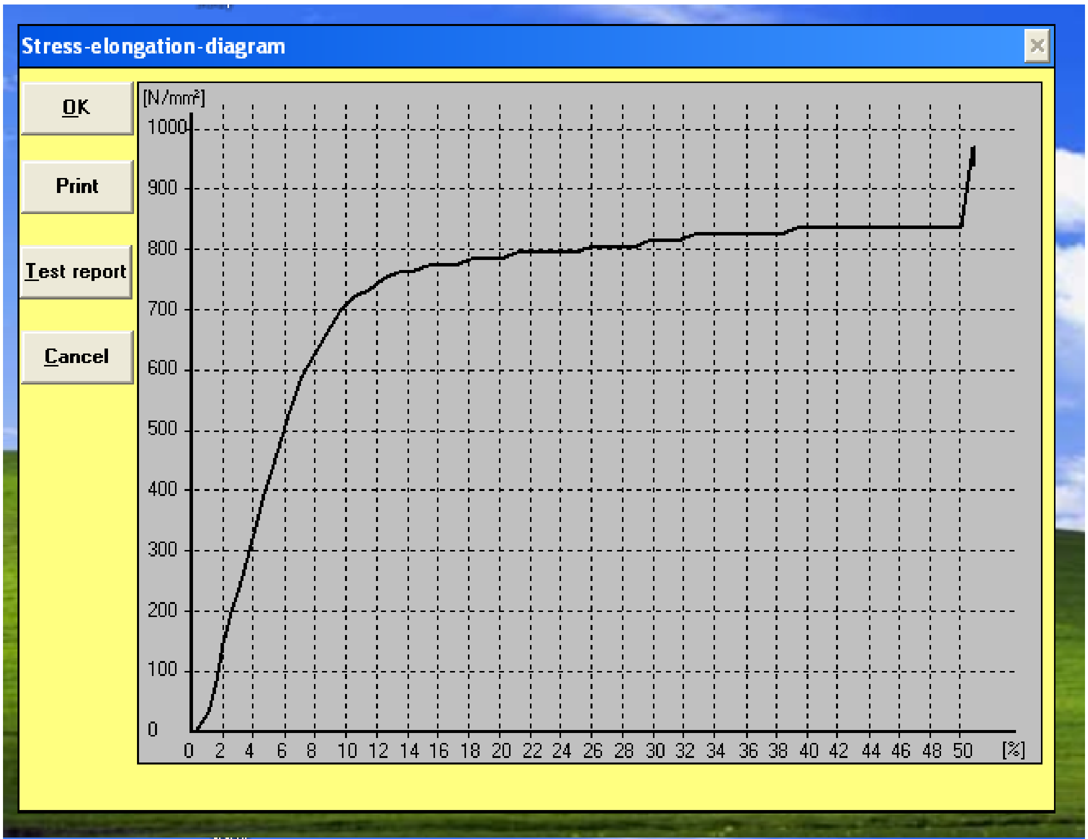

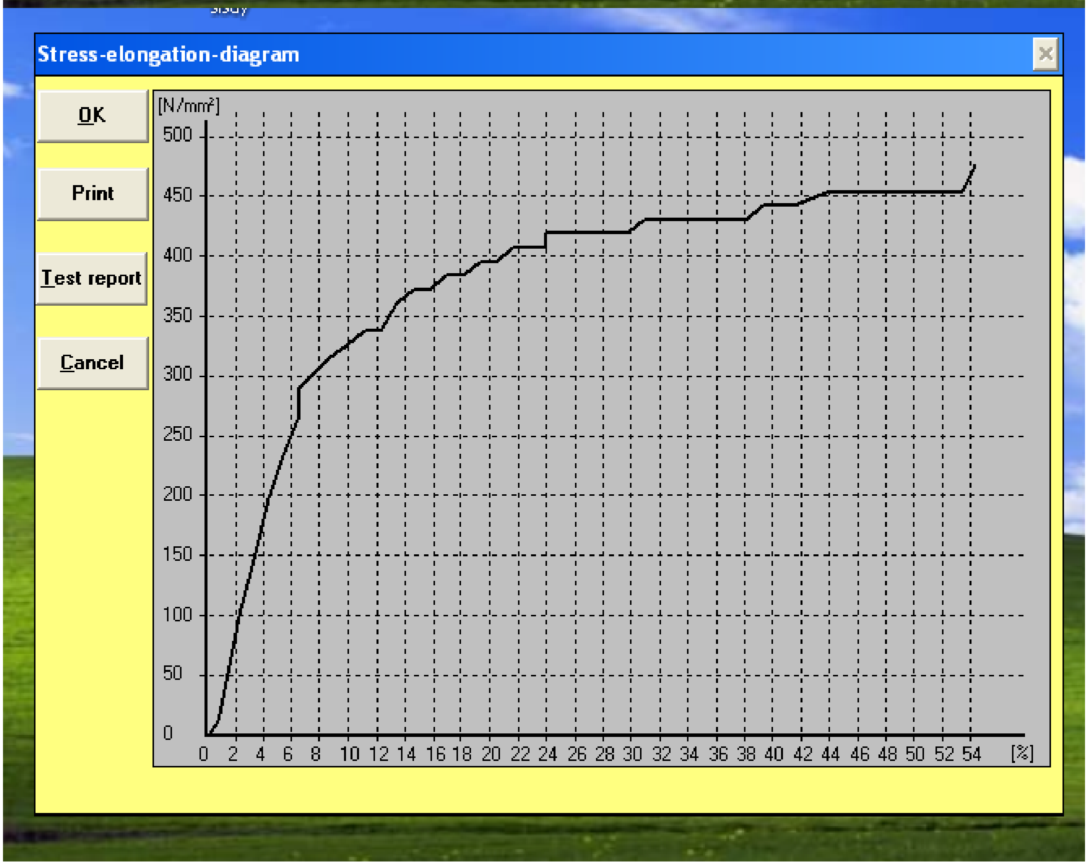

Appendix 6: Minitab 21 Taguchi

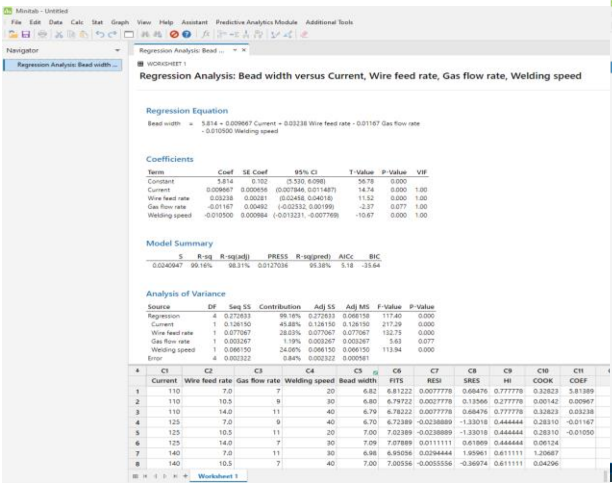

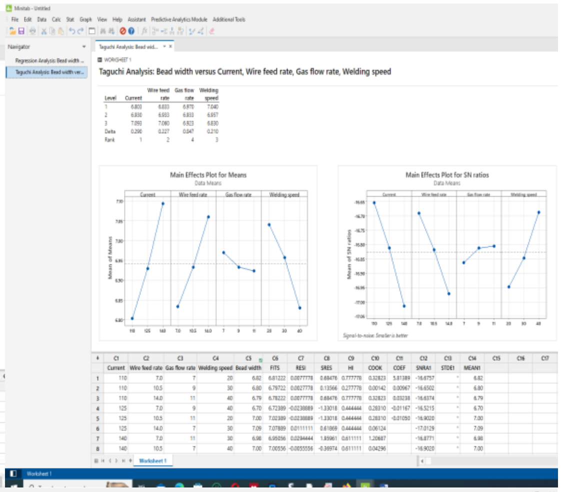

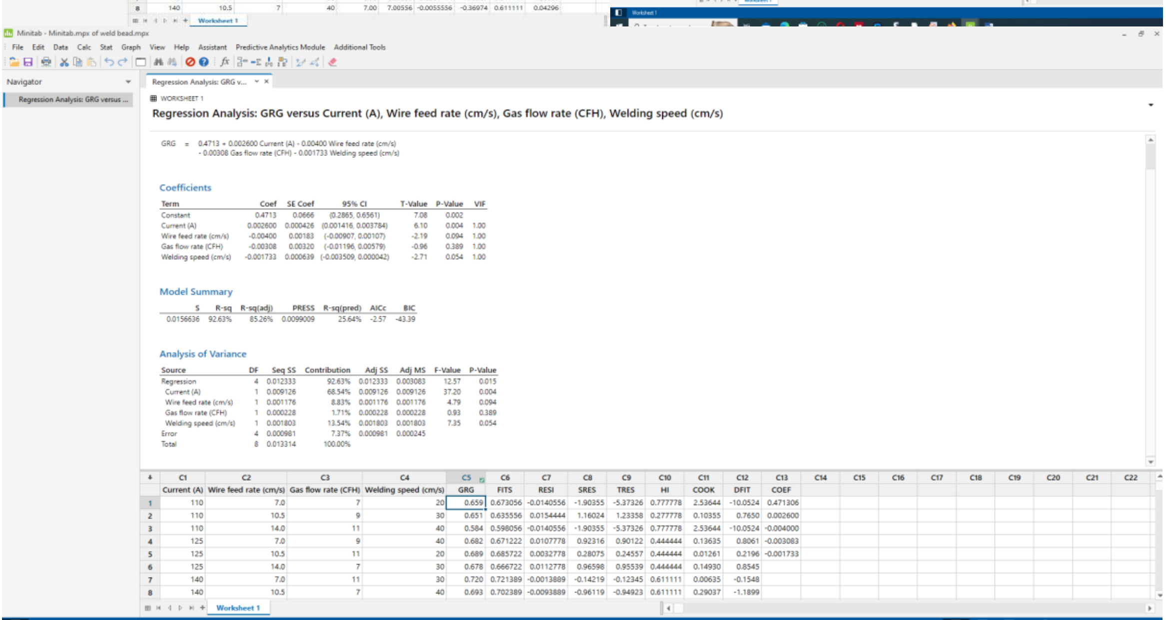

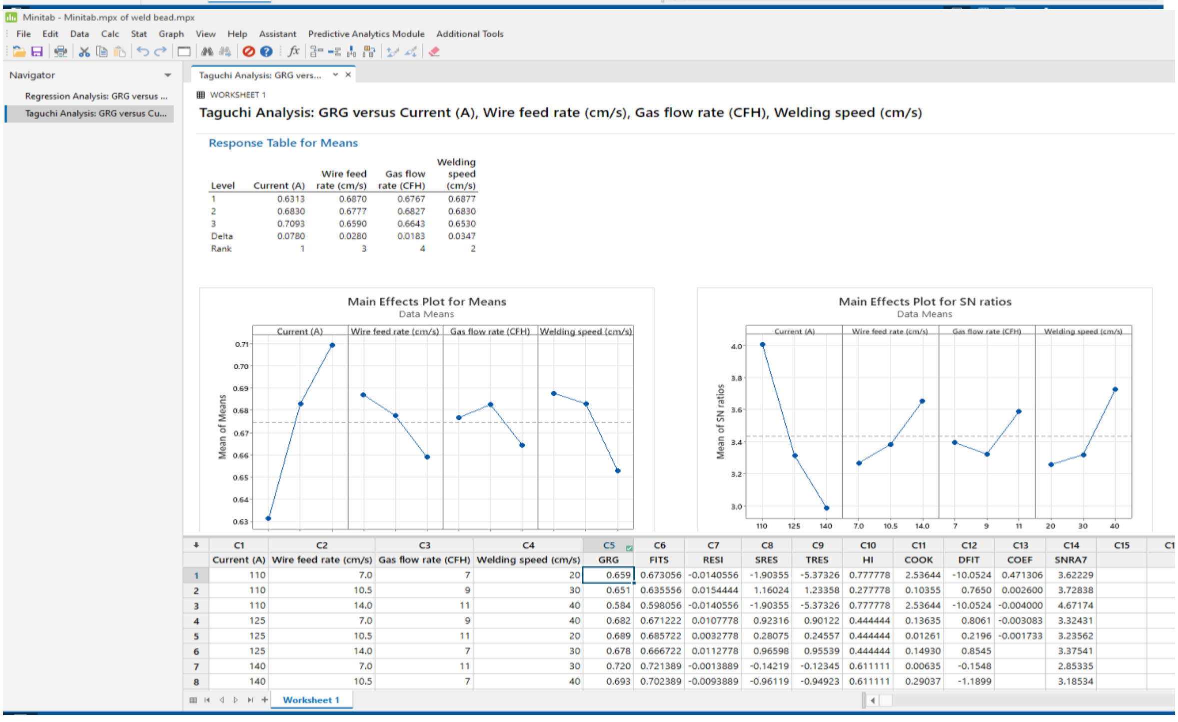

Appendix 6: Spectroscopy test result of SS 316 and AISI 4140

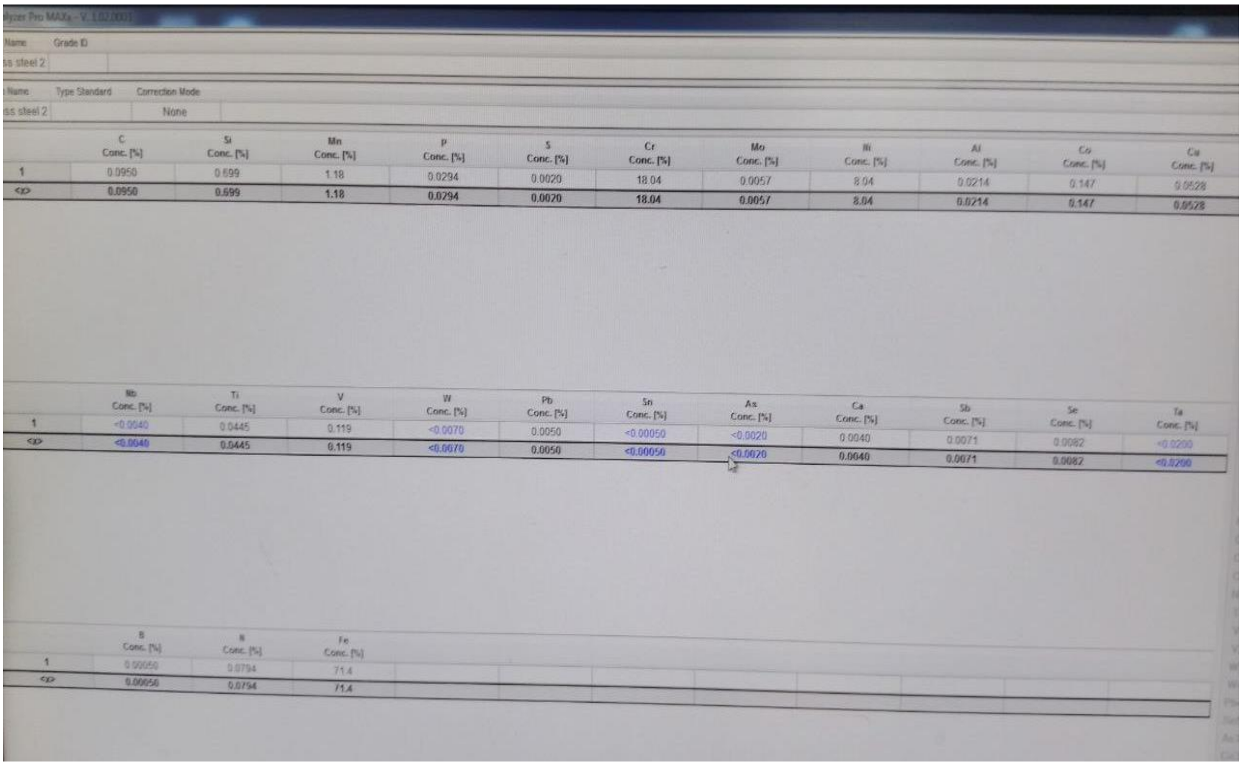

Name	Grade ID
ss steel 2	

Name	Type Standard	Correction Mode
ss steel 2		None

	C Conc. [%]	Si Conc. [%]	Mn Conc. [%]	P Conc. [%]	S Conc. [%]	Cr Conc. [%]	Mo Conc. [%]	Ni Conc. [%]	Al Conc. [%]	Co Conc. [%]	Cu Conc. [%]
1	0.0950	0.699	1.18	0.0294	0.0020	18.04	0.0057	8.04	0.0214	0.147	0.0528
<x>	0.0950	0.699	1.18	0.0294	0.0020	18.04	0.0057	8.04	0.0214	0.147	0.0528

	Nb Conc. [%]	Ti Conc. [%]	V Conc. [%]	W Conc. [%]	Pb Conc. [%]	Sn Conc. [%]	As Conc. [%]	Ca Conc. [%]	Sb Conc. [%]	Se Conc. [%]	Ta Conc. [%]
1	<0.0040	0.0445	0.119	<0.0070	0.0050	<0.00050	<0.0020	0.0040	0.0071	0.0082	<0.0200
<x>	<0.0040	0.0445	0.119	<0.0070	0.0050	<0.00050	<0.0020	0.0040	0.0071	0.0082	<0.0200

	B Conc. [%]	N Conc. [%]	Fe Conc. [%]
1	0.00050	0.0794	71.4
<x>	0.00050	0.0794	71.4